Dissertation

Genomic biomarkers and immune checkpoint Inhibitor response in lung cancer and TZAP induced telomere trimming in ALT cells

submitted by
Melanie KAISER, BSC MSc

for the academic degree of
Doctor of Medical Science (Dr. scient. med.)

at the
Medical University of Graz
Clinical Institute of Medical and Chemical Laboratory Diagnostics

under the supervision of
Assoc.- Prof. Dr. Wilfried Renner

2024

Declaration

I hereby declare that this thesis is my own original work and that I have fully acknowledged by name all those individuals and organizations that have contributed to the research. Due acknowledgement has been made to all other material used. Throughout this thesis and in all related publications I followed the “Standards of Good Scientific Practice and Ombuds Committee at the Medical University of Graz “.

Graz, January 2024 Melanie Kaiser

Disclosures

This dissertation was written at the doctoral school of “Lifestyle-Related Diseases”.

Part of this thesis is based on the following publications:

- Kaiser M, Semeraro MD, Herrmann M, Absenger G, Gerger A, Renner W. **Immune Aging and Immunotherapy in Cancer.** *Int J Mol Sci.* 2021 Jun 29;22(13):7016.
- Moreno SP*, Fusté JM*, Kaiser M, Li JSZ , Nassour J, Haggblom C, Denchi EL, Karlseder J. **TZAP overexpression induces telomere dysfunction and ALT-like activity in ATRX/DAXX-deficient cells.** *iScience*. 2023 Mar 14;26(4):106405.
  * These authors contributed equally

All co-authors have explicitly agreed to the use of the published data in this thesis.

Funding Statement

The first part of this thesis was supported by the *Ingrid Shaker Nessmann Grant* and the second part was funded by the *Marietta Blau Grant* and the Foerderungsstipendium of the Medical University Graz.

Contributions

The following people have contributed to this thesis:

- Wilfried Renner[1] (supervisor, study design, data analysis, data acquisition and interpretation, manuscript writing)
- Markus Herrmann[1] (co-supervisor, study design and data interpretation)
- Armin Gerger[3] (co-supervisor, study design and data interpretation)
- Gudrun Absenger[3] (patient recruitment and data acquisition)

- Donatella Semeraro, BSc, MSc[1] (establishment of telomere related analyses, manuscript writing)
- Sabine Pailer[1] (assay establishment, data interpretation and discussion)
- Renate Jahrbacher[1] (assay establishment, data interpretation and discussion)
- Sara Priego-Moreno[2] (supervisor at the Salk Institute for Biological Studies, study design, data analysis, and interpretation, manuscript writing)
- Jan Karlseder[2] (supervisor at the Salk Institute for Biological studies, study design, data analysis, and interpretation, manuscript writing)
- Javier Miralles Fuste[2] (study design, data analysis, and interpretation, manuscript writing)
- Julia Su Zhou Li[5] (study design, data analysis, and interpretation, manuscript writing)
- Joe Nassour[2] (data interpretation, manuscript writing)
- Candy Haggblom[2] (assay establishment, data interpretation, manuscript writing)
- Eros Lazzerini Denchi[6] (study design, data analysis, and interpretation, manuscript writing)

[1] Clinical Institute of Medical and Chemical Laboratory Diagnostics, Medical University of Graz, 15/1 Auenbruggerplatz, 8036 Graz, Austria.

[2] The Salk Institute for Biological Studies, Molecular and Cell Biology Department, 10010 N. Torrey pines Road, La Jolla, CA 92037, USA.

[3] Department of Oncology, Medical University of Graz

[4] Department of Pulmonology, Medical University of Graz

[5] The Ludwig Institute for Cancer Research, University of California San Diego, 9500 Gilman Drive, La Jolla, CA 92093, USA.

[6] Laboratory for Genome Integrity, National Cancer Institute, Building 37, Room 2144B, Bethesda, MD 20892, USA.

Publications

In addition to the mentioned publications, following articles as first or co-author were written and published during the PhD program:

- **Kaiser M**, Thurner EM, Mangge H, Herrmann M, Semeraro MD, Renner W, Langsenlehner T. Haptoglobin polymorphism and prostate cancer mortality. Sci Rep. 2020 Aug 4;10(1):13117. doi: 10.1038/s41598-020-69333-z. PMID: 32753660; PMCID: PMC7403311.
- Renner W, **Kaiser M**, Khuen S, Trummer O, Mangge H, Langsenlehner T. The Erythropoetin rs1617640 Gene Polymorphism Associates with Hemoglobin Levels, Hematocrit and Red Blood Cell Count in Patients with Peripheral Arterial Disease. Genes (Basel). 2020 Nov 4;11(11):1305. doi: 10.3390/genes11111305. PMID: 33158076; PMCID: PMC7694227.
- Semeraro MD, Smith C, **Kaiser M**, Levinger I, Duque G, Gruber HJ, Herrmann M. Physical activity, a modulator of aging through effects on telomere biology. Aging (Albany NY). 2020 Jun 23;12(13):13803-13823. doi: 10.18632/aging.103504. Epub 2020 Jun 23. PMID: 32575077; PMCID: PMC7377891.
- Semeraro MD, Almer G, **Kaiser M**, Zelzer S, Meinitzer A, Scharnagl H, Sedej S, Gruber HJ, Herrmann M. The effects of long-term moderate exercise and Western-type diet on oxidative/nitrosative stress, serum lipids and cytokines in female Sprague Dawley rats. Eur J Nutr. 2022 Feb;61(1):255-268. doi: 10.1007/s00394-021-02639-4. Epub 2021 Jul 28. PMID: 34319428; PMCID: PMC8783884.

Acknowledgements

Acknowledging the pivotal role of individuals who have contributed to the successful completion of a dissertation is a cherished tradition in the academic realm. In this vein, I would like to express my gratitude to the cornerstone of this endeavor, my dissertation supervisor, Wilfried Renner. Without his guidance, mentorship, and insights, this dissertation would not have reached its full potential. His knowledge and patience were instrumental in shaping this work and I am immensely grateful for the trust placed in me and the opportunities for growth that he has provided during this academic journey. I would also like to convey my sincere appreciation to Donatella, Renate, Barbara and Ernestine for creating the positive spirit that made it easy to come to the lab and especially to Sabine for her incredible support and enthusiasm about science.

I am deeply grateful for Jan Karlseder giving me the opportunity to work along driven and knowledgeable scientists in his lab at the Salk Institute for Biological Studies. I could have not had better guidance then from Sara Priego-Moreno who also became a close friend of mine.

Highly significant in my academic voyage has been the unflagging support from my family and friends. To my parents, Maria Kaiser and Karl Kaiser, and my siblings, Kathrin, Martin, and Benjamin. Your love has been my anchor during difficult phases of this endeavor.

I would be remiss not to extend my deepest gratitude to the Buchroithner family and my loving partner, Armin. Your constant encouragement and unwavering belief in me have been the bedrock upon which this work has been built. Your love and patience have carried me through the most demanding times, and your sacrifices have made my academic aspirations attainable. I am forever grateful for your presence and the countless ways in which you've made this journey not only possible but also more meaningful. This work stands as a testament to our partnership, and I look forward to sharing the fruits of this labor with you as we continue our journey together.

Meiner lieben Mama gewidmet.

Table of Contents

Abbreviations

ACT	Adoptive T cell transfer-based immunotherapy
ADCs	Antibody drug conjugates
ALT	Alternative Lengthening of Telomeres
AMP	Adenosine monophosphate
AMPK	AMP-activated protein kinase
APBs	ALT-associated promyelocytic leukemia bodies
APC	Antigen presenting cell
ATRX	Alpha-thalassemia mental retardation X-linked
ATSA	ALT telomere DNA synthesis in APBs
BLM	Bloom syndrome protein
BRAF	B-raf proto-oncogene
BSA	Bovine serum albumin
BTR	Bloom helicase, topoisomerase 3 and RMI1/2 scaffold protein
CCA	C-circle assay
cDNA	Complementary deoxyribonucleic acid
cECTRs	Circular extrachromosomal telomeric repeats
CI	Confidence interval
CTLA-4	Cytotoxic T lymphocyte-associated protein 4
DAXX	Death domain associated protein
ddTRAP	Droplet digital telomere repeat amplification protocol
DEPC	Diethylpyrocarbonate
DNA	Deoxyribonucleic acid
dNTP	Deoxynucleotide Triphosphate
EdU	5-ehtynyl-2’-deoxyuridine
EV	Empty vector
gammaH2AX	H2A histone family member X
gDNA	Genomic deoxyribonucleic acid
GEP	Gene expression profile
HPD	Hyperprogressive disease
HR	Homologous recombination
ICB	Immune checkpoint blockade
ICI	Immune checkpoint Inhibitor
IFN	Interferon
IHC	Immunohistochemistry
IL	Interleukin
KLRG1	Killer cell lectin-like receptor subfamily G 1
KO	Knock out
LAG-3	Lymphocyte-activation gene 3

MAPK	Mitogen-activated protein kinase
MEK	Mitogen-activated protein kinase kinase
mES	Mouse embryonic stem cells
mRNA	Messenger ribonucleic acid
NSCLC	Non-small cell lung cancer
OIS	Oncogene-induced senescence
OS	Overall survival
PBMCs	Peripheral Blood Mononuclear Cells
PBS	Phosphate buffered saline
PD-1	Programmed cell death protein 1
PD-L1	Programmed cell death protein ligand 1
PML	Promyelocytic leukemia
POT1	Protection of telomeres 1
qPCR	Quantitative polymerase chain reaction
RAP1	Repressor/Activator Protein 1
RMI1	RecQ-mediated genome instability 1
RNA	Ribonucleic acid
ROS	Reactive oxygen species
RT	Room temperature
RT	Reverse Transcriptase
SASP	Senescence-associated secretory phenotype
SNP	Single Nucleotide Polymorphism
SNP	Single nucleotide polymorphism
TBST	Tris-buffered saline 0.1% Tween 20
TCA	T-circle assay
Temra	Effector memory T cells that re-express CD45RA
TERT	Telomerase Reverse Transcriptase
TeSLA	Telomere shortest length assay
TIGIT	T cell immunoreceptor with Ig and ITIM domains
TIL	Tumor infiltrating lymphocytes
TIM-3	T cell immunoglobin and mucin domain-containing protein 3
TIN2	TRF1-interacting nuclear factor 2
TL	Telomere length
TLR8	Toll-like receptor 8
TMB	Tumor mutational burden
TNF	Tumor necrosis factor
TOP3A	DNA Topoisomerase 3 alpha
TOX	Thymocyte selection-associated HMG BOX
TPP1	POT1- interacting protein 1
TRAP	Telomere repeat amplification protocol

Tregs	T-regulatory cells
TRF	Telomeric repeat binding factor
TZAP	Telomeric Zinc finger-Associated Protein
ZBTB48	Zink finger and BTB domain-containing protein 48

Abstract in German (Kurzfassung)

Erster Teil: Telomerdynamik und Antwort auf Immun Checkpoint Inhibitoren bei Lungenkrebs

Die Behandlung von Patienten mit nicht-kleinzelligem Lungenkrebs (NSCLC) hat durch den Einsatz von Immun-Checkpoint-Inhibitoren (ICI) bemerkenswerte Vorteile erfahren. Um eine wirksame Behandlungsstrategie mit verbesserten Ergebnissen zu etablieren, ist es wichtig, Biomarker zu bestimmen, die Responder identifizieren und Immuntoxizitäten vermeiden. Telomere beeinflussen das Proliferationspotenzial von T-Zellen, die in der Immuntherapie die tumorspezifisch aktivierte Population bilden. In dieser Studie wurde die Rolle der Telomerlänge (TL), der TERT-Expression und von Einzelnukleotid-Polymorphismen im Zusammenhang mit der TL untersucht, um ihr Potenzial als prädiktiver Marker für das Überleben von Patienten zu ermitteln, die eine Immun-Checkpoint-Therapie erhalten. Die Proben wurden vor Beginn der Therapie und bei Nachuntersuchungen nach etwa drei Monaten für einen Zeitraum von bis zu einem Jahr entnommen. Die Kaplan-Meier-Analyse ergibt, dass kurze Telomere drei Monate nach Behandlungsbeginn, aber nicht zu Beginn, negativ mit dem Gesamtüberleben verbunden waren. In der multivariaten Analyse, in die Alter, Geschlecht, PDL-1-Expression und Histologie einbezogen wurden, war das Ergebnis statistisch nicht signifikant. Es zeigte sich, dass die Telomerlänge nach drei Monaten, nicht aber das Alter, das Geschlecht oder die PD-L1-Expression, das Überleben vorhersagt. Auch die TERT-Expression und die SNP-Analyse scheinen keinen prädiktiven Wert zu haben. Daher könnte die Bestimmung der Telomerlänge in T-Zellen nach Beginn der Behandlung für individualisierte Behandlungsentscheidungen nützlich sein.

Zweiter Teil: TZAP-induziertes Telomertrimmen in ALT Zellen

Das telomerbindende Protein TZAP hat sich als entscheidender Regulator der Telomerlängen-Homöostase erwiesen, insbesondere in Krebs- und Stammzellen, indem es die Obergrenze der Telomerlänge durch einen als Telomertrimming bekannten Prozess kontrolliert. Trotz seiner Bedeutung war der genaue Mechanismus, mit dem TZAP diese Aufgabe erfüllt, bislang nicht bekannt. Jüngste Erkenntnisse haben die Rekrutierung von TZAP an Telomeren aufgeklärt und gezeigt, dass es eine offene

Chromatinstruktur benötigt. Darüber hinaus scheint der Chromatin-Remodeler ATRX/DAXX eine zentrale Rolle bei der Verhinderung der Dekompaktierung des telomeren Chromatins und des anschließenden Telomertrimmens durch TZAP zu spielen. Auch deuten unsere Daten darauf hin, dass die Bindung von TZAP an Telomere die Telomerverkürzung auslöst, indem sie Replikationsstress auslöst und einen alternativen, der Verlängerung von Telomeren (ALT) ähnlichen Weg aktiviert, der von der Beteiligung des Bloom-Topoisomerase IIIα-RMI1-RMI2 (BTR) Komplexes abhängt.

Abstract in English

First part: Telomere dynamics and immune checkpoint inhibitor response in lung cancer (TILUC)

The treatment of patients with non-small-cell lung cancer (NSCLC) has seen remarkable benefits with the use of immune checkpoint inhibitors (ICIs). To establish an effective treatment strategy with improved outcome it is essential to determine biomarkers that identify responders and to avoid immunotoxicities. Telomeres impact the proliferative potential of T-cells, which make up the tumor-specific activated population in immunotherapy. In this study, the role of telomere length (TL), TERT expression and single nucleotide polymorphisms related to TL were investigated, to determine their potential as a predictive marker regarding survival in patients receiving immune checkpoint therapy. Samples were obtained before initiation of therapy and at follow-up examinations after approximately three months for up to one year. In the Kaplan-Meier analysis, short telomeres at three months after treatment initiation but not at baseline, was negatively associated with overall survival. In multivariate analysis, when age, sex, PDL-1 expression, and histology were included, the result was not statistically significant. It appeared that telomere length at three months but not age, sex or PD-L1 expression was predictive of survival. Furthermore, TERT expression and SNP analysis seem not to be of predictive value. Hence, the determination of telomere length in T-cells after treatment initiation could be useful for individualized treatment decisions.

Second part: TZAP-induced telomere trimming in ALT cells

The telomere binding protein TZAP has recently emerged as a crucial regulator of telomere length homeostasis, specifically in cancer and stem cells, by controlling the upper limit of telomere length through a process known as telomere trimming. Despite its significance, the precise mechanism by which TZAP accomplishes this task has remained elusive. Recent findings have shed light on the recruitment of TZAP to telomeres, revealing that it requires an open telomeric chromatin structure. Additionally, it appears that the chromatin remodeler ATRX/DAXX plays a central role in preventing the decompaction of telomeric chromatin and the subsequent telomere trimming induced by TZAP. Furthermore, our data suggest that TZAP binding to telomeres triggers telomere trimming by inducing replication stress and activating an alternative lengthening of telomeres (ALT)-like pathway that depends on the involvement of the Bloom-Topoisomerase IIIα-RMI1-RMI2 (BTR) complex.

1 Introduction

1.1 Motivation and Aim

Recent research has shed light on the potential use of telomeres as a biomarker in the field of immune checkpoint blockade (ICB). Immune checkpoint inhibitors (ICIs) have revolutionized cancer darftreatment by unleashing the power of the immune system to recognize and attack tumor cells. However, not all patients respond to these therapies, and identifying predictive biomarkers is crucial for patient stratification and treatment optimization. Telomeres, which play a critical role in cellular aging and immune cell function in general [1], have emerged as a promising candidate, which will be discussed in more detail in the next chapter ("Telomere dynamics and immune checkpoint inhibitor response in lung cancer"). In brief, studies have shown that shorter telomeres in tumor tissue and peripheral blood mononuclear cells (PBMCs), are associated with an impaired overall survival and a reduced response to ICIs, respectively. With T-cells being the main target of ICB, these findings led us to hypothesize that telomere dynamics in T-cells could serve as a predictive biomarker in ICB, which would help clinicians to identify patients who are more likely to benefit from these treatments and potentially guide treatment decisions. A thorough literature research showed that further studies are needed to explore the underlying mechanisms linking telomeres and immune checkpoint therapy response, to help pave the way for personalized and effective immunotherapeutic strategies. In this pilot study (Telomere dynamics and immune checkpoint inhibitor response in lung cancer - TILUC), the aim was to find out whether a correlation of ICB treatment response (survival) and telomere dynamics in T cells can be seen. Furthermore, I was given the opportunity together with Wilfried Renner, to analyze the results of a previous study on haptoglobin polymorphism and prostate cancer mortality. This gave me the chance to learn how to analyze data using the Kaplan-Meier curve and Cox regression analysis, which I used in the TILUC study. The study included 690 patients and shows that the polymorphism of the haptoglobin gene, which results in phenotypes with different antioxidant capabilities, does not correlate with overall mortality in prostate cancer [2].

During my PhD I also wanted to gain a deeper understanding of telomere dynamics at the molecular level, since translational analysis builds on basic research. Therefore, I spent 1.5 years at the prestigious Salk Institute for Biological Studies, joining the Molecular and Cell Biology Laboratory of Prof. Jan Karlseder, to learn and set-up techniques essential in the telomere field and to gain a deeper understanding of a special molecule named telomeric zinc finger-associated protein (TZAP) they discovered together with Eros Lazzerini Denchis Lab in 2017. TZAP is a protein that localizes at long telomeres and induces a process of “telomere trimming” which results in shorter telomeres [3].
How the process of trimming telomeres via TZAP exactly works was the research question I tried to answer together with researchers of Jan Karlseders lab at the Salk Institute for Biological Studies.

1.2 Structure of the thesis

First Part: TILUC

Clinical study performed at the **Medical University Graz**

Second Part: TZAP

Study on TZAP and its molecular mechanisms on telomere dynamics performed at the **Salk Institute for Biological Studies.**

First part: **T**elomere dynamics and **I**mmune checkpoint inhibitor response in **Lu**ng **C**ancer (TILUC)

ICB has revolutionized cancer treatment regimens. However, the lack of a durable response in most patients and tumor types, including lung cancer remains a challenge [4,5]. ICB can not only lead to hyperprogressive disease (HPD) but also cause immune-related adverse drug reactions [6, 7]. It is therefore essential to better understand the mechanisms of treatment resistance to allow a more selective and targeted prescription. Lung cancer is the leading cause of cancer incidence and death worldwide [8], but there is still an unmet need for a predictive biomarker of response to immunotherapy [9]. Although measurement of programmed death-ligand 1 (PD-L1) protein expression by immunohistochemistry (IHC) and tumor mutational burden (TMB) are still used, they are imperfect predictors of response [10,11]. With an ample number of new biomarkers emerging and getting tested, it seems that a multimodal approach using a combination of markers will help determine the best treatment strategy [12,13]. Recently, Ferrara et al. showed that T cell senescence measured in peripheral cells, correlated with progression, HPD and poor survival in NSCLC patients undergoing ICB treatment. They assessed several markers including $KLRG1^{+}$, $CD28^{-}$ and $CD57^{+}$ on T cells of the periphery [14]. It also has been shown before that shorter telomeres in leukocytes goes along with a higher risk of early death after cancer diagnosis [15]. Since short telomeres is a hallmark of senescent cells [16], we wanted to assess whether measuring telomere length in T-cells has any predictive value regarding overall survival in patients undergoing ICB. A study performed by Faugeras et al. demonstrated that short telomeres measured in biopsies of patients suffering from NSCLC treated with Nivolumab negatively affects overall survival [17]. Furthermore, Rolles et al. proposed that TL of leukocytes in the periphery is associated with overall survival but not with treatment response to ICB [18].

Our hypothesis was that telomere dynamics in T-cells is predictive of survival in NSCLC patients receiving ICB treatment. Within the first part of the thesis project, telomere dynamics was assessed by analysis of telomere length, TERT expression, telomerase activity and determination of specific SNPs that are known to correlate with telomere

length in humans. Blood samples for these measurements were drawn before ICB and in three-month-intervals for a follow-up time of up to one year. The primary outcome is overall survival (OS). Although the present study focuses on lung cancer, the results also provide valuable scientific information on the role of ICB response prediction in other cancer types, since not the cancer itself but T-cells which are affected by ICB treatment, are investigated.

2 Background (TILUC)

2.1 Structure and function of telomeres

Telomeres play a crucial role in the aging of cells and the development of cancer, with their length and integrity influencing the overall health and longevity of an organism. They are localized at the end of each chromosome with a range of 2-20 kb in humans, depending on the chromosome [19]. These repetitive DNA sequences, consisting of TTAGGG repeats in humans, act as protective caps and prevent the erosion and degradation of chromosomes during cell division and DNA replication [20]. In addition to the DNA sequence, telomeres are also comprised of a diverse array of proteins. A total of six proteins form the so-called shelterin complex that binds to telomeric DNA and contributes to telomere structure and function (Figure 1). These proteins include Telomeric Repeat-binding Factor 1 (TRF1), Telomeric Repeat-binding Factor 2 (TRF2), TRF1-interacting Nuclear Factor 2 (TIN2), POT1-interacting Protein 1 (TPP1), Protection of Telomeres 1 (POT1), and Repressor/Activator Protein 1 (RAP1). Each protein within the shelterin complex has specific roles and interactions that contribute to the regulation and stability of telomeres [21]. TRF1 and TRF2 bind DNA that is double stranded, helping to protect the chromosomal ends and prevent degradation and fusion events [30]. TIN2 serves as a bridge, connecting TRF1 and TRF2 to the rest of the shelterin complex and helps with recruiting the telomerase enzyme [22,23,24]. TPP1 interacts with POT1, both also involved in facilitating the recruitment of telomerase, form a protective cap over the single-stranded telomeric DNA. POT1 binds specifically to the single-stranded telomeric DNA and prevents its recognition as a DNA break, maintaining the integrity of the telomere [25,26,27]. RAP1 together with TRF2 prevents

telomeres from homologous recombination-triggered deletions and fusions [28]. This array of proteins together essentially prevent telomere shortening by inhibiting the action of DNA repair enzymes that may mistake the natural ends of chromosomes for damaged DNA. Additionally, shelterin proteins contribute to the formation of a protective telomere loop structure, known as the T-loop, which further shields the telomere ends [29]. Overall, the structure and function of telomeres are tightly regulated by the shelterin complex, ensuring the maintenance of genomic stability, and preventing aberrant DNA repair processes [30].

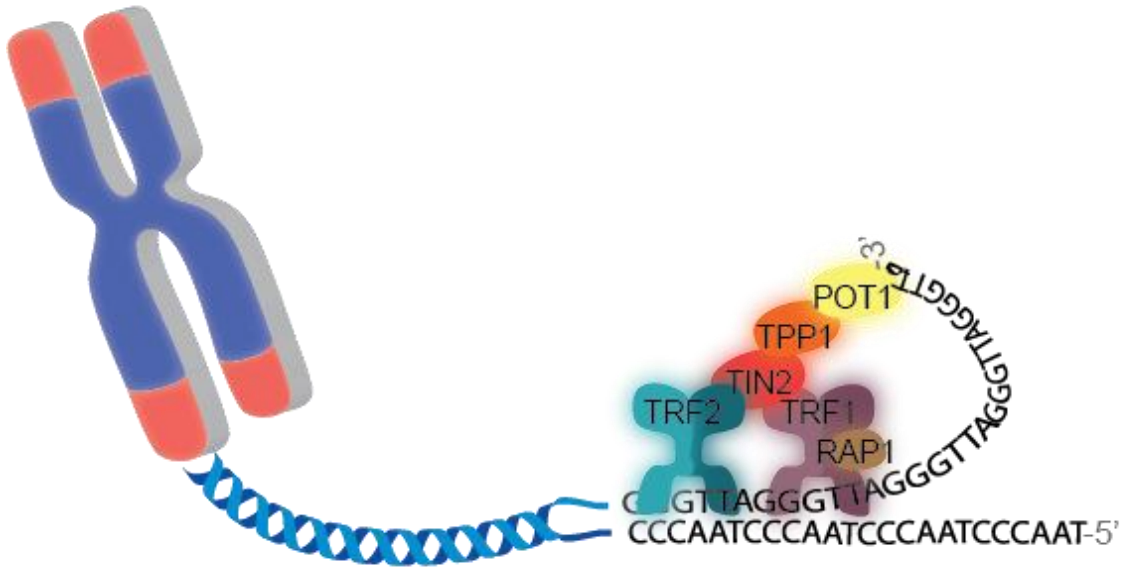

Figure 1: Telomeric bound shelterin complex. Image was created in Adobe Illustrator 2024.

During each cell division, telomeric DNA shortens (50-200 base pairs) because of the DNA replication machinery being unable to fully copy the ends of linear chromosomes and the lack of telomerase expression in somatic cells. This phenomenon is known as the "end replication problem" [31, 32]. Furthermore, somatic cells lack the ability to express telomerase enzyme [33] Telomeres act as sacrificial sequences that protect the essential genetic information contained within the chromosomes. As cells divide repeatedly, telomeres become progressively shorter, eventually reaching a critically short length. At this point, cells go into replicative senescence or undergo apoptosis, resulting in a decline of tissue function and contributing to the aging process [34]. To counteract the gradual telomere shortening, the enzyme telomerase is present in some

cells, especially stem cells, germ cells, and certain types of cancer cells [35]. Telomerase adds repetitive DNA sequences to the ends of chromosomes, replenishing and extending telomere length. This activity enables these cells to maintain their proliferative capacity and avoid premature senescence. However, in most somatic cells, telomerase activity is low or absent, leading to a progressive loss of telomeric DNA with each cell division [36].

2.2 Telomeres and their role in aging and carcinogenesis

Telomere shortening and cellular aging are interconnected processes. In terms of aging, telomeres act as a molecular clock where progressive shortening of telomeres is associated with natural aging processes in various tissues and organs, characterized by altered gene expression, impaired functionality, and reduced regenerative capacity. As cells age and telomeres become critically short, the ability to maintain tissue homeostasis declines, leading to age-related physiological changes and increased susceptibility to age-related diseases such as cardiovascular disease, osteoporosis and immune system decline amongst others [37]. Telomeres also have a significant role in cancer development. Cancer cells possess the ability to bypass the normal mechanisms of telomere shortening and maintain their telomere length, thereby achieving immortality and unlimited replicative potential (Figure 2). In most cancer cells, the activation of telomerase or alternative lengthening of telomeres (ALT) mechanisms allows the cells to continually extend their telomeres. This prevents the cells from entering replicative senescence or undergoing cell death, enabling them to divide indefinitely and form tumors [38]. Telomerase activation is observed in almost all human cancers, making it an attractive target for cancer therapies. Inhibiting telomerase activity or disrupting the telomere maintenance mechanisms in cancer cells could potentially halt their uncontrolled growth and lead to their demise. Several approaches to targeting telomerase, such as small-molecule inhibitors and immunotherapeutic strategies, are being explored in cancer research and clinical trials [39, 40]. While telomerase activation is prevalent in many cancers, a subset of tumors utilizes the ALT mechanism to maintain their telomere length. ALT is a telomere maintenance mechanism that operates through recombination-based processes, allowing cancer

cells to elongate their telomeres without activating telomerase. The ALT-positive cancers tend to have distinct genetic and epigenetic alterations, and targeting ALT remains a challenge due to its complexity and variability across different tumor types [41]. Understanding the intricate relationship between telomeres, aging, and cancer is of great importance and has opened new avenues for therapeutic interventions and disease management. Targeting telomeres and telomerase has emerged as a promising therapeutic treatment avenue. Moreover, telomere length and telomere-related markers are being investigated as potential biomarkers for cancer, response to therapy like ICB, aging and age-related diseases. By deciphering the complex mechanisms underlying telomere biology, it is possible to gain deeper insights into the aging process, develop strategies for promoting healthy aging, and devise novel therapeutic approaches for cancer management. In Chapter 6 I will address the two telomere maintenance pathways with greater detail.

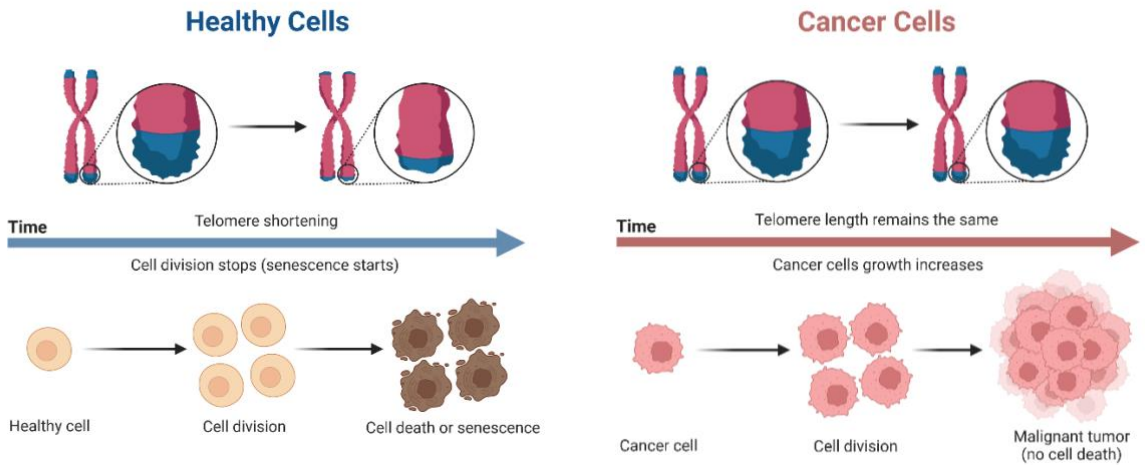

Figure 2: Telomere biology in healthy cells compared to cancer cells. In healthy somatic cells telomeres shorten with every cell division until they become senescent and stop divide. In cancer cells on the other side telomeres don't become short because of various telomere elongating mechanisms that can be activated in cancer cells, and therefore they can proliferate indefinitely and bypass senescence. Image was created with BioRender.com.

2.3 Immunological decline and ICB

The following chapters are partially based on a review article that has already been published [42]. With age the functions of our immune system decline, and cancer

incidence rises. The discovery of these checkpoints of the immune system has not only transformed cancer treatment, but also generated a great deal of interest in finding biomarkers that can predict treatment response, as only one-third of patients benefit from this therapy. The process of aging has a major impact on immunity and therefore also on T cells, the cells mainly targeted in immune checkpoint blockade.

2.3.1 Innate and adaptive immune response

A complex system of proteins and cells makes up an immune system that defends our body against pathogens like bacteria or viruses and that eliminates cancerous or damaged cells. It comprises two distinct cellular responses. The first is the innate response with an immediate line of defense. It is made up of specific proteins and phagocytic cells that recognize pathogen-associated molecular patterns, via the Toll-like receptors [43]. The adaptive immune response can specifically recognize and remember pathogens, providing a targeted and long-lasting defense. It is established through the generation of memory cells, including memory B cells and memory T cells, which are formed during the initial encounter. These memory cells can quickly mount a robust and targeted immune response, leading to a faster and more effective elimination of a pathogen [44]. As we grow older, alterations in our immune system occur, leading to its inability to support adequate wound healing and protection against cancer cells and foreign pathogens. As we age, innate immune functions continue to evolve, creating a chronic, low-grade inflammatory state called "inflammaging". As adaptive immune responses weaken, accumulation of dysfunctional T cells arise [45,46,47]. I will mainly describe changes in acquired immunity with a focus on T cells in the upcoming chapters.

2.3.2 Senescence vs Immunosenescence

Cellular senescence is a state of cell cycle arrest in G-1 phase in which cells cease to divide and undergo characteristic changes in their morphology and function. Senescence can be triggered by various stressors, including DNA damage, telomere shortening, oncogene activation, and other forms of cellular stress. In the beginning of the 1960s, pioneering research was conducted that unveiled a critical revelation:

primary human cells ultimately lose their ability to replicate due to a limited number of cellular divisions. This limitation primarily arises from telomere attrition, a process that incites a robust DNA damage response and is termed as replicative senescence [48, 49, 50, 51]. Notably, cellular growth arrest can also be initiated through oncogenic signaling, denoted as oncogene-induced senescence (OIS). OIS materializes as a consequence of activating mutations in oncogenes, activation of tumor suppressors such as $p16^{INK4a}$, or their loss, exemplified by PTEN. Epigenetic disturbances and external stressors like DNA damage or oxidative challenges can similarly induce a state termed stress-induced premature senescence [52, 53, 54, 55, 56, 57, 58]. At the core of orchestrating a durable growth arrest are the master regulators, p53 and the $p16^{INK4a}$-pRb tumor suppressor pathways [59]. OIS, critically, serves as a robust defense mechanism against tumorigenesis, curbing the proliferative potential of cancerous cells. In contrast, replicative senescence aligns more closely with the natural aging process and the development of degenerative diseases [60,61]. Importantly, beyond their static growth arrest, senescent cells undergo extensive alterations in metabolic and transcriptional activity representing key features of their distinctive phenotype [62]. In contrast to apoptosis, an alternative cellular program leading to cell-cycle exit, senescent cells not only maintain viability but also exhibit a remarkable characteristic known as the senescence-associated secretory phenotype (SASP). This phenotype involves the secretion of an array of proinflammatory cytokines, chemokines, growth factors, and proteases, which can potentially exert adverse effects on the local microenvironment [63,64]. The expression of SASP is typically triggered by various disruptions, including genomic, mitogenic, and oxidative perturbations, with oncogene activation being one example. Intriguingly, SASP expression is notably absent when cyclin-dependent kinases like $p16^{INK4A}$ or p21 are active [65]. Although SASP remains partially understood, it is proposed to necessitate the presence of persistent DNA damage, a condition that is not met when $p16^{INK4A}$ or p21 is ectopically expressed [66]. While the acquisition of SASP is essential in processes such as wound healing and embryogenesis, it can also exert modulatory effects on close by cells, also cells of the immune system, potentially transforming fibroblasts that are senescent into proinflammatory cells. This, in turn, can facilitate tumor development [67, 68, 69, 70].

Immunosenescence is used to describe weakened immunity in old people [71]. The term was first used by Roy Walford when he hypothesized that aging is pathogenetically related to defective processes of the immune system [72]. Later, the main features of immunosenescence were determined as an inability to respond to new antigens, a buildup of memory T cells, a persistent low-grade inflammation, and a concomitant decrease in naive T cells [73, 74].

2.3.3 When T-cells age

T cells play a crucial role in orchestrating and upholding immune responses within the body. Their journey commences with their development from hematopoietic stem cells. Following this, progenitor cells embark on a migratory path to the thymus, subsequently undergoing a series of transformation phases. The emerging thymocytes that do not have specific traits are subjected to apoptosis. Once matured, naive T cells, characterized as $CD4^+$ and $CD8^+$ cells, enter the bloodstream. CD4 T cells are responsible for a wide array of functions, including the activation of innate immune cells, B-lymphocytes, and cytotoxic T cells. They also play an essential part in curbing excessive immune responses [75].

Within the peripheral T cell pool, various subsets coexist. This includes naive T cells, primed to respond to novel antigens, memory T cells, originating from prior antigen encounters and ensuring long-term immunity, and T-regulatory cells (Tregs), responsible for maintaining immune equilibrium [76].

One of the most significant alterations in the immune system is thymic involution, a process contributing to the age-related decline in T cell immunity, particularly observed in mice. In contrast, the dynamics of T cell homeostasis in humans differ notably from mice. In human adults, the generation of T cells predominantly relies on the peripheral proliferation of naive T cells [77]. Intriguingly, there is an age-associated discrepancy in the maintenance of naive T cell subsets, with naive $CD8^+$ T cells showing less resilience compared to their $CD4^+$ counterparts [78]. Consequently, a conspicuous reduction in circulating naive $CD8^+$ T cell numbers stands out as the most reliable indicator of and aging immune system [79].

As T cells grow older, with a typical lifespan of four to six months, they may enter a state of senescence [80]. It's worth noting the importance of distinguishing between states of senescence, anergy, and exhaustion, as they each have distinct origins despite sharing some similar traits.

Anergy denotes a functional dampening in $CD4^+$ and $CD8^+$ T cells, where T cells exhibit reduced responsiveness characterized by the absence of proliferation and diminished secretion of the key T cell growth factor IL-2 upon encountering an antigen and subsequent T cell receptor (TCR) activation. In addition to this, these cells also display diminished levels of cytokines like IFN-γ and TNF-α [81, 82, 83]. Despite that there is no specific surface marker that distinctly identifies those cells, epigenetic mechanisms like histone modifications mediated by Sirtuin 1, along with the involvement of the early growth response gene 2, seem to be implicated in the establishment and maintenance of this anergic state [84, 85, 86, 87].

Exhaustion in T cells characterizes a gradual decline in effector function and a diminished capacity for proliferation due to prolonged antigen exposure, typically stemming from chronic infections or tumor development. In this state, T cells demonstrate reduction of effector cytokines like Interleukin-2, Interferon-γ, or Tumor necrosis factor [88]. They also exhibit heightened expression of various chemokines and an increase of inhibitory receptors, including PD-1 [89],TIM-3 [90,91], LAG-3 [92], CTLA-4 [93], (TIGIT) [94], among others. These receptors collectively dampen the response of the immune system towards tumor cells [95,96]. However, it's worth noting that $CD8^+$ T cell exhaustion appears crucial in preserving the immunological reserve necessary for surveilling chronic infections, as proposed recently [97]. Therefore, the impact of T cell exhaustion depends on the context, exerting significant influence on the outcomes of autoimmune diseases, infections, and cancer [98,99].

Exhaustion is externally regulated by immunological control mechanisms, whereas senescence is intrinsically managed through cellular stress responses [100]. The regulation of T cell senescence predominantly revolves around the mitogen-activated protein kinase (MAPK) signaling pathways, whereas T cell exhaustion primarily involves signaling associated with inhibitory receptors [101]. Replicative senescent T cells exhibit specific characteristics, including shortened telomeres, the absence of

CD28 and CD27, plus an increase of heightened senescence-associated-ß-galactosidase (SA-ß-Gal) [102]. They are found in both the $CD4^+$ and $CD8^+$ T cell compartments and notably display increased levels of CD57 and Killer cell lectin-like receptor subfamily G (KLRG1) surface markers. Recent research emphasizes CD57 as a pertinent marker, attributed to the seriously compromised proliferative capacity of CD57-expressing T cells [103].

Another category of T cells, characterized by the absence of CD27 and CD28 while expressing CD45RA, is referred to as effector memory T cells that re-express CD45RA, often denoted as T_{emra} cells (See Figure 3). Interestingly, they have a few key attributes of senescent cells. They display a notable reduction in telomerase activity. Additionally, T_{emra} cells exhibit diminished proliferative capabilities, more DNA damage as evidenced by increased phosphorylated H2A histone family member X (γH2AX) levels, a component of the DNA damage response pathway observed in senescent cells. Intriguingly, although these cells lack very short telomeres, indicating a different mechanism driving their senescent state, T_{emra} cells still undergo senescence, possibly due to DNA damage induced by reactive oxygen species (ROS) [104,105]. Furthermore, the upregulation of cell cycle regulatory proteins like p16 and p21 is noted in T_{emra} cells, primarily stemming from the loss of CD27 and CD28 [106]. This elevation impedes the transition from the G1 phase of the cell cycle to the S phase, contributing to senescence [107]. They also display a senescence-associated secretory phenotype (SASP), encompassing a spectrum of cytokines. This includes both immunosuppressive cytokines like IL-10 and TGF-ß, as well as proinflammatory ones such as TNF, IFNγ, IL-2, IL-6, and IL-8 [108,109,110]. The SASP observed in T cells is further under the influence of p38 MAPK signaling, playing a role in age-related inflammation [111].

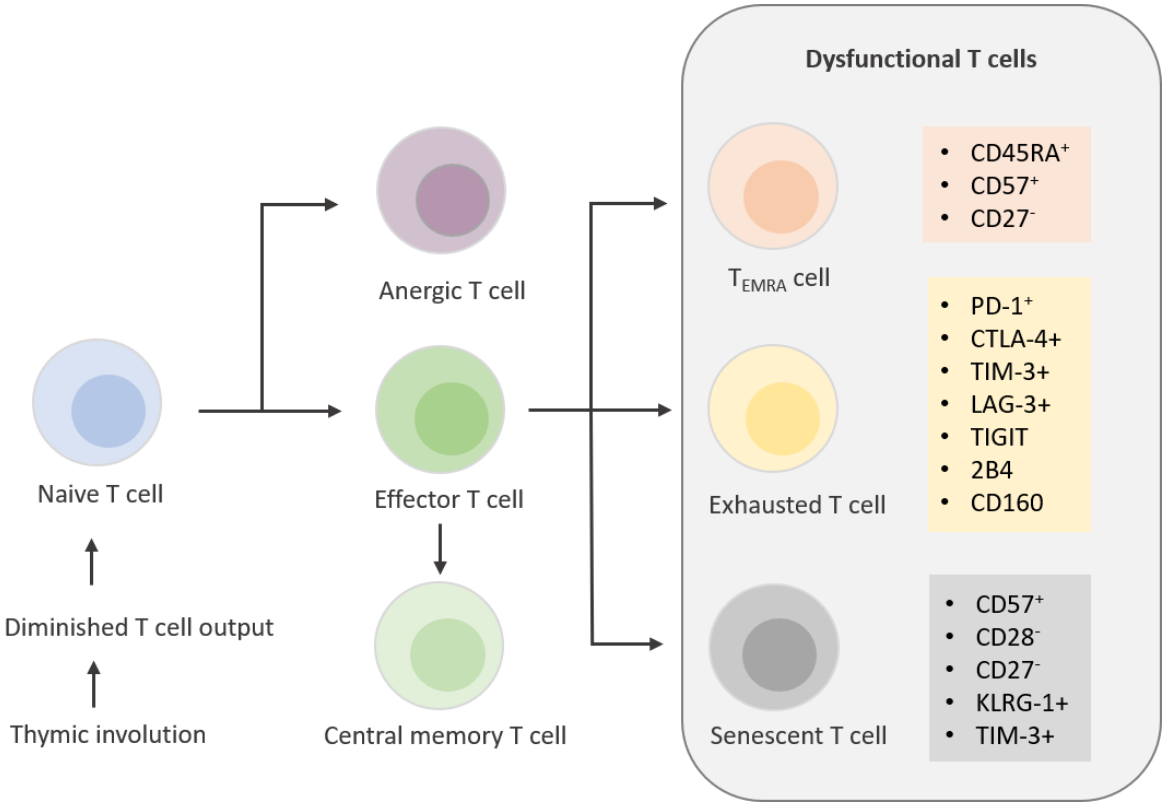

Figure 3: T cell development over the course of aging. Copyright © 2021 by the authors, with kind permission of the publisher.

2.4 Cancer and Immunotherapy

2.4.1 Immune checkpoint blockade

Immune checkpoint inhibitors are monoclonal antibodies that can modulate the immune response. The ones most explored and used in cancer treatment are PD-1 (programmed cell death protein 1), PD-L1 (programmed death-ligand 1), and CTLA-4 (cytotoxic T-lymphocyte-associated protein 4).

T cells play a crucial role in the immune response, recognizing and eliminating abnormal cells, including cancer cells. The surface receptor PD-1 is found on T cells and can trigger apoptosis when activated in antigen specific T cells and lowers apoptosis of regulatory T cells [112]. PD-L1 on the other hand is expressed on the membrane of cancer cells but also some other immune cells. PD-L1 on cancer cells

can bind to the receptor (PD-1) in T cells which leads to an inhibitory signal that shuts down the T cell. This inhibitory signal prevents the T cell from attacking the cancer cell effectively, allowing the cancer cell to evade an effective response of the immune system. Monoclonal antibodies targeting the receptor PD-1 (Pembrolizumab, Nivolumab) or the ligand PD-L1 (Atezolizumab, Durvalumab and Avelumab) block this interaction and promote survival and activation of T cells. As a result, the inhibitory signal is in theory to be lifted, and the T cells should be able to attack cancer cells more effectively [113,114] (See Figure 4B).

Another checkpoint is CTLA-4 on the membrane of T cells. It is important in the regulation of T cell activation at the early stages. CTLA-4 competes with CD28 (a co-stimulatory molecule) for binding to B7-1 (CD80) and B7-2 (CD86) on dendritic cells (antigen-presenting cells). CTLA-4 can bind B7-1/B7-2, which leads to an inhibitory signal that dampens T cell activation. This prevents excessive immune responses and helps maintain immune homeostasis. Checkpoint inhibitors targeting CTLA-4 (Ipilimumab) block the inhibitory signals, that should allow sustained activation of immune system and therefore T cells [115, 116] (See Figure 4A).

The profound significance of uncovering immune checkpoints which lead the way to ICB, was underscored by James Allison and Tasuku Honjo getting the Nobel Prize in Physiology or Medicine in 2018 [117]. Successful implementation of PD-1/PD-L1 and CTLA-4 inhibitors led to several clinical trials investigating other immune checkpoint like adenosine A2A receptor, CD47, B7H3, CD39 and CD73, with hopefully new treatment options soon [118,119].

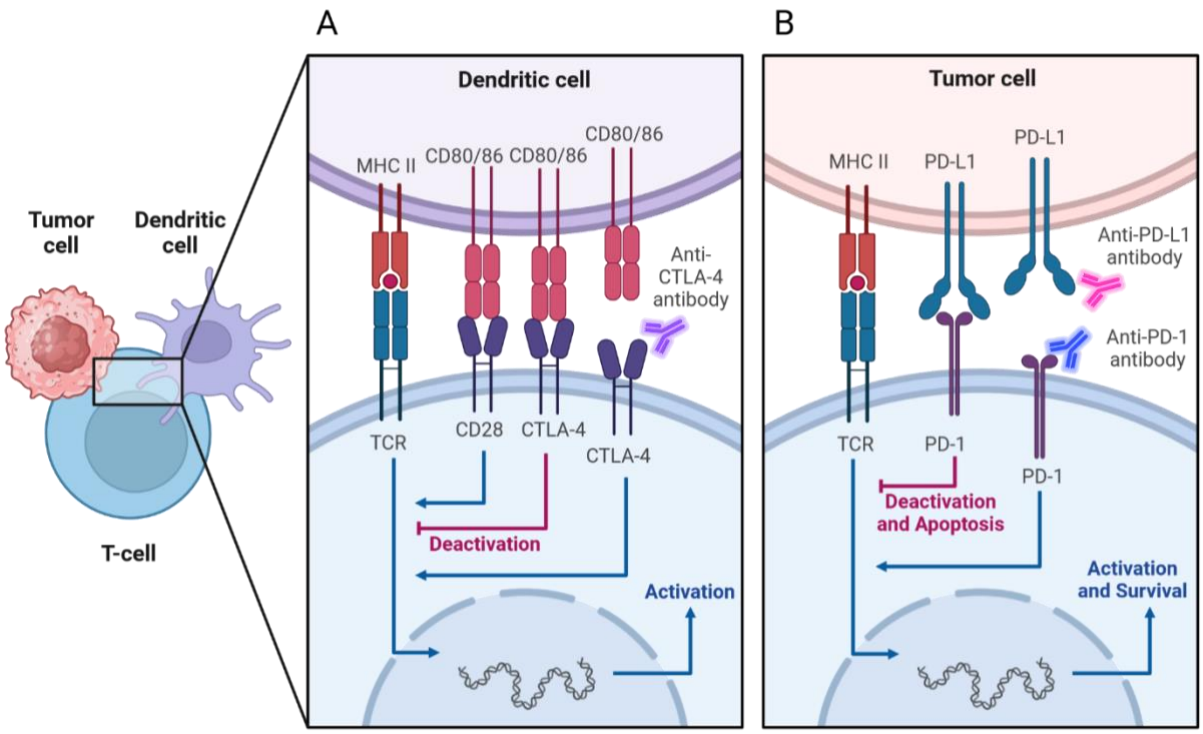

Figure 4: Overview of the mechanism of immune checkpoint blockade. (A) A dendritic cell binds via MHC II to the TCR receptor and CD80/86 to DC28 on the T cell leading to the activation of the T cell. CTLA-4 competes with CD28 to bind to CD80/86 and blocks T cell activation. The CTLA-4 antibody binds to the receptor on T cells and therefore inhibits binding to CD80/86, leading to activation of the T cell. (B) A tumor cell binds via MHC II to the TCR receptor of the T cell. The PD-1 receptor is a surface receptor on T cells. Tumor cells that express PD-L1 on their surface can bind to T cells and therefore promote deactivation and apoptosis of certain T cells. When Anti-PD-L1 antibody or Anti-PD-1 antibody bind to the ligand or receptor, respectively, activation and survival of the T cells is promoted. Image created with BioRender.com.

As mentioned before, despite the remarkable efficacy of ICB, up to two-thirds of patients receiving these therapies still exhibit resistance, highlighting the imperative need for deeper investigations into the mechanisms of treatment resistance and the development of more efficacious therapeutic approaches. Besides HPD, ICB can, in rare instances, induce life-threatening or irreversible autoimmune toxicities. Consequently, it becomes imperative to enhance patient selection, minimize toxicity, and avert HPD in individuals who may not respond favorably to such treatments.

Historically, immune checkpoint therapy primarily concentrated on reversing T cell exhaustion through inhibition of PD-1, PD-L1, and CTLA-4. Nonetheless, not every patient experiences the benefits of ICB. As a result, considerable interest has emerged in targeting additional immune checkpoints, such as LAG3. It is shown that LAG3, along

with PD-1, is notably upregulated on tumor-infiltrating lymphocytes (TILs) and collaborates synergistically to facilitate immune evasion by tumors [120,121]. Consequently, a substantial body of preclinical data has propelled LAG3 to the forefront as the third immune checkpoint to be investigated in clinical settings, with nearly a dozen therapeutic approaches currently under scrutiny [122,123].

The conventional clinical biomarkers for treatment response, namely PD-L1 expression and overall Tumor Mutational Burden (TMB), have encountered limitations due to their inability to predict responses with complete accuracy [124]. Thus far, PD-L1 expression has been the most widely used marker for guiding patients' selection. Nevertheless, the practicality of PD-L1 testing greatly differs depending on the type of cancer and the treatment context. The variability arises from differences in the specific PD-L1 assay used, the defined PD-L1 expression thresholds, and the types of cells analyzed. Deciphering the diverse testing methodologies continues to present a formidable challenge [125].

While PD-L1 expression holds relevance as a biomarker, it falls short of being the ideal one. Nonetheless, it currently stands as the sole pertinent biomarker in specific cancer types and is notably linked to improved outcomes in cancers like NSCLC or gastric cancer amongst others, when treated with PD-1 inhibitors, or breast cancer when PD-L1 inhibitors are used as therapy [126]. Nonetheless, it becomes less obvious in treatments when combining chemotherapy or other immune checkpoint inhibitors. Additionally, more trials prove the effectiveness of checkpoint inhibitors in cancers lacking PD-L1 expression [127]. Consequently, relying solely on PD-L1 assessment through immunohistochemistry (IHC) appears insufficient for patient selection in most cancer cases [128]. Hence, the ongoing pursuit involves the discovery of a marker, especially one that is not invasive, as well as the exploration of therapeutic approaches beyond the targeting of PD-1/PD-L1 and CTLA-4.

2.5 T cells as a biomarker in the context of ICB – what markers have already been explored?

It's a natural process in the aging body that non-functional T cells amass, but they can also result from chronic infections or cancer. Malignant tumors have the capacity to

induce two critical dysfunctional states, namely T cell exhaustion and senescence, both of which coexist in individuals with cancer. These states play pivotal roles in sustaining a suppressive tumor microenvironment, thereby impeding effective antitumor immune responses [129]. Numerous studies have provided evidence that T cells can become senescent within patients afflicted by chronic viral infections and can be observed in tumor-infiltrating lymphocytes (TILs) in different malignant tumors [130, 131, 132, 133]. This suggests that T cell senescence represents another way of how cancer cells can evade the body's immunity [134]. The accumulation of such evidence has not only positioned senescence as a burgeoning target for immunotherapy but has also led to its utilization as a marker for ICB [135].

The enzyme telomerase plays a central role in preserving telomere length, also in T cells, which is crucial for their proliferative capacity and therefore an effective immune response. This led Weng et al. to propose that enhancing telomerase activity could potentially enhance T cell function in older individuals [136]. There is evidence, particularly in adoptive cell transfer therapies, that shorter telomeres in T cells exhibit lower suitability for a persisting immune response against cancerous cells because of their weakened proliferative potential [137,138]. Which makes me hypothesize that short telomeres in T cells might contribute to non-responsiveness to ICB because of the diminished capacity to proliferate, raising the question if it could serve as a marker alongside other recently promising measures such as the T cell–inflamed gene expression profile (GEP), PD-L1, and clonal TMB [139, 140, 141, 142].

Interestingly, the CD28 marker on the surface of T cells which is lost upon senescence, has been shown to be essential for the proliferation of $CD8^+$ T cells following checkpoint blockade (PD-1) [143, 144]. Essentially, T cell proliferation restricted by PD-1 is dependent on blocking CD28 stimulation. It has been demonstrated recently that CD28 co-stimulation plays a vital part when it comes to ICB [145,146]. Furthermore, they show that $CD8^+$ T cells that respond to ICB do have CD28 on the cell surface. A recent study indeed explored markers of senescence and ICB response and they found that loss of certain markers (CD57, Tim-3, CD28) were correlated with negative treatment response [147]. However, this study involved only 10 patients, and further research with

larger cohorts is necessary to validate these results. Another study (which I already mentioned in the beginning of my thesis) claims that senescent T cells correlate with progression and hyperprogressive disease in patients with lung cancer treated with ICB [148]. It has also been suggested that cytotoxicity of T cells at tumor the tumor does go along with cytotoxic activity of those T cells in the periphery, emphasizing that T cells are a valid option for studying T cell responses in tumors [149]. In NSCLC patients, they propose that response to PD-1 inhibition can be estimated by the cytotoxic activity of T cells in the periphery. Additionally, it is claimed in another study that subsequent to ICB, the amplification of T cell clones that go into the tumor did not originate from existing TILs [150]. Instead, it arose from new clone variants from the peripheral regions. Intriguingly, clonotypes initially identified before initiation of therapy in tumor microenvironments persisted after therapy [150], which suggests not only that infiltrating lymphocytes possess restricted capacity for rejuvenation, but also that proliferation of those infiltrating lymphocytes originating in peripheral sources significantly contributes to the response to treatment. In fact, when clonotypes of T cells were tracked with deep T cell receptor sequencing after immune checkpoint (PD-1) blockade in lung cancer, it was observed that the cells that underwent expansion in the blood amass within the tumor tissue in people who exhibited a positive response to the therapy [151].

Also, T cells within the tumor microenvironment can serve as predictive indicators of immune responses to immunotherapy across various tumors, including colorectal, breast, and urothelial cancers [152,153,154]. An insightful study recently revealed that just by analysis of TCF7 alone (a transcription factor), observed on T cells within a tumor specimen, it is possible to accurately forecast the treatment effectiveness in melanoma patients. This finding underscores that the functional state, alongside their quantity and spatial distribution of $CD8^+$ cells within a patient's tumor, plays a pivotal role in initiating effective antitumor immune response [155]. Furthermore, a recent investigation identified a subset of T cells within the tissue of lung cancer samples, that spread in the tumor and that play a role in non-responsive tumors in ICB. This unique $CD8^+$ subset, referred to as "Ebo," exhibits distinctive functional characteristics. While they share certain characteristics with T cells that are exhausted, like expressing

inhibitory receptors such as PD-1 or TIM-3 or a limited IFNγ response, they display remarkably high proliferation activity. This suggests that non-responsiveness to ICB may be mechanistically linked to an accumulation of TILs that are not functional. In essence, ICB could prevent these T cells from undergoing apoptosis, and not help reverse T cells exhausted state. These findings imply that depleting this subset of cells might create room for actual effective cancer fighting T cells. Alternatively, measuring these Ebo cells in the TME might help predict response to ICB [156]. It is worth noting that the response to ICB stemming from pre-existing TILs in the cancer and the reaction of T cells external to the tumor to the treatment are not mutually exclusive. Instead, they might signify interlinked mechanisms of response. Within this context, the expression of the immune cytokine CXCL13 emerges as a promising biomarker. Its predictive value for ICB response has been observed upon analyzing it in cancer samples before treatment. Additionally, it is correlated with ICI response when measured in TILs that show an elevated PD-1 expression, in certain type of cancers including lung cancer [157, 158]. The predictive significance of this marker was underscored in another paper where they claim that CXCL13 and CCR5 are intrinsic markers in T cells for immune checkpoint response across a spectrum of cancers [159]. Consequently, it appears that combining markers from the periphery with markers that are present in tumor microenvironments hold promise for enhancing the precision of therapy response predictions.

2.6 Evolving treatment strategies

Once believed to be an irreversible process, senescence has seen notable advancements in our understanding. However, in the early 2000s, it was revealed that replicative senescence, hinging on p16 of pRB, may not always be permanent [160]. Further insights unveiled how T cells that are senescent employ AMPK for the recruitment of p38 to TAB1. Their study showed that by obstructing AMPK-TAB1-dependent p38 activation, the senescent phenotype was abrogated [161]. Intriguingly, in vitro experiments demonstrated that inhibiting both p38MAPK and PD-1 led to the recovery of cell division capacity and TNF-α release of T_{EMRA} cells. This effect couldn't be achieved by blocking either pathway in isolation, suggesting a connection between

an exhausted state and senescence state in T cells [162]. The cytokine TNF-α can inhibit tumor growth and even promote shrinking of the cancer [163, 164]. This is controlled by p38 MAPK signaling, which is pivotal in regulating SASP [165].

Like I described earlier, this unique secretory profile of senescent cells can influence cells that are close-by and therefore reshape the TME. Consequently, it becomes intriguing to explore whether modifying the SASP through manipulation of P38 MAPK pathway or other treatments, such as using senostatic or senlolytic drugs to stall senescence or to eliminate cells, respectively, could enhance the response to immunotherapy. In another study it is discussed whether manipulating various actors of sestrin-MAPK could regulate changes in T cell function that are related to senescence. Although, they raise concerns that extended sestrin suppression might promote expansion of cells that are senescent with DNA damage, which could lead to malignancy [166]. Therefore, short-term sestrin inhibition may represent a more beneficial immunotherapeutic strategy [167].

Recent studies have investigated the manipulation of the MAPK pathway using inhibitors against BRAF and MEK, with mixed outcomes. However, not only preclinical but also clinical trials have demonstrated improved antitumor immunity and tolerability when these inhibitors are combined with ICB. Specifically, targeting MEK did not only lead to the proliferation of effector T cells but also a reduction in T cells that are exhausted and apoptosis [168, 169, 170, 171, 172]. Notably, Gurusamy et al. highlighted the significance of p38 inhibition not only in rejuvenating older T cells but also in blocking it`s expression in "younger" T cells [173].

Furthermore, it seems that chimeric antigen receptor (CAR) T-cell treatment in conjunction with PD-1 inhibitors positively impact the exhausted state of T cells [174]. This encourages the hypothesis that using CAR T cell therapy, ICB, and inhibition of p38 at the same time, may constitute an effective therapy in certain contexts. Additionally, studies have shown that T cell senescence mediated by regulatory T cells or cancers might be blocked or overturned by Toll-like receptor 8 (TLR8) signaling [175, 176, 177]. Given that establishing an immunosuppressive TME comes with a significant difficulty to effective ICB, focusing on TLR8 activation may present a different avenue to promote functionality of T cells in conjunction with ICIs.

Emerging evidence also shows the importance in cellular-level alterations, specifically on an epigenetic level, in achieving lasting responses to ICB. TOX (Thymocyte selection-associated HMG BOX), has an important function in priming T cells for exhaustion at the transcriptional and epigenetic levels, and has gained attention in this regard [178, 179, 180, 181, 182, 183, 184]. This suggests that epigenetic modifiers might hold promise in combination with ICB.

Several other combination treatments focused on PD-1 plus for example LAG-3 have shown promising results. In a recent study of melanoma patients, it is shown that when focusing on TIGIT and PD-1 concurrently led to an actual synergistic restoration of CD8 T cell performance including elevated proliferative capacity in both peripheral blood and the cancer [185].

Despite substantial advancement in comprehension and addressing different states like senescence or exhaustion of T cells, an optimal therapy and indicator capable of perfectly distinguishing responders from non-responders remain elusive. Ultimately, a multifaceted interventional strategy is necessary to enhance therapeutic results. Therefore, it will be necessary to measure several markers, originating from both tumor and peripheral sources, to tailor the most successful therapy. Employing a vast range of markers from diverse sources within the tumor and combining treatments to either abolish or reconfigure T cell subsets holds the potential to significantly enhance cancer treatment outcomes. With the TILUC study we were hoping to help clinicians by bringing them closer to better treatment decisions.

3 Materials and Methods

3.1 Patient characteristics, recruitment, and study design

The study includes 35 cancer patients recruited at the *Department of Oncology and Pulmonology* at the *Medical University Hospital* in Graz between April 2019 and October 2020. Only patients who did not undergo previous ICB were included in the study. Upon study entry, each participant donated a tube of EDTA-blood (used for SNP measurements and for isolation of T cells) and a Pax gene tube (for gene expression analysis). Samples were obtained before initiation of therapy and at follow-up examinations after approximately three months (Figure 5).

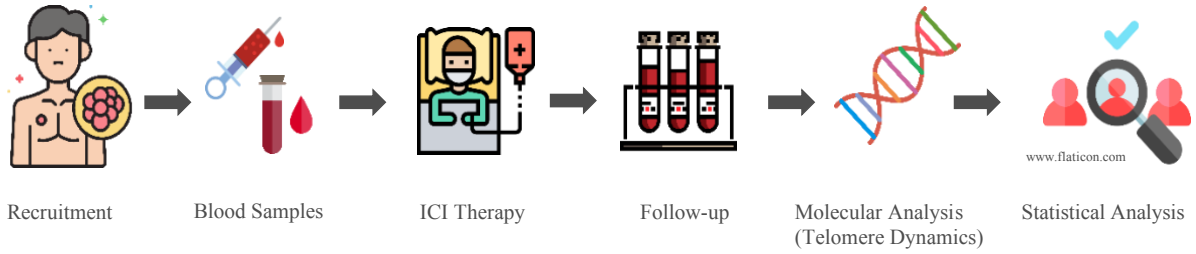

Figure 5: Study design. Lung cancer patients were recruited. Blood samples were taken before and after therapy initiation with a follow-up after three months and telomere parameters were determined and statistically analyzed. Icons are freely available at www.flaticon.com [186], image composition was created with Microsoft PowerPoint.

The clinical trial at hand has been approved by the Ethical Committee of the Medical University of Graz and informed consent was acquired. Clinical parameters were obtained from medical records. Detailed patient characteristics can be found in Table 1. For all patients we documented age at diagnosis, sex, cancer type, PDL-1 expression, type of treatment, follow-up of two years and overall survival (OS). We decided to analyze overall survival because data acquisition for determining progression free survival turned out to be rather difficult since patients were recruited in two different departments.

3.2 T-cell isolation: Fluorescence-activated cell sorting (FACS)

Human peripheral blood mononuclear cells (PBMCs) were isolated from fresh EDTA blood by Ficoll density gradient centrifugation (Cytiva Ficoll® Paque Plus, Sigma

Aldrich). The cells were stained with a monoclonal anti-CD3/PE-Cy7 antibody (Clone SK7, Biolegend) in FACS staining buffer for 20 minutes at room temperature. $CD3^+$ cells were sorted on a FACSAria™ IIIu cell sorter (BD Biosciences) and subsequently snap frozen in liquid nitrogen and stored at −80 °C until further analysis. T cell sorting was carried out by the Imaging Facility at Medical University Graz.

3.3 Telomere length

3.3.1 Quantitative real time PCR

The protocol of the qPCR assay for relative telomere length measurement used, is based on Cawthon [187] and was established by Wilfried Renner and Sabine Pailer. The DNA of T cells was isolated using the MagNA Pure LC instrument (Roche). For this procedure the Total Nucleic Isolation Kit (Roche) was used. Input volume was 200µl and output volume was set to 100µl. After the instrument finished isolation, DNA was stored at -20º Celsius until further use.

Subsequently, relative telomere length was measured in triplicates. This assay measures the template amount of TL (T) and a reference single-copy gene. These measurements were then used to determine the relative telomere length as the T/S ratio. 36B4 (acidic ribosomal phosphoprotein P0) was used as a reference gene and amplification control for each sample. To get the T/S ratio for each sample, the median 36B4 threshold cycle (C_t) value was subtracted from the median telomere C_t value. Then the relative T/S ratio was calculated by subtracting the T/S ratio of the standard curve point from the T/S ratio of each unknown sample.

All qPCR analyses were performed on a CFX384 TouchTM (Biorad) instrument. Each run included a positive control (Hela DNA, New England Biolabs) and a standard curve based on dilutions of a pool of healthy donor control DNA to determine the quantity of targeted templates in each sample relative to the control DNA. If variance of result of telomere length exceeded 20%, the measurement was repeated.

The following primers were used in the reaction:

Telomere For:	5'-CGGTTTGTTTGGGTTTGGGTTTGGGTTTGGGTTTGGGTT-3'
Telomere Rev:	3'-GGCTTGCCTTACCCTTACCCTTACCCTTACCCTTACCCT-5'
36B4 For:	5'-CAGCAAGTGGGAAGGTGTAATCC-3'
36B4 Rev:	3'-CCCATTCTATCATCAACGGGTACAA-5'

In more detail, pool DNA for the standard curve was diluted with Elution buffer from the Magna Pure Isolation Kit as follows:

1:2	120 µl Pool DNA	+	120 µl Elution Buffer
1:8	60 µl from dilution 1:2	+	180 µl Elution Buffer
1:32	60 µl from dilution 1:8	+	180 µl Elution Buffer
1:128	60 µl from dilution 1:32	+	180 µl Elution Buffer
1:512	60 µl from dilution 1:128	+	180 µl Elution Buffer

The positive control was diluted 1:160 in Elution Buffer and the sample DNA was used undiluted. Reaction for telomer length and for the single copy gene (36B4) was prepared using 10 µl of Universal Mastermix (UMM 2x), 2 µl of Sybergreen (10x), Primer 1 (100 µm) 0.06 µl, Primer 2 (100 µm) 0.06 µl, 3.88 µl ddH_20 and 4 µl of DNA (sample or pool DNA). The thermal cycling profile was 10 min at 95 °C followed by 35 cycles of 15 s at 95 °C, 30 s at 58 °C and 30 s at 72 °C including fluorescence data collection. All primers have been purchased from Metabion, Austria.

3.3.2 Telomere shortest length assay (TeSLA)

The TeSLA assay methodology was adapted from a protocol in Andrew Ludlow´s lab and Lai et al [188]. Prof. Ludlow also recommended the Gentra Puregene Cell Kit from Quiagen for DNA isolation as described below.

Isolation of DNA for TeSLA using the Gentra Puregene Cell Kit (Quiagen) according to manufacturer's protocol:

Isolated T-cells were thawed and centrifuged for 5 sec at 14.000g x to pellet the cells. Supernatant was discarded and pellet was vortexed vigorously in the residual liquid. 300 µl Cell Lysis Solution were then added to the resuspended cells and vortexed on high speed for 10 sec to lyse the cells. Then 100 µl Protein Precipitation Solution was

added, vortexed vigorously for 20 sec at high speed and centrifuged for one minute at 14.000 x g. 300 µl isopropanol were pipetted into a clean 1.5 ml microcentrifuge tube and the supernatant from the previous step was transferred by pouring carefully. When combined, the tube was inverted gently about 50 times. Then the tube was centrifuged for 1 min at 14,000 x g. The supernatant was then discarded and 300 µl of 70% ethanol was added and inverted several times to wash the DNA pellet followed by centrifugation of 1 minute at 14.000 x g. Supernatant was again discarded and pellet air dried for 5 minutes. 20 µl of DNA Hydration Solution was then added and vortexed for 5 sec at medium speed. The mix was then incubated at 65°C for 1 hour to dissolve the DNA followed by an incubation overnight at room temperature with gentle shaking. The DNA was then centrifuged briefly and stored at -20°C.

Oligo preparation for TeSLA PCR

40µl of each adapter (100µM p22TA and p22AT) was combined with 40µl of TeSLA ADR1 C3S (100µM) and 20µl of 5x STE buffer (50mM Tris pH 8.0, 250mM NaCl, 5mM EDTA) and incubated in a thermocycler at 95 ºC for 5 min and brought gradually to 25 ºC using the ramp option (0.1 ºC down/s). These pre-annealed 40µM stock Oligos were then stored at -20 ºC until further use. Also, Telo 1,2,3,4,5 and 6 were combined to make for 10nm of each single Telo component.

gDNA was quantitated using the Qubit fluorometer and the dsDNA BR assay kit (Invitrogen) but no DNA could be detected anymore, very likely due to long shipping times. Therefore, the maximum amount of 17 µl of input was used from the TILUC samples. Sample was mixed with 2µl of 10x CutSmart Buffer (New England Biolabs), 2µl of 10 mM ATP (New England Biolabs), 1µl of 10nM Telo 1-6 and 0.5µl of T4 ligase (New England Biolabs, 2000000 units/ml). Mixture was subjected to 35 ºC on the thermocycler overnight.

Oligos for telomeric DNA ligation

TeSLA Telo 1	ACTG GCC ACG TGT TTT GAT CGA CCC TAA C
TeSLA Telo 2	ACTG GCC ACG TGT TTT GAT CGA TAA CCC T
TeSLA Telo 3	ACTG GCC ACG TGT TTT GAT CGA CCT AAC C
TeSLA Telo 4	ACTG GCC ACG TGT TTT GAT CGA CTA ACC C
TeSLA Telo 5	ACTG GCC ACG TGT TTT GAT CGA AAC CCT A
TeSLA Telo 6	ACTG GCC ACG TGT TTT GAT CGA ACC CTA A

Oligos for Subtelomeric DNA ligation

TeSLA ADR1 C3S	GGT TAC TTT GTA AGC CTG TC
TeSLA P22 TA	TA GAC AGG CTT ACA AAG TAA CCA TGG TGG AGA ATT CTG TCG TCT TCA CGC TAC ATT
TeSLA P22 AT	AT GAC AGG CTT ACA AAG TAA CCA TGG TGG AGA ATT CTG TCG TCT TCA CGC TAC ATT

Oligos for TeSLA PCR

TeSLA Adapter	TGT AGC GTG AAG ACG ACA GAA
TeSLA TP	TGG CCA CGT GTT TTG ATC GA

On day one, DNA was diluted to 10ng/uL in 10uM Tris (pH 8) and the following mixture of 20 µl of 5 µl DNA (10ng/ µl), 2 µl 10X CutSmart Buffer (New England Biolabs), 2 µl 10mM ATP (New England Biolabs), 1 µl Telo 1-6, 0.5 µl T4 ligase (New England Biolabs 2000000 units/ml) and 9.5 µl ddH_2O was prepared and incubated overnight at 35 °C. On the second day the reaction from day one was subjected to 65℃ for 10 min to inactivate enzymes. Then reaction of day one (20 µl) was mixed with 1 µl 10X CutSmart Buffer, 0.2 µl CviAII (New England Biolabs 10000units/ml) and 8.8 µl ddH_2O and incubated at 25℃ for 2 hours. Afterwards 1 µl 10X CutSmart Buffer, 0.2 µl MseI (New England Biolabs 10000 units/ml,), 0.1 µl NdeI (New England Biolabs 20000 units/ml), 0.2 µl BfaI (New England Biolabs 10000 units/ml) and 8.5 µl ddH_2O was added to the reaction and incubated at 37℃ for 2 hours. Reaction from previous step (40 µl) was then mixed with 1 µl 10X CutSmart Buffer, 1 µl rSAP (New England Biolabs 1000 units/ml) and 8 µl ddH_2O and incubated at 37℃ for 1 hour, then heated to 80℃ for 20 min and then gradually reduced temperature to be room temperature. Then 10 µl of the previous reaction (1 ng DNA/ µl) was mixed with 5 µl ddH_2O, 1 µl 10X CutSmart Buffer, 2 µl 10 mM ATP, 0.5 µl AT adapter (40 µM), 0.5 µl TA adapter (40 µM) and 0.5 µl T4 ligase which was incubated overnight at 16°C. On day three the reaction from day two was incubated at 65℃ for 10 min. Then reaction from was diluted to be 10 pg DNA/ µl (50X dilution) = 4 uL of ligation into 196 uL ddH2O. The rest of the ligation was stored at -20ºC. Then a PCR containing 2 µl DNA (10 pg/µl), 12.5 µl 2X Mix H (epicenter), 0.5 µl Adapter (10 µM), 0.5 µl TeSLA TP (10 µM), 0.5 µl FailSafe polymerase (epicenter) and 9 µl ddH_2O was then set up and subjected to a hot start, followed by 94 °C for 2

min, and 26 cycles of 94 °C 15 sec, 60 °C 30 sec, 72 °C 10 min. This was followed with 72 °C for 15 minutes. An illustration of the assay is given in Figure 6.

After PCR, a 0.85% gel (SeaKem LE-Agarose) using 1xTAE was prepared and Southern blotting performed using telomere probe. In Figure 6 an overview of the principle of the TeSLA assay is given.

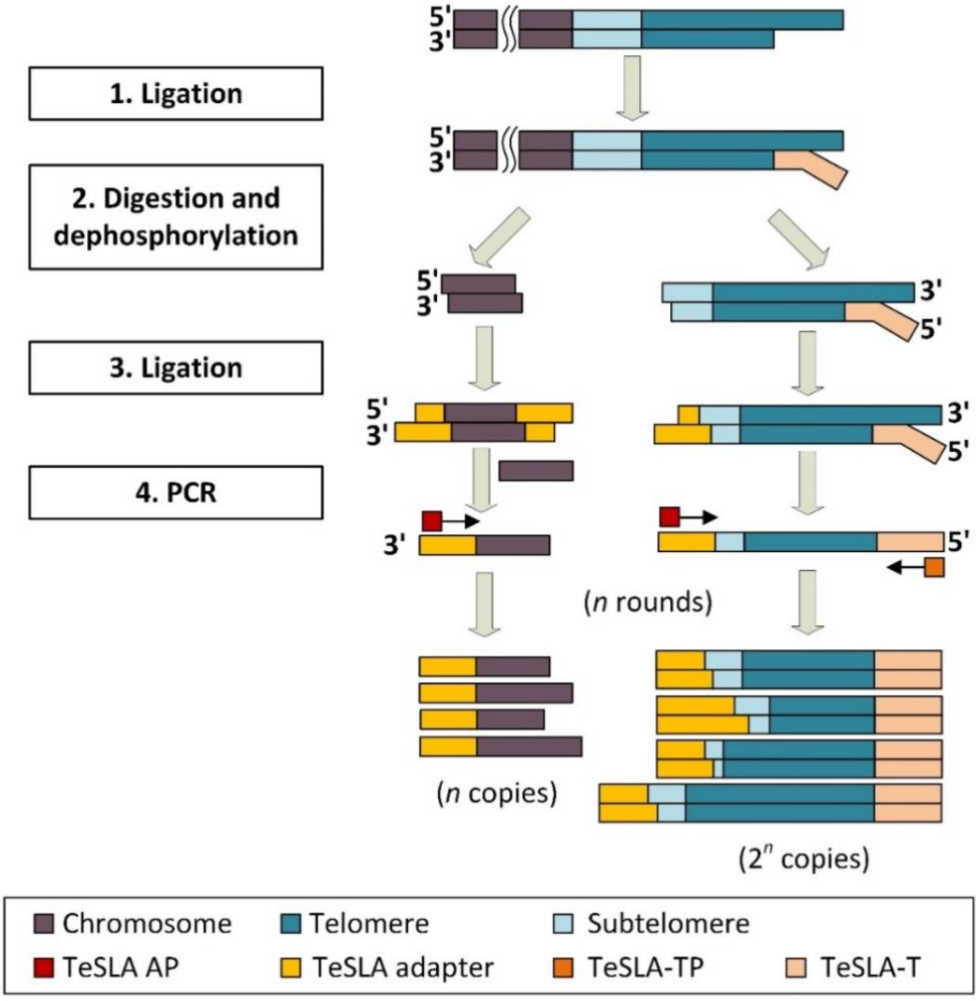

Figure 6: Illustration of the TeSLA assay. Image was created in MS Visio Professional 2013.

The entire sample (25µl plus 6x Orange-G loading dye) was loaded plus DNA Molecular weight marker II (0.12-23.1kbp, λDNA HinIII digested). Gel was run in 1xTAE buffer overnight at 30 V.

The next day the gel was soaked in depurination solution (0.25 M HDI) for 10 minutes, 2x15 minutes in denaturation solution (1.5 M NaCl; 0.5 M NaOH) and 2x15 minutes in neutralization solution (1 M Tris 7.4; 1.5 M NaCl). After the washing steps the gel was blotted onto a positively charged nylon transfer membrane (#RPN203B) overnight and crosslinked at 120 mJ/cm². The membrane was hydrated in miliQ H_20 and then equilibrated in 20xSSC buffer. In Figure 7 the set-up of the blot is illustrated.

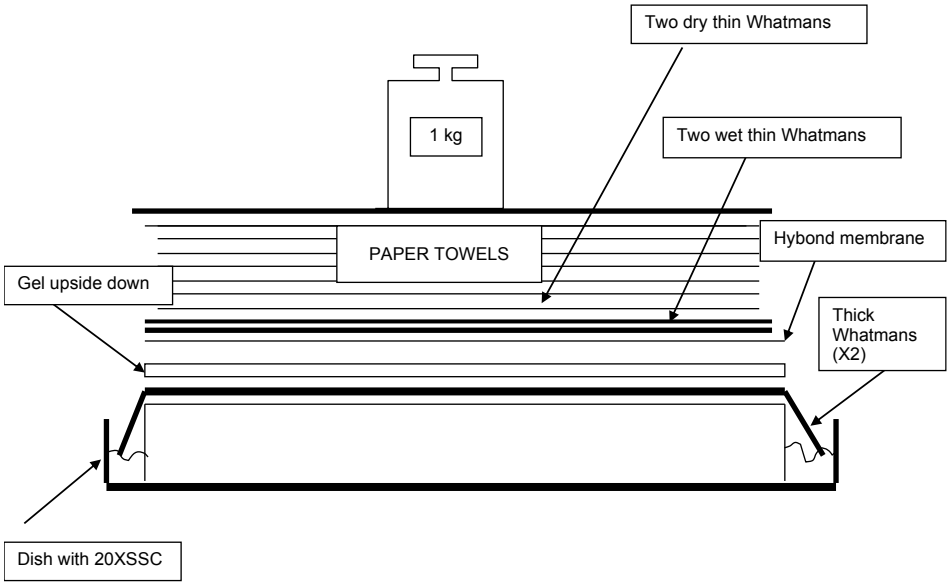

Figure 7: Illustration of southern blot. Image was created with MS Visio Professional 2013.

The membrane was subjected to prehybridization buffer (5x SSC, 0.1% sarkosyl, 0.04% SDS) for 1-2 hours at 65 °C and then hybridized with DIG-TelG probe (1.3 nM final concentration in prehybridization buffer) overnight at 65 °C. Furthermore, it was then washed 3x15 min at RT using wash buffer 1 (2xSSC; 0.1% SDS), 1x15 min with wash buffer 2 (2xSSC). Then membrane was incubated in blocking solution (Roche) at RT for 30 min to prehybridize. Anti-DIG-AP antibody (Roche) was added to fresh blocking solution and membrane was incubated at RT for 30 min. then developed using CDP-star ready to use (Roche) and visualized in a Syngene G-Box imager and analysed using TeSLA-Quant Software which automatically quantifies TeSLA Southern blot images and generates statistical outcomes as can be seen in Figure 8.

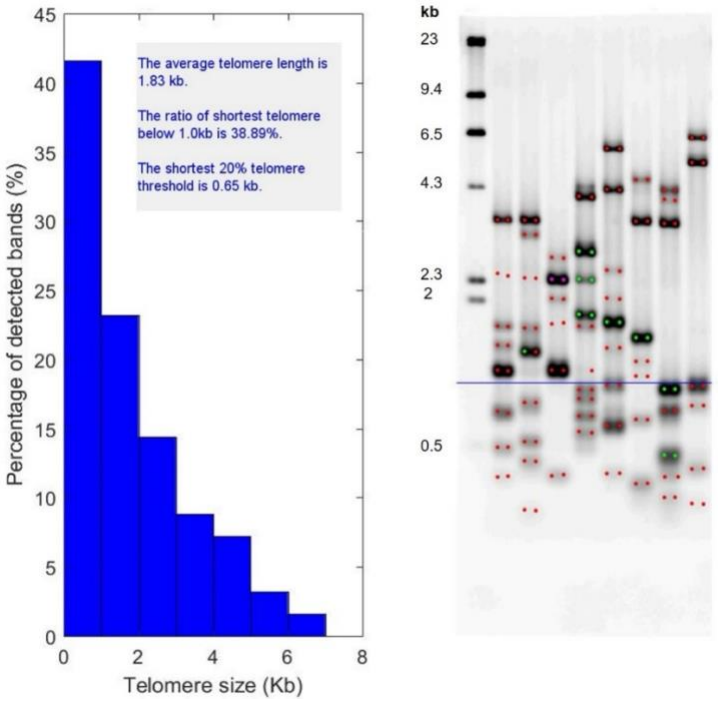

Figure 8: TeSLA assay on IMR90hpv^{E6E7} PD 65.4. The average TL is 1.83 kb with the ratio of shortest telomere below 1.0 kb being 38.89%. The shortest 20% telomere threshold is 0.65 kb. Image was created with TeSLA-Quant Software.

3.4 TERT mRNA expression

RNA was isolated using the PAXgene Blood RNA Kit (Quiagen) according to user's manual. Before starting the procedure, the PAXgene tube which was stored at -20 ºC was thawed at room temperature for two hours.

Purification initiates by subjecting the contents of the PAXgene Blood RNA Tube to centrifugation (10 minutes at 4000g), causing nucleic acids to form a pellet. This pellet undergoes a washing and resuspension process, followed by incubation in optimized buffers containing proteinase K. This enzymatic treatment facilitates protein digestion. Subsequently, a supplementary centrifugation utilizing the PAXgene Shredder spin column is performed to standardize the cell lysate and eliminate any lingering cellular debris. The resulting supernatant from this process was carefully transferred to a fresh microcentrifuge tube. To fine-tune the binding conditions, ethanol is introduced. The lysate is then introduced to a PAXgene RNA spin column. During a brief centrifugation step, RNA selectively adheres to the PAXgene silica membrane, while impurities

proceed through. To eliminate residual contaminants, a sequence of efficient washing steps was executed. Between the initial and subsequent washing steps, the membrane undergoes DNase I treatment to eradicate trace amounts of bound DNA. After the washing procedure, RNA is released using an elution buffer and then subjected to heat-induced denaturation.

Afterwards the mRNA got transcribed into complementary DNA with Quanti-Tect Reverse Transcription Kit (Qiagen).

After the RNA purification process, a brief incubation in genomic DNA (gDNA) Wipeout Buffer (2 minutes, 42º Celsius) was carried out to efficiently eliminate any contaminating genomic DNA. The resulting RNA sample was directly employed in reverse transcription. This involves utilizing a master mix composed of Quantiscript Reverse Transcriptase (RT), Quantiscript RT Buffer, and RT Primer Mix. The unique capabilities of Quantiscript Reverse Transcriptase enable transcription to occur at lower temperatures, accommodating complex secondary structures within the RNA molecule and thereby preserving its integrity. This entire reaction unfolds at a consistent temperature of 42°C (15 minutes), followed by inactivation at 95°C (3 minutes) (visualized in Figure 9). Samples of cDNA were then stored at -20º Celsius until further use.

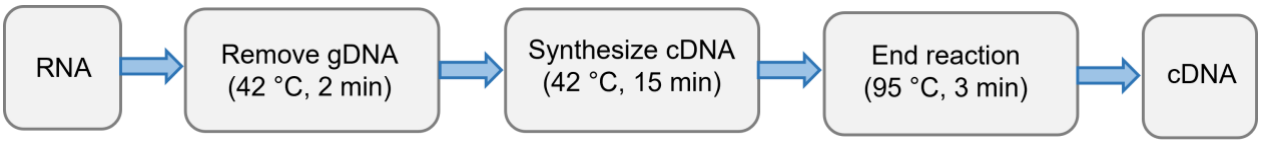

Figure 9: Overview of QuantiTect Reverse Transcription Procedure. Image created with Microsoft PowerPoint.

Finally, mRNA expression of TERT was analyzed with qPCR analysis using TaqMan probes (Life Technologies). The instrument used for the expression analysis was the The LightCycler® 480 System (Roche Diagnostics). Finally, the ΔΔCT method (with GAPDH as a reference gene), was used to determine the expression level. The following oligonucleotides were used:

GAPDH: 5’ -CACCTAGACAAGGATGCAGAG-3’

TERT: 5′-ATCGAGCAGAGCATCTCCATGAATG-3′

3.5 Telomerase activity

3.5.1 TRAP qPCR

To measure telomerase activity, I used the Telomeric-repeat-amplification-protocol (TRAP) in combination with quantitative real-time PCR. This assay was already established at the Institute and is based on the protocol of Skvortsov et al. [189].
The process of telomeric repeat amplification protocol can be segmented into three primary phases: primer elongation, amplification of DNA synthesized by telomerase, and lastly, its detection. During the elongation phase, telomeric repeats are attached to an oligonucleotide that mimics the telomere structure (TS) by the telomerase enzyme present in the cell extract. Subsequently, DNA synthesized by telomerase is amplified through PCR using specialized primers (ACX) (visualized in
Figure 10).

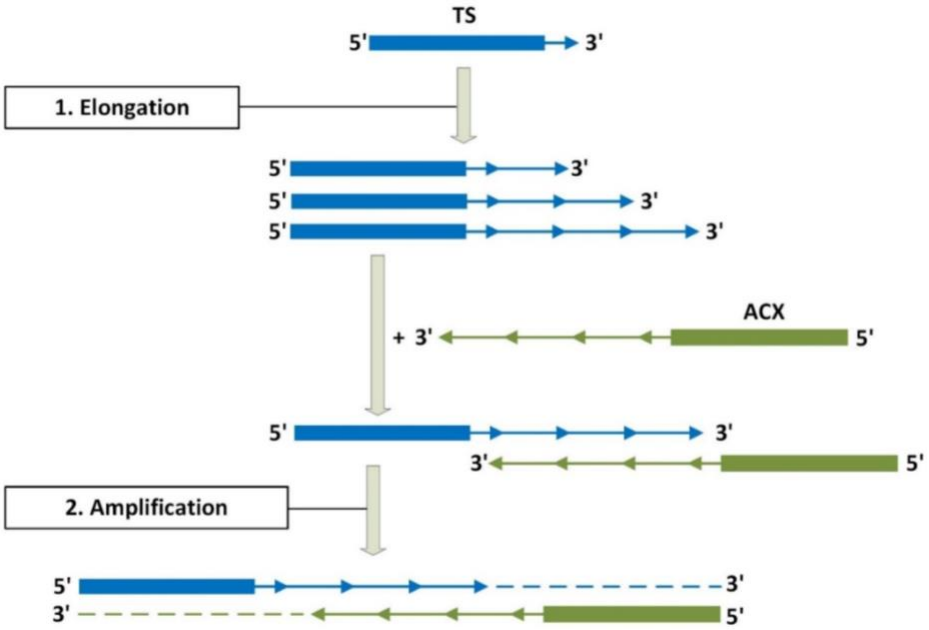

Figure 10: Illustration of TRAP. The first step of the assay is elongation of telomeric repeats (1) which is followed by the amplification of the synthesized DNA (2). Image was created with MS Visio Professional 2013.

Preparation of protein extract for telomerase expression measurement

Isolated T-cells were pelleted at 2000 x g for five minutes and supernatant was discarded. Cells were then resuspended in 20 µl 1x CHAPS (Alfa Aeser #J60812) + SUPERase (Thermo Fisher AM2694), (100Units/ml), vortexed briefly and incubated on ice for 30 minutes. Immediately after, cells were centrifuged at 16 000 x g for 20 minutes at 4° C. Supernatant was then used for measuring telomerase activity. The rest was stored at -80 °C until further use.

In more detail, pool protein extracts from healthy donor cells for the standard curve was diluted with 1x Chaps buffer as follows:

1) 1:5	8 µl Plasma-pool	+	32 µl Chaps
2) 1:10	20 µl Standard 1	+	20 µl Chaps
3) 1:20	20 µl Standard 2	+	20 µl Chaps
4) 1:40	20 µl Standard 3	+	20 µl Chaps
5) 1:80	20 µl Standard 4	+	20 µl Chaps
6) 1:160	20 µl Standard 5	+	20 µl Chaps
7) 1:320	20 µl Standard 6	+	20 µl Chaps
8) 1:640	20 µl Standard 7	+	20 µl Chaps
9) 1:1280	20 µl Standard 8	+	20 µl Chaps
10) Only Chaps butter – negative control			

Standard 3 to 10 were used since we were expecting low expression values in T-cells.

Each reaction contained 10 µl Universal Mastermix (UMM 2x), 5.6 µl ddH_20, 2 µl Sybergreen (10x), 0.2 µl TS (100 µm), 0.2 µl ACX (100 µm), 2 µl Protein extract.

The thermal cycling profile was 30 min at 25 °C, 10 min at 95 °C followed by 40 cycles of 15 sec at 95 °C and 30 sec at 55 °C and 60 sec at 72 °C including fluorescence data collection.

All measurements were done in duplicates. Protein extracts were not diluted due to the expected low expression of telomerase in T-cells.

3.5.2 Droplet digital telomere repeat amplification protocol (ddTRAP)

The droplet digital telomere repeat amplification protocol (ddTRAP) was developed by Dr. Andrew T. Ludlow and the method described is based on his protocol [190].
Since this method is supposed to have increased sensitivity and repeatability compared to the basic TRAP assay and we were dealing with aliquots of 10^5 cells with an expected low expression of telomerase, we decided to implement this assay.
I had the opportunity to visit the lab of Dr. Steven Smith at the Konrad-Lorenz-Institute in Vienna where the method was well established. I took samples (T cells, 10^5 aliquots) with me to analyze them on site in their lab.
First, cell aliquots were lysed by adding 40µl NP40 lysis buffer (10 mM Tris-HCl, pH 8.0; 1 mM MgCl2; 1 mM EDTA; 1% (vol/vol) NP-40; 25 mM sodium deoxycholate; 10% (vol/vol) glycerol; 150 mM NaCl; 5 mM ß-mercaptoethanol; 0.1 mM AEBSF (4-(2-Aminoethyl)benzenesulfonyl fluoride hydrochloride)) to the cells and incubated on ice for 40 minutes. Extension reaction was prepared on ice as follows: 5 µl of 10xTRAP buffer (200 mM Tris-HCl, pH 8.3; 15 mM MgCl2; 630 mM KCl; 0.5% Tween 20; 10 mM EGTA) was mixed with 36.6 µl DEPC-treated (Diethylpyrocarbonate) dH2O (Ambion), 0.4 µl of 50 mg/mL BSA (Sigma), 1 µl TS Primer (10 µM), 5 µl of 2.5 mM dNTPs and 1 µl cell lysate. The thermal cycling profile was 40 min at 25 °C followed by 5 min at 95 °C and sample was then held on 12 °C. As a positive control HeLA cells (New England Bio Labs) were used. The ddPCR was set up at room temperature as follows: 10 µl of 2x Evagreen ddPCR Super Mix v2.0 (Bio-Rad) were mixed with 0.1 µl of 10 µM TS primer, 0.1 µl of 10 µM ACX primer, 2 µl of extension product from previous reaction and 7.8 µl DEPC-treated dH_2O. For droplet generation whole sample (20 µl) was loaded onto cartridge of the droplet generator (DG8 Bio-Rad 186–3008). Then 60 µl of droplet generation oil (Bio-Rad 186–3005) was added to the oil chamber. Then the droplet cartridge gasket (Bio-Rad 186–3009) was placed on the cartridge and then put into the droplet generator. After droplets were generated, samples were gently transferred to new PCR tubes (96 well plate), sealed with foil (Bio-Rad) using the Bio-Rad plate sealer (PX1 PCR plate sealer) and placed in the thermocycler (Bio-Rad T100). The cycling profile was 95 °C for 5 min (activation of hot-start polymerase), followed by 40 cycles of 95 °C for 30 sec, 54 °C for 30 sec, 72 °C for 30 sec. Then the sample was subjected

to 4 °C for 5 min, 90 °C for 5 min (to stabilize the droplets) and then held on 12 °C. Ramp rate was set for 2.5 °C/sec in between all steps to allow sample to evenly reach required temperature. Plate was then transferred into the droplet reader (Bio-Rad QX150/200). Program for absolute quantification and dye type FAM/Vic (for ddTRAP) was chosen.

Regarding data analysis, at least 10.000 droplets should be generated for reliable results. The threshold should be set above 2000 fluorescent units above the negative droplet line. Background noise has to be subtracted from samples using the negative control. After background correction for the value of molecules per microliter (given by the Quantasoftware) one has to multiply this value by 20 (PCR volume) and then divided by 50 (number of cell equivalents used for extension reaction). See Figure 11 for a simple overview of the workflow.

Following primers were used in this assay:

TS Primer:	5'-AATCCGTCGAGCAGAGTT-3'
ACX Primer:	5'-GCGCGGCTTACCCTTACCCTTACCCTAACC-3'

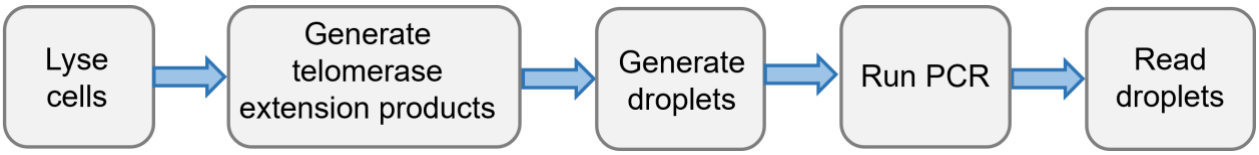

Figure 11: ddTRAP workflow. First, cells were lysed, then telomerase extension products were generated, followed by generation of droplets, the PCR and the readout of the droplets. Image created with Microsoft PowerPoint.

3.6 Single nucleotide polymorphism analysis

According to previous literature the KIMCL lab established the method with the following SNPs (Table 1) which I also used in the TILUC study [191, 192, 193]. The method and tables are based on and can be found in more detail in the bachelor thesis of Viktoria Topler “Leukozyten-Telomerlänge als prognostischer Marker für das Prostatakarzinom” [194].

Table 1: SNP identity, location on the chromosome, name of gene, nucleotide exchange and allele for elongation.

No	SNP Identity (ID)	Chromosome	Location	Gene	Nucleotide exchange	Allele for elongation
1	rs11125529	2	54475866	ACYP2	C>A	A
2	rs6772228	3	58376019	PXK	T>A	T
3	rs12696304	3	169492101	TERC	C>G	C
4	rs10936601	3	169528449	TERC	C>T	C
5	rs7675998	4	164007820	NAF1	A>G	G
6	rs2736100	5	1286516	TERT	C>A	C
7	rs9420907	10	105676465	OBFC1	C>A	C
8	rs4387287	10	105677897	OBFC1	A>C	A
9	rs3027234	17	8136092	CTC1	C>T	C
10	rs8105767	19	22215441	ZNF208	A>G	G
11	rs412658	19	22359440	ZNF676	C>T	T
12	rs6028466	20	38129002	DHX35	G>A	A
13	rs755017	20	62421622	ZBTB46	A>G	G

For each patient, 13 SNPs were determined by PCR using TaqMan probes. The SNPs were determined in separate assays and thus a separate assay mix was required for each SNP examined. The assay mixes were manufactured by Thermo Fisher. They each consist of two different probes, a forward primer and a reverse primer. More detailed information on the assay IDs and the analyzed gene sequences can be obtained from Table 2. The allele to which the VIC-labeled probe binds is listed first in the parenthesis, and the allele to which the FAM-labeled probe binds is listed second.

Table 2: Assay ID´s and DNA sequences (from Thermo Fisher Scientific)

No	Assay ID	Context Sequence [VIC/FAM]
1	C___1166977_10	GAAGAAAAGAAGATGACTAAAACAT[A/C]ATCTTGGCCCTTGAA GAACTTAAAA
2	C__31685604_10	AATATTTTATATAACCATGGCACAT[A/T]TATCAAAACTAGAAGT GAATATTAG
3	C____407063_10	GCGATCTTAGATCACCTTGAGTAAA[C/G]TGAGGCTTACTGAAG CTGAGCTACT
4	C_____29091_30	GAATAGGTCTTATTATCAAGTAAGT[C/T]TGAGAAGTACTAAAAT AAACAAAAC
5	C__11248528_10	TTGTTAAATAAATAAATAAATAAAT[A/G]ACTGATGTGTAAGTGC ATTCTTAAA
6	C___1844009_10	GAAAAGCAGGGCGGGGGCAAAGCTA[A/C]AGAAACACTCAACA CGGAAAACAAT
7	C___2818534_10	CTATTTGTGAATTATTACACAGCTA[A/C]GTGAATTATTTAAATC CACCCCAAA
8	C___2818531_10	GCCGCCTGCAGCTCCAGGAGCCCTG[A/C]GACCTGGCCCTTCC GGCGCTCGGAG
9	C__15770320_10	GTTCTCTGCCTGCCATACAAGTCTC[C/T]CAGAAGTTGTTGATT GACATGTGTC
10	C___8169004_30	CAGAGAGTTACATCACCTGGGTATC[A/G]GACTCAGCTACATGT CAAAATGGCC
11	C__11463190_10	TTTTGTTTCCTAGTAAATTAGACAT[C/T]TTATTAAATGCTTTGTG GTTTCAAT
12	C__30071974_10	CTATAAAAGAGTCAAAAGCAGATAC[A/G]TGTGTCAAGGATGAA CAGAAAGGCT
13	C____993807_20	CCAGCCACGGGGAGATGCTCCTCCC[A/G]GCCATCACGGCCG AGATGAGAGCTT

Each reaction contained 5 µl of 2x PerfeCTa® qPCR SuperMix (Quantabio, $MgCl_2$, dNTPs, AccuStart Taq DNA-Polymerase), 0,25 µl Assay Mix (40x), 2,75 µl ddH_20 and 2 µl sample DNA. The thermal cycling profile was 1 min at 95 °C followed by 40 cycles of 10 sec at 95 °C, 30 sec at 60 °C. The reaction was then kept at 8° C. Afterwards, fluorescent signals (VIC and FAM) were detected using the Flex Station 3 Microplate Reader (Molecular Devices).

The evaluation of the data was done by their representation in a scatterplot, which allowed an assignment to the genotype. Assuming a base exchange from A to G due to a SNP, a patient can either be homozygous for allele A, homozygous for allele G or heterozygous. Since the probes used are designed to be allele specific, this is also

reflected in the fluorescence signals detected. Assuming the probe for allele A is labeled with the fluorescent dye VIC and the probe for allele G is labeled with the fluorescent dye FAM, a lot of fluorescent signal from VIC will be detected in the sample of a patient who is homozygous for allele A. The fluorescence signal from VIC will be very high. In the sample from a patient who is heterozygous, fluorescent signal from both VIC and FAM will be detected. However, these will not be as strong as in patients with a homozygous genotype. When the measured fluorescence signals are plotted on a scatterplot, three clusters are obtained corresponding to the three possible genotypes. Negative controls were included in each analysis. These should not fall into any of the three clusters. If the negative controls were not assignable to any cluster, the results could be analyzed. Genotype-associated telomere lengthening was taken from previously published genome wide association studies (195,196,197,198). From these, an estimate of telomere elongation in kbp per presence of the associated allele, referred hereafter to as beta, is obtained. The values for beta are illustrated in Table 3.

Table 3: Genetic variants associated with TL as reported in prior genome wide association studies.

No	SNP ID	Beta in kbp
1	rs11125529	0,065
2	rs6772228	0,041
3	rs12696304	0,100
4	rs10936601	0,087
5	rs7675998	0,048
6	rs2736100	0,085
7	rs9420907	0,142
8	rs4387287	0,120
9	rs3027234	0,103
10	rs8105767	0,064
11	rs412658	0,086
12	rs6028466	0,058
13	rs755017	0,019

Beta was multiplied by the number of elongating alleles possessed by the patient. For a homozygous genotype (for an allele associated with telomere elongation), beta was multiplied with a factor of 2. For a heterozygous genotype (for an allele associated with telomere elongation), beta was multiplied with a factor of 1. If the allele was not present

at all, beta was multiplied by a factor of 0. This was done for all 13 SNPs analyzed. The genetic telomere score is the cumulative result of all 13 SNPs.

3.7 Statistical analysis

IBM SPSS statistics 28 software (IBM) was used for statistical analyses. Overall survival (OS) was defined as the time between the date of diagnosis and the date of death from any cause, estimated using the Kaplan-Meier method and compared by the logrank test. The Cox proportional hazards regression model was used to estimate hazard ratio (HR) and to determine 95% confidence intervals (CI). The criterion for statistical significance was $p < 0.05$. Correlation analysis was done using linear regression analysis.

4 Results

4.1 Telomere length (TeSLA assay, qPCR)

I established the TeSLA assay at the Salk Institute for Biological Studies and before having the TILUC samples as planned, shipped from the Clinical Institute of Medical and Chemical Laboratory Diagnostics (KIMCL) lab in Graz I tried using as little as 10^5 cells to make sure the assay will work on the probes. However, the amount of DNA in the T cell aliquots of 10^5 cells isolated was lower than expected. See Table 4.

Table 4: Values for DNA isolated and measured in T-cells at the KIMCL lab.

Sample	ng/µl	ng/µl	mean
1a	0.239	0,144	0.192
2a	0.020	0,268	0.144

Although I was not able to detect any DNA when samples arrived at the Salk Institute, I anyway tried to analyze the samples with the TeSLA method with the highest sample input possible for the assay which was 17 µl in the first PCR reaction. Unfortunately, the amount of DNA in the T cell samples were too low since no bands were detected (See Figure 12). I also tried using various input amounts plus varying input of sample in the final PCR before running the gel but with no success. The recommended input for the assay is 50 ng of DNA compared to 3.3 ng (0.192 ng times 17 µl) I had for sample 1a.

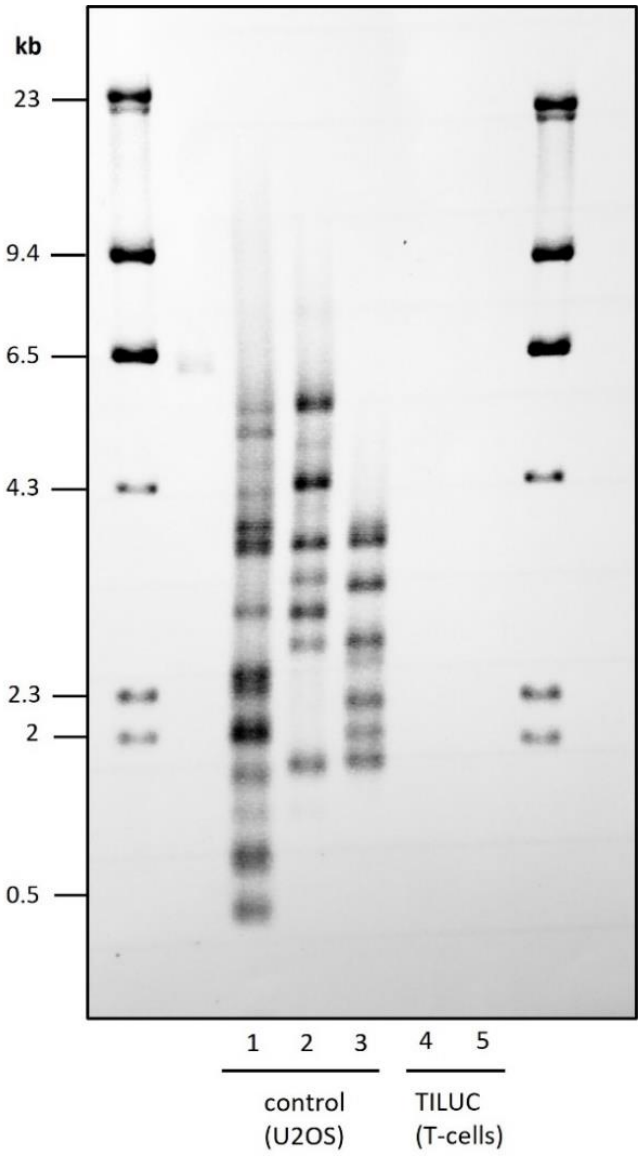

Figure 12: TeSLA assay on positive control (U2OS) and TILUC samples. Number 4: T cell sample 1a, Number 5: T cell sample 2a.

We then decided to analyze telomere length with the qPCR method which worked out. See Table 5 for values of average telomere length results, and Figure 13 for a representation of the range of relative TL that was measured. Before therapy initiation, TL in 34 samples could be determined. At the first follow-up, second follow-up, third follow-up and fourth follow-up, it was 26 samples, 18 samples, 12 samples and 6 samples that were measured, respectively.

Table 5: relative T/S values for telomere length using qPCR method.

	T/S at various timepoints				
PATIENT NO	a	b	c	d	e
1	0.734	0.599	0.522	0.571	0.701
2	0.505	0.725	0.620	0.545	1.020
3	0.546	0.601	0.586	0.622	0.416
4	0.571	0.694	0.672		
5	0.543	0.707	0.389	0.850	0.335
6	0.588	0.641			
7	0.658				
8	0.632	0.785	0.510	0.631	0.254
9	0.673				
10	0.721	0.719			
11	0.679				
12	0.643	0.460	0.601	0.647	
13	0.727	0.706	0.719		
14	0.494	0.600	0.875		
15		0.646			
16	0.401	0.396			
17	0.681				
18	0.433				
19	0.500				
20	0.576	0.531	0.668	0.281	
21	0.490	0.460	0.535	0.395	
22	0.634	0.595	0.607	0.598	0.279
23					
24	0.613	0.587			
25	0.547				
26	0.615				
27	0.867	0.743			
28	0.782	0.788	0.433	0.580	
29	1.464	1.048	1.653	1.144	
30	0.604	0.534	0.387		
31	0.440	0.395	0.301		
32	0.592				
33	0.555	0.527			
34	0.486	0.435	0.486	0.346	
35	0.535	0.398			
36	0.405	0.384	0.448		

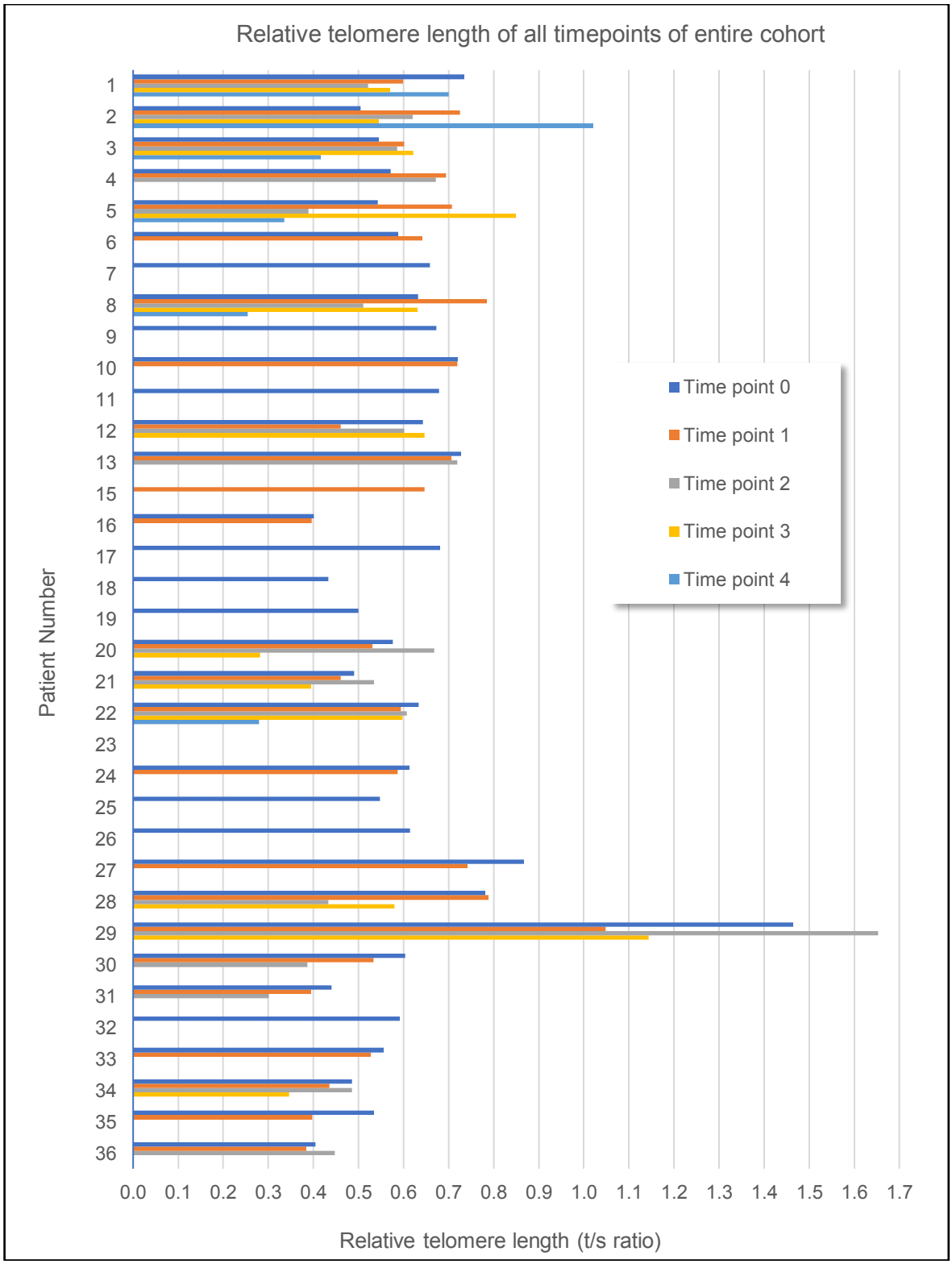

Figure 13: Relative telomere length (t/s ratio) for all patients and all time points measured using qPCR.

A correlation analysis (Figure 14) showed that relative TL at baseline is significantly correlated with relative TL at follow-up of the same patient. In Figure 15 one can see that according to our data there is no statistically significant correlation between relative TL and age in females or males.

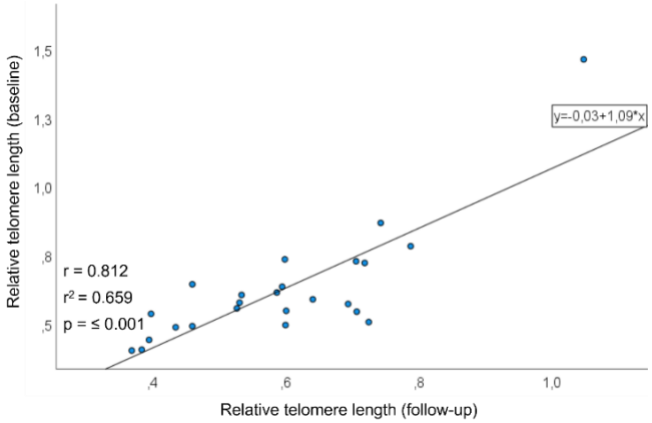

Figure 14: Scatterplot showing the correlation between relative TL at baseline and relative TL at first follow-up considering all patients.

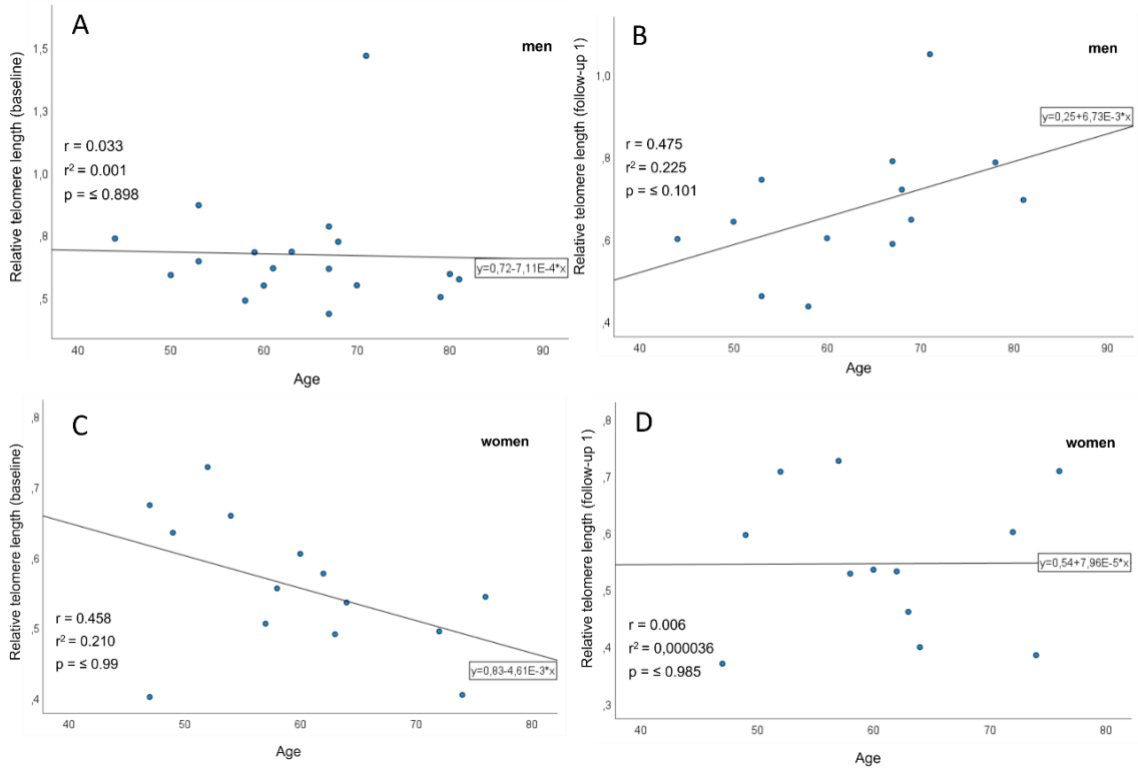

Figure 15: Scatterplot showing the correlation between relative TL (y-axis) and age (x-axis) in males and females. (A) Correlation of relative TL at baseline and age in men. (B) Correlation of relative TL at follow-up 1 and age in men. (C) Correlation of relative TL at baseline and age in women. (D) Correlation of relative TL at follow-up 1 and age in women.

4.2 Single nucleotide polymorphism analysis and relative telomere length

To determine whether there is a correlation between the relative telomere length and the SNP score, I did a Pearson correlation analysis. In Figure 16, a scatterplot including linear regression analysis can be seen for the complete study cohort. No significant relationship was found between relative TL before initiation of therapy (baseline, Figure 16A) or relative TL after initiation of therapy (follow-up, Figure 16B) and the SNP score.

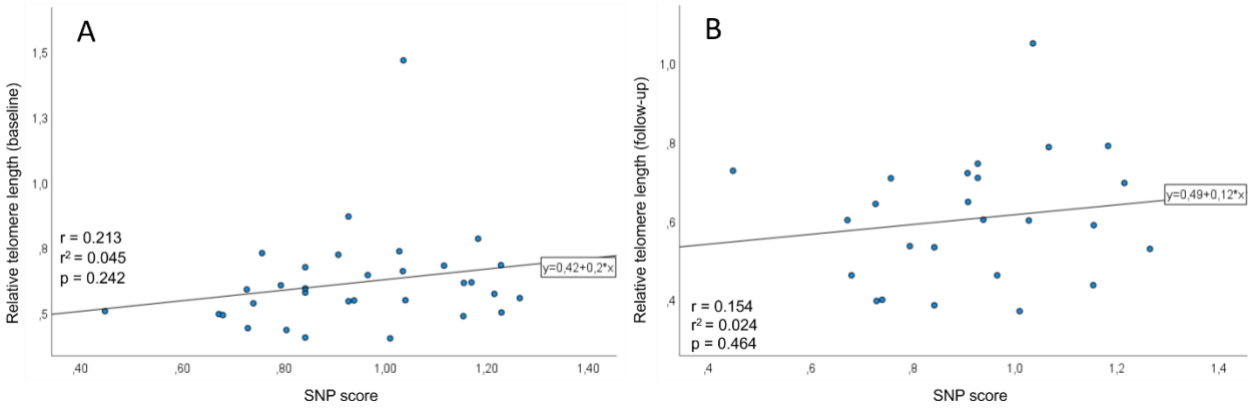

Figure 16: Correlation analysis between relative TL and SNP score considering all patients. (A) In the first graphic TL before initiation of therapy (baseline) is considered (x-axis). On the y-axis the SNP score is displayed. (B) In the second graphic TL after initiation of therapy (follow-up 1) is considered.

4.3 Telomerase activity (ddTRAP and qPCR)

Although having been trained by experts using the ddTRAP assay and successfully establishing it in the KIMCL lab, it seems that there was not enough telomerase activity in T cells of the TILUC study for it to be detected. A representative image of the ddTRAP assay is depicted in Figure 17. Various troubleshooting was done to make sure it was not a technical problem. We tried not only different amounts of input of cell-lysates but also using different types of lysis buffer (NP-40 as described in the original protocol by Ludlow et al. and Chaps lysis buffer (100mM Tris-HCl pH 7.4, 220mM NaCl, 10mM EDTA, 2% Chaps)). We then decided to try the qPCR approach anyway, if anything just to verify that there is definitely no telomerase activity in these samples. Indeed, we couldn't detect any activity with TRAP qPCR either.

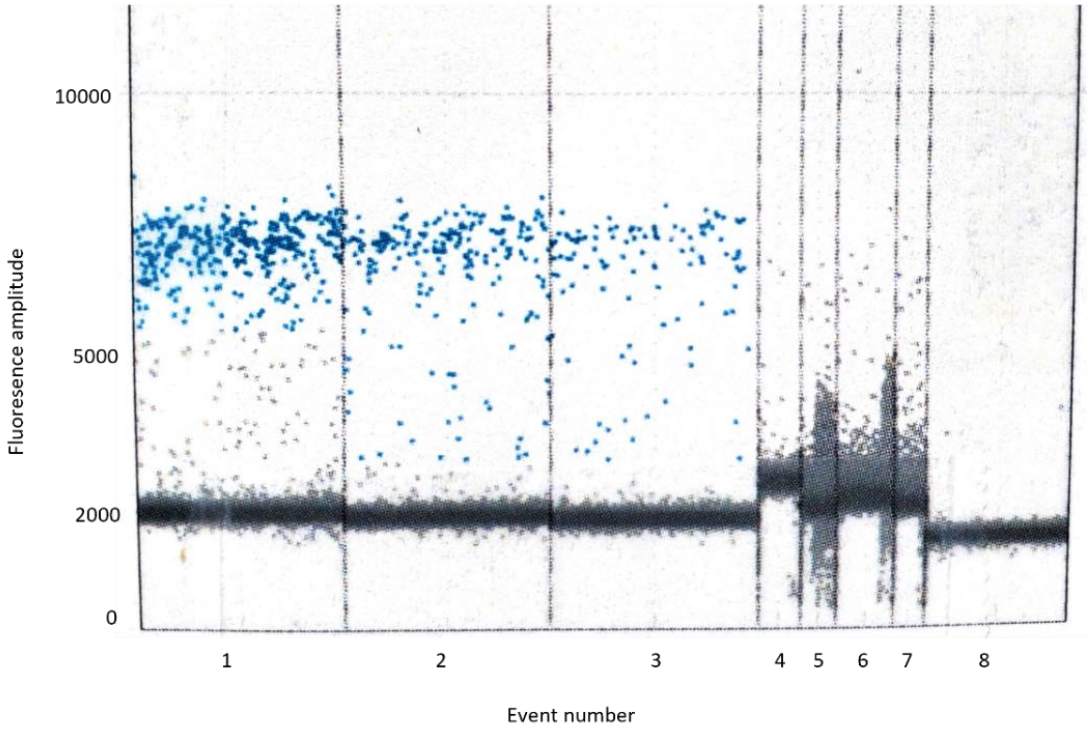

Figure 17: Representative image of ddTRAP results on A549 cell line and PBMCs. Sample 1: 250.000 cells (20.980 droplets), Sample 2: 1:2 dilution of sample 1 (20.726 droplets), Sample 3: 1:4 dilution of sample 2 (21.145 droplets), 4-7: 100.000 cells (PBMCs) in each sample, 8: neg control. The amplitude is the detected fluorescence for every droplet in the assay.

4.4 Patients Characteristics

We decided to analyze the complete study group and a subgroup of patients that all got Pembrolizumab as ICB regimen to get a more homogeneous cohort.

Complete study group

Baseline relative telomere length (TL0) was successfully measured in 34 (97 %) patients and follow-up after initiation of therapy (TL1) in 26 (74 %). For the measurements that are missing, either not enough DNA was available, or the patient deceased during follow-up before another blood sample could be taken. Characteristics of patients are shown in Table 6. All subjects were diagnosed with non-small cell lung cancer. Follow-up time was 24 months and 25 (71 %) patients died during that time. The study cohort consisted of 20 men (57 %) and 15 women (43 %). 24 patients

received Pembrolizumab, 5 patients Nivolumab, 3 patients Atezolizumab and 3 patients Durvalamab as ICB regimen for the first time. In 20 patients PDL-1 expression was higher than 50 % and in 15 patients the expression was lower than 50 %.

Table 6: Patients characteristics of complete study cohort. No, number; NSCLC, non-small cell lung cancer; ICI, immune checkpoint inhibitor.

Parameter	Study Cohort
Cancer patients, no.	35
Age at diagnosis (median and range)	63 (44-81)
Gender [%]	
male	57
female	43
PDL-1 Expression, no.	
<50%	15
≥50%	20
ICB regimen [%]	
Pemprolizumab	24
Nivolumab	5
Others (e.g Atezolumab, Durvalamab)	6
Histology	
Adenocarcinoma	25
Squamous cell carcinoma	10
Deceased during follow-up [%]	
Yes	71
No	29

Study group receiving Pembrolizumab as ICB regimen

Baseline relative telomere length (TL0) was successfully measured in 22 (92 %) patients and follow-up after initiation of therapy (TL1) in 18 (75 %). For the measurements that are missing, either not enough DNA was available, or the patient deceased during follow-up before another blood sample could be taken. Characteristics of patients are shown in Table 7. All subjects were diagnosed with non-small cell lung cancer. Follow-up time was 24 months and 16 (67 %) patients died during that time. The study cohort consisted of 15 men (62 %) and 9 women (38 %), and everyone received Pembrolizumab as ICB regimen for the first time. In 16 patients PDL-1

expression was higher than 50 % and in 8 patients the expression was lower than 50 %.

Table 7: Patients characteristics of cohort receiving Pembrolizumab. No, number; NSCLC, non-small cell lung cancer; ICB, immune checkpoint inhibitor.

Parameter	Study Cohort
Cancer patients, no.	24
Age at diagnosis (median and range)	63 (44-81)
Gender [%]	
male	62
female	38
PDL-1 Expression, no.	
<50%	8
≥50%	16
ICB regimen [%]	
Pemprolizumab	100
Histology, no.	
Adenocarcinoma	17
Squamous cell carcinoma	7
Deceased during follow-up [%]	
Yes	67
No	33

4.5 Kaplan-Meier survival and Cox-regression analysis

4.5.1 Telomere length in T cells and SNP score

Complete study group (Kaplan-Meier survival curve)

Due to our relatively small study cohort, we use the median as cut-off value in the Kaplan-Meier analysis, therefore two groups of roughly the same size are compared. When using the median TL1 (0.599) as a cut-off value in the Kaplan-Meier analysis, we observed a (non-significant) trend (p= 0.088) of an impaired OS in patients with a TL shorter than the cut-off value (Figure 18B). The median overall survival in these patients was 12 months. The same trend could not be seen in telomere length measurement at baseline before initiation of treatment, where the median survival time was estimated to be nine and 12 months for patients with short or long telomeres respectively (Figure

18A). In the follow-up measurements two (p= 0.333) and three (p= 0.377), no significant difference in survival was found. Furthermore, no significant difference can be seen in survival when analyzing men (p= 0.661) and women (p= 0.825) separately (See Figure 19).

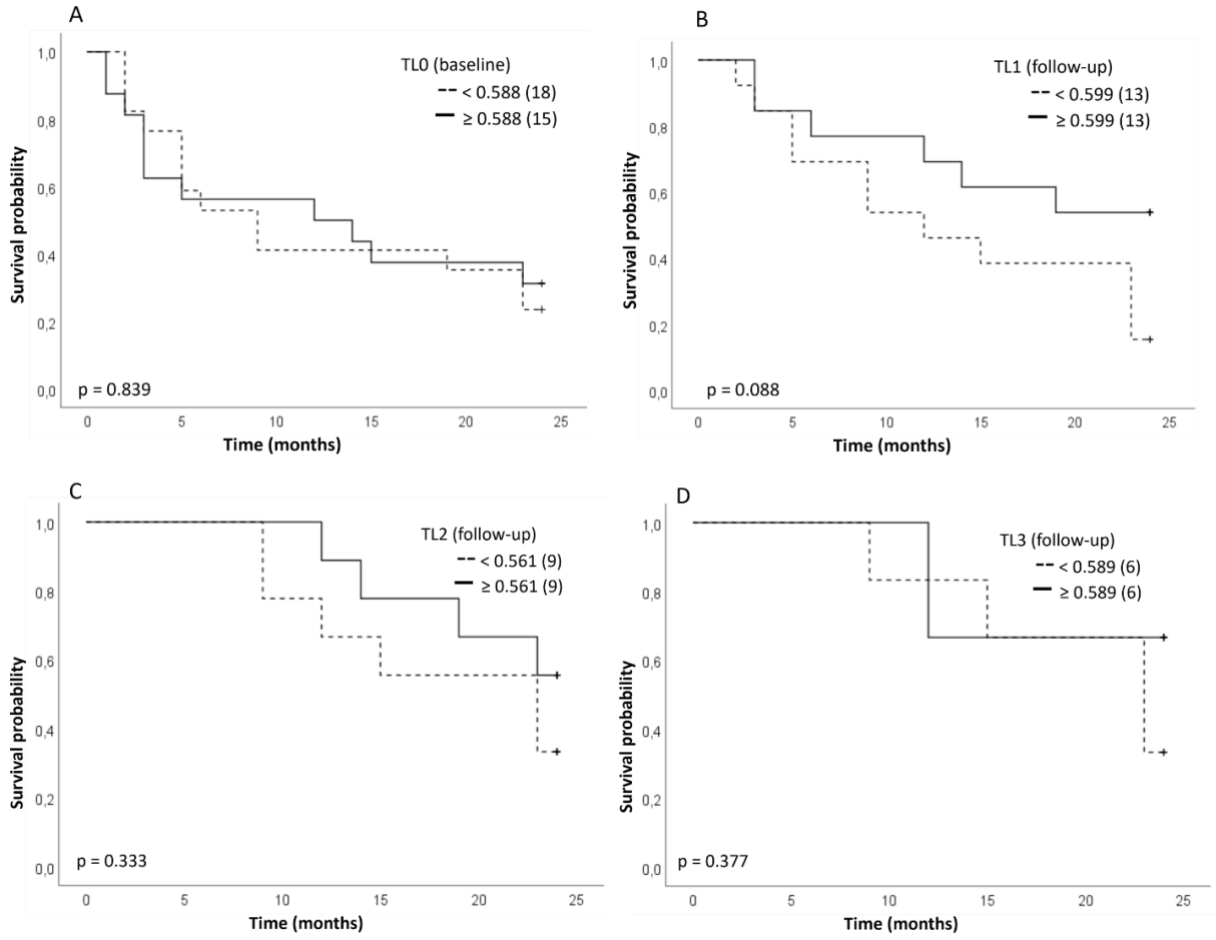

Figure 18: Kaplan-Meier curves of survival considering TL for all patients. Probability of survival is depicted in relation to the course of time. Subjects were divided into two groups based on the median of TL. **(A)** In the first graphic, TL at baseline is considered, a relative TL of 0.588 (median) was taken for the cut-off value, resulting in 18 subjects in the group of shorter telomeres and 15 subjects in the group of longer telomeres. **(B)** In the second graphic, the first measurement after therapy initiation is considered, a relative TL of 0.599 (median) was taken for the cut-off value, resulting in 13 subjects in the group of shorter telomeres and 13 subjects in the group of longer telomeres. **(C)** The second follow-up measurement after therapy initiation is considered, a relative TL of 0.561 (median) was taken for the cut-off value, resulting in 9 subjects in each group. **(D)** The third follow-up measurement after therapy initiation is considered, a relative TL of 0.589 (median) was taken for the cut-off value, resulting in 6 subjects in each group.

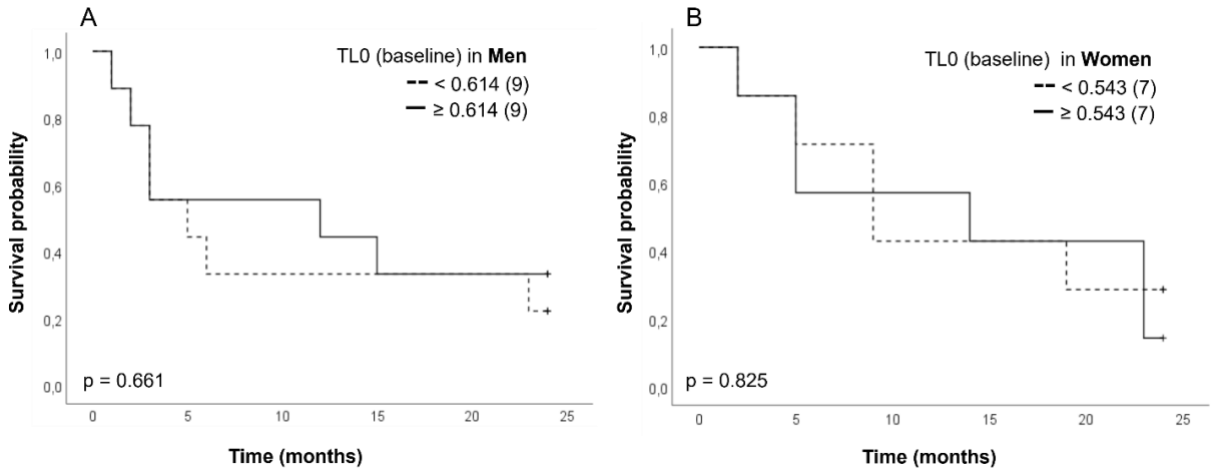

Figure 19: Kaplan-Meier curves of survival considering TL at baseline considering all patients for women and men separately. Probability of survival is depicted in relation to the course of time. Subjects were divided into two groups based on the median of TL. **(A)** In the first graphic, the TL at baseline for men is considered, a relative TL of 0.614 (median) was taken for the cut-off value, resulting in 9 subjects in each group. **(B)** In the second graphic, the TL at baseline for women is considered, a relative TL of 0.543 (median) was taken for the cut-off value, resulting in 8 subjects in each group.

Study group receiving Pembrolizumab as ICB regimen (Kaplan-Meier survival curve)

Due to our relatively small study cohort, we use the median as cut-off value in the Kaplan-Meier analysis, therefore two groups of roughly the same size are compared. When using the median TL1 (0.597) as a cut-off value in the Kaplan-Meier analysis, we observed a (non-significant) trend (p= 0.065) of an impaired OS in patients with a TL shorter than the cut-off value (Figure 20B). The median overall survival in these patients was nine months. Since only two patients survived, no value for median overall survival time was given by the statistical software SPSS. The same trend could not be seen in telomere length measurement at baseline before initiation of treatment, where the median survival time was estimated to be six and 14 months for patients with short or long telomeres respectively (Figure 20A). Of note, correlation analysis between TL0 and TL1 turned out to be statistically significant (p = 0.001).

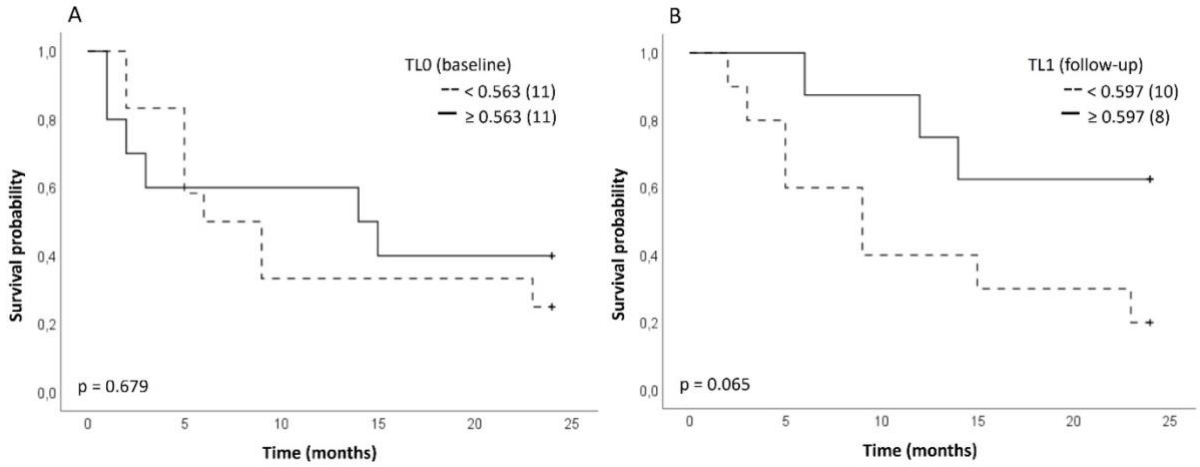

Figure 20: Kaplan-Meier curves of survival considering TL for patients receiving Pembrolizumab as ICB regimen only. Probability of survival is depicted in relation to the course of time. Subjects were divided into two groups based on the median of TL. **(A)** In the first graphic, the TL at baseline (TL0) is considered, a relative telomere length of 0.563 (median) was taken for the cut-off value, resulting in 11 subjects in each group. **(B)** In the second graphic, the second measurement after therapy start is considered, a relative TL of 0.597 (median) was taken for the cut-off value, resulting in 10 subjects in the group of shorter telomeres and 8 subjects in the group of longer telomeres.

Complete study group (Cox regression analysis)

The univariate Cox regression analyses for TL1 (median) did show a similar trend like in the Kaplan-Meier curve (HR: 0.441, 95% CI: (0.163-1.197), p = 0.108) (Table 8). However, when including other parameters of prognostic relevance in univariate analysis into a multivariate Cox-regression analysis (Sex, age at diagnosis and PDL-1 expression), the prognostic role of TL1 was found to be in part dependent of these confounders (HR: 0.519, 95% CI: (0.149-1.805), p = 0.302). A reasonable explanation for this might also be our small study cohort. Although patients with Adenocarcinoma seemed to have a 120% higher risk of mortality compared to people with squamous cell carcinoma, the hazard ratio for TL1 changed only from 0.441 to 0.519 in univariate compared to multivariate Cox regression analysis, respectively (Table 8). Furthermore, although not statistically significant, ΔTL (the change of TL0 to TL1) seemed to have no prognostic relevance according to our data (HR: 1.000, 95% CI: 1.000-1.001, p = 0.773). The SNP-score itself does not seem to have a statistically significant effect on survival on its own but in multivariate Cox regression when including TL1 (follow-up) the p-value changes from p=0.108 to p=0.058 and the hazard ratio changing from 0.441 (0.163-1.197) to 0.380 (0.140-1.034).

Table 8: Uni- and multivariate Cox-regression analysis of telomere length in T-cells for the prediction of overall survival including all patients.

Parameter	Univariate Cox-regression		Multivariate Cox-regression	
	p-value	Hazard-Ratio (95%CI)	p-value	Hazard-Ratio (95%CI)
TL0 (baseline)	0.763	1.132 (0.506-2.529)	0.861	0.924 (0.383-2.232)
TL1 (follow-up)	0.108	0.441 (0.163-1.197)	0.302	0.519 (0.149-1.805)
TL2 (follow-up)	0.362	0.555 (0.156-1.969)	0.393	0.484 (0.091-2.559)
TL3 (follow-up)	0.407	0.487 (0.089-2.667)	0.124	0.129 (0.009-1.760)
Age	0.479	0.985 (0.964-1.027)		
Sex	0.759	0.884 (0.401-1.949)		
PDL-1 Expression	0.570	0.796 (0.363-1.748)		
Histology	0.116	2.199 (0.824-5.872)		

Table 9: Uni- and multivariate Cox-regression analysis of telomere length in T-cells, including SNP-score in all patients.

Parameter	Univariate Cox-regression		Multivariate Cox-regression	
	p-value	Hazard-Ratio (95%CI)	p-value	Hazard-Ratio (95%CI)
TL0 (baseline)	0.763	1.132 (0.506-2.529)	0.587	1.260 (0.546-2.907)
TL1 (follow-up)	0.108	0.441 (0.163-1.197)	0.058	0.380 (0.140-1.034)
SNP-score	0.707	1.455 (0.206-10.256)		

Study group receiving Pembrolizumab as ICB regimen (Cox regression analysis)

The univariate Cox regression analyses for TL1 (median) did show a similar trend (HR: 0.310, 95% CI: 0.082-1.177, p = 0.085) (Table 10). However, when including other parameters of prognostic relevance in univariate analysis into a multivariate Cox-regression analysis (Sex, age at diagnosis and PDL-1 expression), the prognostic role of TL1 was found to be in part dependent of these confounders (HR: 0.372, 95% CI: 0.076-1.809, p = 0.220). A reasonable explanation for this might also be our small study cohort. Of note, the hazard ratio itself changed only from 0.310 to 0.369 (Table 10). It was TL1 but not Age, Sex or PD-L1 expression that seemed to be of predictive value

according to the Cox Regression analysis. Furthermore, ΔTL (the change of TL0 to TL1) seemed to have no prognostic relevance according to our data (HR: 0.994, 95% CI: 0.981-1.008, p = 0.390). The SNP-score itself does not seem to have a statistically significant effect on survival in the Pembrolizumab group on its own but in multivariate Cox regression when including TL1 (follow-up) the p-value changes from p=0.085 to p=0.044 and the hazard ratio changing from 0.310 (0.082-1.177) to 0.249 (0.064-0.964) in univariate to multivariate analysis respectively.

Table 10: Uni- and multivariate Cox-regression analysis of telomere length in T-cells for the prediction of overall survival in patients receiving Pembrolizumab as ICB regimen.

Parameter	Univariate Cox-regression		Multivariate Cox-regression	
	p-value	Hazard-Ratio (95%CI)	p-value	Hazard-Ratio (95%CI)
TL0 (baseline)	0.342	0.601 (0.211-1.716)	0.402	0.609 (0.191-1.941)
TL1 (follow-up)	0.085	0.310 (0.082-1.177)	0.217	0.369 (0.076-1.794)
Age	0.813	0.994 (0.949-1.042)		
Sex	0.870	0.919 (0.333-2.537)		
PDL-1 Expression	0.339	0.617 (0.229-1.662)		
Histology	0.118	2.737 (0.775-9.665)		

Table 11: Uni- and multivariate Cox-regression analysis of telomere length in T-cells, including SNP-score in Pembrolizumab group.

Parameter	Univariate Cox-regression		Multivariate Cox-regression	
	p-value	Hazard-Ratio (95%CI)	p-value	Hazard-Ratio (95%CI)
TL0 (baseline)	0.342	0.601 (0.211-1.716)	0.951	0.967 (0.334-2.810)
TL1 (follow-up)	0.085	0.310 (0.082-1.177)	0.044	0.249 (0.064-0.964)
SNP-score	0.974	1.046 (0.071-15.40)		

4.5.2 TERT expression (in PBMCs)

The expression analysis for TERT was done in PBMCs and not in T-cells alone, therefore I analyzed them separately from telomere length. Due to our relatively small

study cohort, we use the median as cut-off value in the Kaplan-Meier analysis, therefore two groups of roughly the same size are compared. No significant difference in survival could be seen between patients with higher compared to lower expression of TERT at baseline (TERT0) or at follow-up (TERT1) (Figure 21). The same conclusion applies to analysis of Pembrolizumab group only (Figure 22).

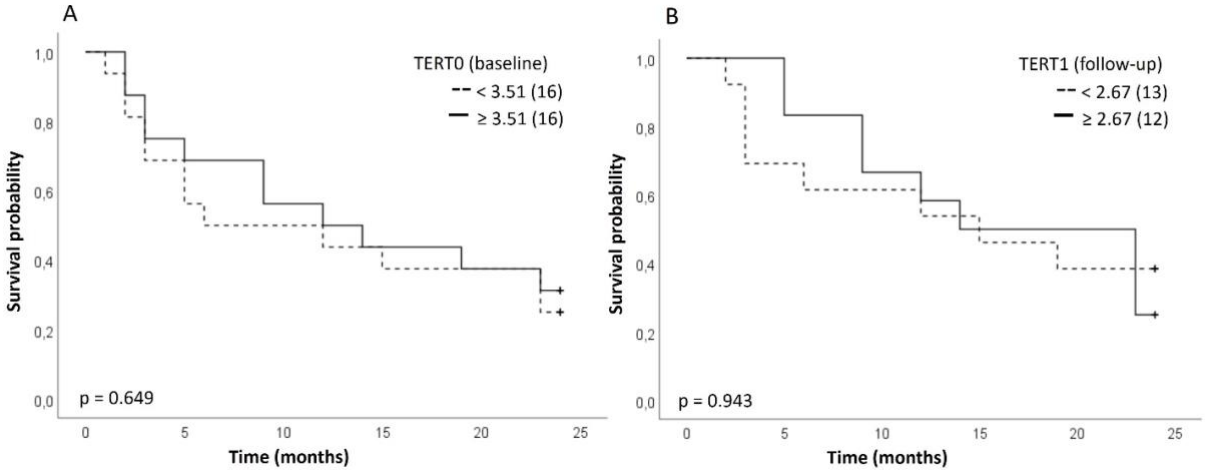

Figure 21: Kaplan-Meier graph of TERT0 (baseline) and TERT1 (follow-up) including all patients. Probability of survival is depicted in relation to the course of time. Subjects were divided into two groups based on the median of TERT **(A)** TERT expression at baseline is considered, a median of 3.51 was used as a cut-off value, resulting in 16 subjects in each group. **(B)** The second measurement after therapy start is considered, a median of 2.67 was used as a cut-off value, resulting in 13 subjects in the group of shorter telomeres and 12 subjects in the group of longer telomeres.

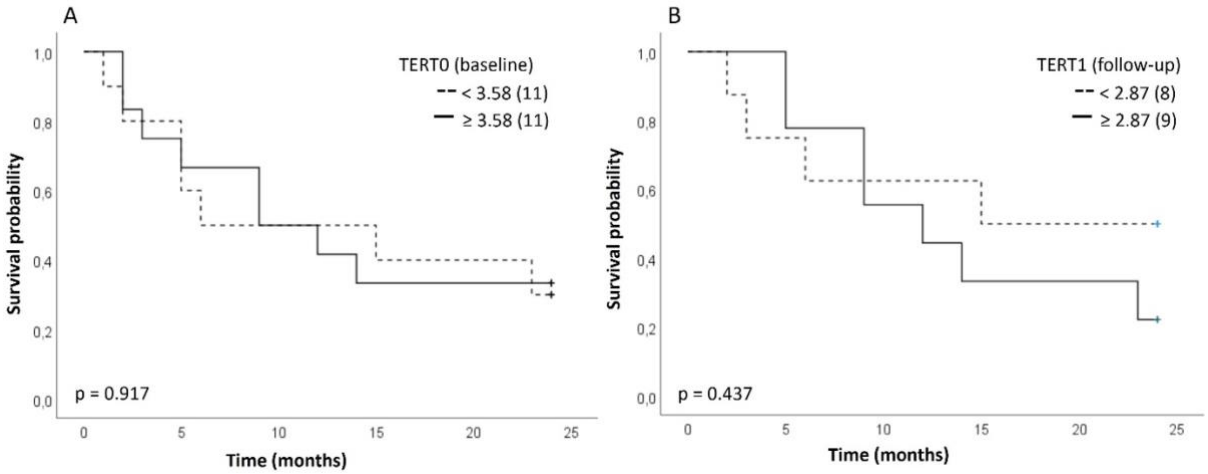

Figure 22: Kaplan-Meier graph of TERT0 (baseline) and TERT1 (follow-up) for patients receiving Pembrolizumab as ICB regimen only. Probability of survival is depicted in relation to the course of time. Subjects were divided into two groups based on the median of TERT **(A)** TERT expression at baseline is considered, a median of 3.58 was used as a cut-off value, resulting in 11 subjects in each group. **(B)** The second measurement after therapy start is considered, a median of 2.87 was used as a cut-off value, resulting in 8 subjects in the group of shorter telomeres and 9 subjects in the group of longer telomeres.

In uni- and multivariate Cox regression analysis no statistically significant result could be obtained. Interestingly, while the hazard ratio for TERT1 (follow-up) doesn't change much from uni- to multivariate analysis, TERT0 (baseline) seems to be partially dependent on the included confounders (age, sex, PDL-1 Expression and histology), with the hazard changing from 0.834 or 0.884 in univariate to 1.504 or 1.754 in multivariate analysis when including all patients or pembrolizumab group, respectively.

Table 12: Uni- and multivariate Cox-regression analysis of TERT expression in PBMCs for the prediction of overall survival including all patients.

Parameter	Univariate Cox-regression		Multivariate Cox-regression	
	p-value	Hazard-Ratio (95%CI)	p-value	Hazard-Ratio (95%CI)
TERT0 (baseline)	0.664	0.834 (0.368-1.891)	0.414	1.504 (0.565-4.003)
TERT1 (follow-up)	0.945	1.034 (0.398-2.686)	0.937	1.042 (0.372-2.922)
Age	0.479	0.985 (0.964-1.027)		
Sex	0.759	0.884 (0.401-1.949)		
PDL-1 Expression	0.570	0.796 (0.363-1.748)		
Histology	0.116	2.199 (0.824-5.872)		

Table 13: Uni- and multivariate Cox-regression analysis of TERT expression in PBMCs for the prediction of overall survival in patients receiving Pembrolizumab as ICI regimen.

Parameter	Univariate Cox-regression		Multivariate Cox-regression	
	p-value	Hazard-Ratio (95%CI)	p-value	Hazard-Ratio (95%CI)
TERT0 (baseline)	0.812	0.884 (0.320-2.442)	0.380	1.754 (0.501-6.139)
TERT1 (follow-up)	0.448	1.617 (0.467-5.596)	0.456	1.662 (0.437-6.320)
Age	0.813	0.994 (0.949-1.042)		
Sex	0.870	0.919 (0.333-2.537)		
PDL-1 Expression	0.339	0.617 (0.229-1.662)		
Histology	0.118	2.737 (0.775-9.665)		

5 Discussion

Although immune checkpoint inhibitors (ICIs) have widely been used across different types of tumors, only a limited number of factors has been identified to predict treatment response and overall survival (OS) in ICI therapy [199]. Furthermore, the ideal combination of biomarkers for patient selection still needs to be determined. T-cells play a critical role in tumor defense and significantly contribute to sustaining an anti-tumoral immune response, particularly in the context of immune checkpoint inhibitor (ICI) therapy [200]. In this study, we propose that enhanced telomere shortening in T-cells could potentially serve as a biomarker for worse survival in NSCLC patients treated with Pembrolizumab. In line with our results, several other studies have identified telomere parameters as predictive biomarkers in different cancer settings. Rolles et al., for instance, demonstrated that across several cancer types (including NSCLC) and regardless of the underlying disease, improvement in OS but not in treatment response correlated with longer telomeres compared to those with shorter telomeres measured in PBMCs [13]. However, they measured TL only in PBMCs and not in a subpopulation which they also stated as one of their methodological constraints. In a recent study, Faugeras et al. measured TL in tumor tissue of NSCLC patients before treatment initiation and showed that short telomers in tumor biopsies go along with shorter survival and a worse response to ICI treatment [17].

According to our study, overall survival seems not to be correlated with TL in T-cells before ICI therapy was started (TL0). However, a trend towards overall survival being improved in the subgroup with longer telomeres (after treatment initiation, TL1) was observed (Figure 20B, Figure 18B). According to our data age does not correlate significantly with TL of T cells in cancer patients (Figure 15) although it has been found that TL in cancer patients is shorter in white blood cells compared to healthy individuals of the same age, we cannot draw this conclusion since we did not include a healthy cohort [201]. A possible explanation for age not playing a significant role in TL in cancer patients might be the advanced disease stage and treatment effects on telomeres, masking any potential correlation with age [202]. Rolles et al. for instance showed that adaptation of TL in PBMCs for age does not change the results for overall survival in ICI therapy in different types of cancer [13]. Furthermore, T-cells have the capability of

changing TL through mechanisms like expression of telomerase, that are influenced by various factors that have not yet been completely unraveled, which might also explain why ΔTL had no prognostic relevance in the study at hand.

It must be noted that the same trend was observed for TL1 (HR: 0.310; 95% CI: 0.082-1.177; p = 0.085) in univariate analysis. Although the p-value changes to p = 0.217 in multivariate Cox-regression analysis, when including age, sex, PDL-1 expression and histology, the hazard ratio was relatively stable and independent of the additional factors. Patients with Adenocarcinoma seem to have a 170% higher risk of mortality compared to people with squamous cell carcinoma. However, patients with longer telomers in T-cells have a 69 % or 63 % lower risk of mortality compared to those with shorter telomeres in the univariate or multivariate Cox regression analysis respectively. In other words, longer telomeres indicated a reduced risk of mortality compared to patients with shorter telomers when undergoing ICI treatment independently of the type of cancer. Additionally, when including the SNP-score in Cox-regression analysis, the hazard of 0.249 proves to be statistically significant (p=0.044) meaning the group with longer telomeres in T cells have a 75% lower risk of mortality compared to patients with shorter telomeres. Nevertheless, a bigger cohort is needed to verify our results. It is tempting to speculate that the T cells proliferative potential was higher due to their capability to elongate telomeres, and therefore trigger a proper immunological response. It must be stressed that replicative senescence, as shown by Beauséjour et al. may not be permanent [203]. Furthermore, Lanna et al. revealed that senescent T-cells utilize AMPK to recruit p38 to the scaffold TAB1. Through the inhibition of AMPK-TAB1-dependent p38 activation, they successfully reversed the proliferative impairment of senescent T-cells [204]. Moreover, in vitro experiments demonstrated that the combination of p38MAPK inhibition with PD-1 inhibitors resulted in the restoration of the proliferative potential [205]. It might be of relevance to measure telomere length at earlier time points, since TL in T cells can change relatively fast, and effects therefore might be seen earlier in treatment [206]. A more extensive discussion on T-cell parameters in immunotherapy and emerging therapeutic avenues can be found elsewhere [207].

There might be several reasons why we could not detect any correlation between TL0 (baseline) and survival in ICI therapy. First, we recruited only patients who had not undergone ICI treatment before. Meaning that the T-cell compartment had not been stimulated by monoclonal antibodies (ICIs) to proliferate, which for patients who respond to treatment only happens when ICI therapy is initiated. Second, cellular senescence, amongst other factors, is primarily determined by one critically short telomere, rather than the average length of telomeres in a cell. It might help to determine TL using the Telomere Shortest Length Assay (TeSLA) to see subtle differences. Another limiting factor was the small study group. A bigger cohort is needed to substantiate the hypotheses presented in this paper. Furthermore, we did not include a control group, for example NSCLC patients undergoing chemotherapy treatment only. Ferrara et al. nicely showed that a senescent immune phenotype in T-cells ($CD28^-$, $CD57^+$, $KLRG1^+$) was associated with a lack of benefit from ICI, but not with platinum-based chemotherapy in patients with NSCLC. It also might be interesting to measure telomere dynamics and several senescence markers in one cohort, including telomere length, telomerase activity, TERT expression, shelterin complex genes (TRF1, TRF2, POT1, TPP1, RAP1 and TIN2), surface markers like $CD28^-$, $CD57^+$, $KLRG1^+$ and IgM-Rheumatoid factor. Faugeras et al. had already demonstrated that aberrant expression of shelterin genes in NSCLC tumor biopsies correlates with significantly shorter survival [17]. It would be of value to determine whether the same is true in the periphery when measured e.g., in T-cells, which would allow a non-invasive evaluation. Furthermore, Ugolini et.al showed that serum IgM-RF can serve as a predictive factor for the early progression development and a prognostic factor for reduced progression-free survival and overall survival in anti-PD-1 treated NSCLC patients [208]. They speculate that the capacity of IgM-RF to bind to naïve and central memory T-cells and hinder their migration might explain the decrease in the tumor-reactive $CD137^+$ T-cell population, potentially leading to the inefficacy of these T-cell targeting drugs like Pembrolizumab. Due to the complexity of the immune response, it is therefore essential to measure various biomarkers with the aim of finding ideal combinatorial treatment regimens. Numerous clinical trials are presently underway, exploring the combined use of immune checkpoint inhibitors and antibody-drug conjugates (ADCs), with the aim of enhancing

the effectiveness of these treatments and potentially augmenting the impact of immunotherapy [209,210,211]. Hence, there is hope that improved combination of therapies in conjunction with predictive biomarkers will lead to more effective treatment strategies.

According to our data, TERT expression in PBMCs does not play a role in survival of NSCLC patients undergoing ICB treatment. While this is the first study measuring TERT expression in PBMCs in patients undergoing ICB, a very recent study by Kuhn et al concluded that TERT expression and promoter mutations in tumor cells could also not be associated with survival of melanoma patients undergoing ICB treatment [212].

Overall, while telomere length in T-cells appears to be a viable candidate as a potential biomarker for ICI response and overall survival in NSCLC, further research is needed to establish its clinical significance and utility in guiding treatment decisions. It would be interesting to see how early after treatment initiation one could see the correlation of shorter telomeres and decreased survival. Therefore, one should increase the timepoints and samples taken before the first timepoint (three months) of the TILUC study.

Despite challenges like tumor heterogeneity or the dynamic nature of the tumor-immune microenvironment, advancements in technologies, multi-omics approaches, artificial intelligence, and collaborative research initiatives are tools, which hold the potential to uncover additional robust and reliable biomarkers in the future [213]. These biomarkers can not only aid in patient selection for ICIs but also help with treatment monitoring, and the development of personalized immunotherapeutic strategies.

In conclusion this study provides proof of principle for a correlation of accelerated telomere shortening in T cells of non-small lung cancer patients receiving Pembrolizumab and overall survival. However, it is important to note that the current understanding of telomere length and immune checkpoint therapy response is limited, and more research is needed. The relationship between telomere length, T-cell function, and treatment outcomes is complex, and additional studies with larger patient cohorts and long-term follow-up are required for a more comprehensive understanding.

Second Part: TZAP-induced telomere trimming is mediated by an ALT-like pathway and suppressed by the ATRX/DAXX complex

The following research is based on a paper that has already been published [214]. I am second author on the publication. All experiments done in triplicates or duplicates I performed at least one time including counting colocalizations, confocal microscopy sessions conducted on Zeiss LSM 880 microscope and using Imaris software for the analysis. I was not involved in the CRISPR Cas 9 and TRF experiments. Thanks to the core facility at the Salk Institute for Biological Studies for teaching me how to use the microscope and Sara Priego Moreno and other members of the Karlseder lab for teaching me all the assays and the data analysis using Imaris Software. Statistical analysis (Graphpad) and figures were compiled by Sara Priego-Moreno, except Figure 38 and Figures in the materials and method section.

6 Background (TZAP)

6.1 ALT (Alternative lengthening of telomeres) vs Telomerase and its implications in cancer development

Alternative Lengthening of Telomeres (ALT) and the action of telomerase are fundamentally different. However, both play essential roles in preserving telomere length and ensuring cell viability.

ALT - Alternative Lengthening of Telomeres

ALT is a telomerase-independent mechanism that some cancer cells and a subset of normal human cells employ to maintain telomere length [215, 216]. Unlike telomerase, which adds telomeric repeats to the ends of chromosomes, ALT relies on a recombination-based process involving homologous recombination (HR) and DNA repair mechanisms. ALT is typically associated with certain types of cancers, such as osteosarcomas and glioblastomas, and is characterized by distinct features at the molecular level [217].

In ALT-positive cells, telomeres exhibit unique properties. These cells often display heterogeneous telomere lengths, with a subset of ultra-long telomeres [218]. Furthermore, they rely on a mechanism called Break-induced Replication (BIR), where the telomere invades a telomeric-repeat-containing template, followed by conservative DNA synthesis to elongate the telomere [219, 220]. Moreover, they display extrachromosomal telomeric DNA circles (C-circles) and ALT-associated promyelocytic leukemia (PML) bodies (APBs) [221]. These APBs are thought to be specialized structures that facilitate the exchange of telomeric DNA between different chromosome ends, promoting homology-directed recombination and telomere synthesis.

The regulation of ALT is not fully understood, but several factors have been implicated in its activation and maintenance. The ATRX/DAXX complex plays a crucial role in the context of ALT. ATRX (Alpha Thalassemia/Mental Retardation Syndrome X-Linked), and DAXX (Death-Domain Associated Protein) are two evolutionarily conserved proteins that form a chromatin remodeling complex, and their functional interplay is integral to various cellular processes, including transcriptional regulation and heterochromatin organization. Recent research has illuminated the intricate involvement of the ATRX/DAXX complex in the maintenance of telomeres through the ALT pathway [222].

The ATRX/DAXX complex's role in ALT was initially evidenced by its frequent mutation or loss in ALT^+ tumors, which implied its significance in regulating ALT-associated telomere maintenance [223]. ATRX, a member of the SWI/SNF family of chromatin remodeling factors, possesses ATP-dependent helicase activity, and contributes to chromatin regulation through nucleosome assembly and histone variant deposition, particularly the H3.3 histone variant [224]. DAXX, on the other hand, interacts with histones and plays a role in regulating gene expression and chromatin stability [225]. Mechanistically, ATRX and DAXX collaborate to deposit the H3.3 histone variant at telomeres. This process ensures proper telomere structure and function, including the maintenance of a repressive chromatin environment that prevents undesired recombination events and DNA damage response activation [226]. In the absence of ATRX/DAXX or their functional impairment, telomeric chromatin can become destabilized, leading to aberrant homologous recombination-based telomere

elongation, a hallmark of ALT [227]. Furthermore, ATRX/DAXX involvement extends beyond their role in telomere chromatin regulation. They influence the transcription of non-coding RNAs from telomeric regions, such as Telomeric Repeat-containing RNA (TERRA), which participate in the telomere maintenance process [228]. Dysregulation of TERRA expression, driven by ATRX/DAXX deficiency, may contribute to the altered telomeric chromatin landscape observed in ALT^+ cells, further facilitating recombination-based telomere lengthening. The discovery that ATRX/DAXX-deficient tumors exhibit ALT activity underscores the complex interplay between these proteins, telomeric chromatin structure, and ALT-associated telomere maintenance. ATRX/DAXX mutations or loss-of-function alterations are recurrent in several cancers, including gliomas and pancreatic neuroendocrine tumors, where they correlate with ALT activity [229]. Of note, the expression of ATRX in ALT-positive (ALT^+) cells leads to the reversal of ALT markers, indicating ATRX's significant role as a key suppressor of the ALT mechanism [230,231]. Consequently, therapeutic strategies targeting ALT-positive cancers may involve exploiting vulnerabilities arising from ATRX/DAXX dysfunction.

Telomerase: The Classic Telomere Lengthening Pathway

Telomerase, a specialized reverse transcriptase enzyme, is responsible for adding telomeric repeats to the ends of chromosomes. It carries an intrinsic RNA template, which it uses as a guide to synthesize the telomeric DNA repeats. Telomerase activity is highly regulated, and its expression is tightly controlled in normal human cells, with most somatic cells lacking significant telomerase activity [232]. However, telomerase is highly active in germ cells, stem cells, and some cancer cells, allowing them to maintain telomere length indefinitely [233,234]. Telomerase extends telomeres by adding telomeric DNA repeats to the 3' overhang of the telomere. The RNA component of telomerase serves as a template, allowing the reverse transcriptase activity of the enzyme to synthesize new telomeric repeats. This action elongates the telomere, compensating for the loss that occurs during DNA replication. The regulation of telomerase activity involves a complex interplay of various factors, including telomerase RNA, telomerase reverse transcriptase protein (TERT), telomere-associated proteins, and intricate signaling pathways. TERT, the catalytic subunit of telomerase, is often

upregulated in various cancers, allowing cells to elongate their telomeres and evade replicative senescence [235,236]. This activation is frequently achieved through mutations in the TERT promoter region, enabling increased expression [237]. The implications of telomerase in cancer extend beyond mere cellular immortality. Telomerase activation is intricately linked to tumor initiation, progression, and therapeutic resistance [238, 239]. Telomerase activation has been correlated with increased metastatic potential and poor prognosis in various cancer types, underlining its significance as a prognostic marker [240]. Therefore, targeting telomerase has emerged as a promising avenue for cancer therapy. The unique presence of telomerase in most cancer cells, along with its absence or minimal activity in most normal somatic cells, offers a potential therapeutic window. Strategies to inhibit telomerase activity include direct telomerase inhibition through small-molecule inhibitors, gene therapy approaches to silence TERT expression, and immunotherapeutic targeting of telomerase-expressing cells [241]. Encouragingly, several telomerase inhibitors have entered clinical trials, displaying promising outcomes in certain cancers. However, challenges remain, including potential off-target effects and the emergence of resistance mechanisms. Telomerase inhibitors could be particularly effective in combination therapies. Combining telomerase inhibition with conventional chemotherapy or radiation therapy may sensitize cancer cells to treatment, as cells with critically short telomeres become more susceptible to DNA damage-induced cell death [242]. Moreover, telomerase inhibition might enhance the efficacy of immune checkpoint blockade therapies by targeting cells with active telomerase and high antigenicity, potentially boosting the immune response against cancer cells [243, 244].

Intriguingly, recent research has unveiled the complexity of telomerase function beyond telomere maintenance. Telomerase has been implicated in non-canonical roles, influencing cellular processes such as DNA damage repair, gene expression regulation, and mitochondrial function [245]. These non-telomeric functions of telomerase may contribute to its roles in cancer beyond telomere elongation. For example, telomerase activation has been associated with enhanced DNA damage repair mechanisms, allowing cancer cells to resist therapy-induced DNA damage.

Additionally, telomerase overexpression has been linked to altered gene expression patterns that facilitate cancer cell survival, proliferation, and immune evasion [238].
Both ALT and telomerase pathways have profound implications for cellular biology and human health. As mentioned in the previous chapter of my thesis, telomerase is crucial for the immortalization of germ cells, stem cells, and certain cancer cells, enabling them to evade senescence and continue dividing indefinitely. In contrast, ALT provides an alternative means of telomere maintenance, particularly in cancers where telomerase activity is repressed.

6.2 TZAP and its role in telomere length regulation

TZAP, also referred to as ZBTB48 (Zinc Finger and BTB Domain-Containing Protein 48), was identified and characterized by the Karlseder Lab in 2017 as a new protein that binds to telomeres which is involved in the regulation of TL [3]. The discovery of TZAP marked a significant advancement in our understanding of the intricate dynamics governing telomere maintenance. Unlike many other telomere-binding proteins associated with telomere shortening, TZAP exhibits a rather unexpected function in promoting telomere elongation. Studies have revealed that TZAP preferentially associates with long telomeres in human cells. When TZAP is upregulated or overexpressed, it leads to telomere loss that goes along with the build-up of circular extra-chromosomal telomeric repeats (cECTRs) and an elevation of ALT-associated PML bodies (APBs). These cellular changes ultimately culminate in cell death, underscoring the importance of balanced telomere length regulation [3]. Conversely, when TZAP is downregulated, a cutback in the levels of cECTRs is observed in ALT-positive (ALT^+) cells and mouse embryonic stem cells (mES), along with significant telomere elongation in mES cell [3]. This implies that TZAP may play a role in maintaining telomere length homeostasis by associating with and promoting the trimming of excessively long telomeres. Such trimming activity prevents telomeres from becoming overly elongated and ensures the stability of the genome. The molecular mechanisms underlying TZAP's role in telomere length regulation are complex and multifaceted. One hypothesis posits that the concentration of shelterin at telomeres may serve as a crucial determinant for TZAP recruitment. Longer telomeres have lower

shelterin concentration, possibly triggering TZAP recruitment to ensure appropriate telomere trimming. However, further investigations are needed to fully decipher the precise mechanisms by which TZAP interacts with shelterin and other telomeric components to regulate telomere length.

At the Salk Institute, we investigated the molecular mechanisms that are triggered when TZAP is overexpressed in human cancer cells.

7 Materials and Methods

For easier readability the material and methods referred to in this section are structured in a way that indicates the main steps with graphical elements. Icons were sourced from and created with BioRender.com.

7.1 t-circle assay

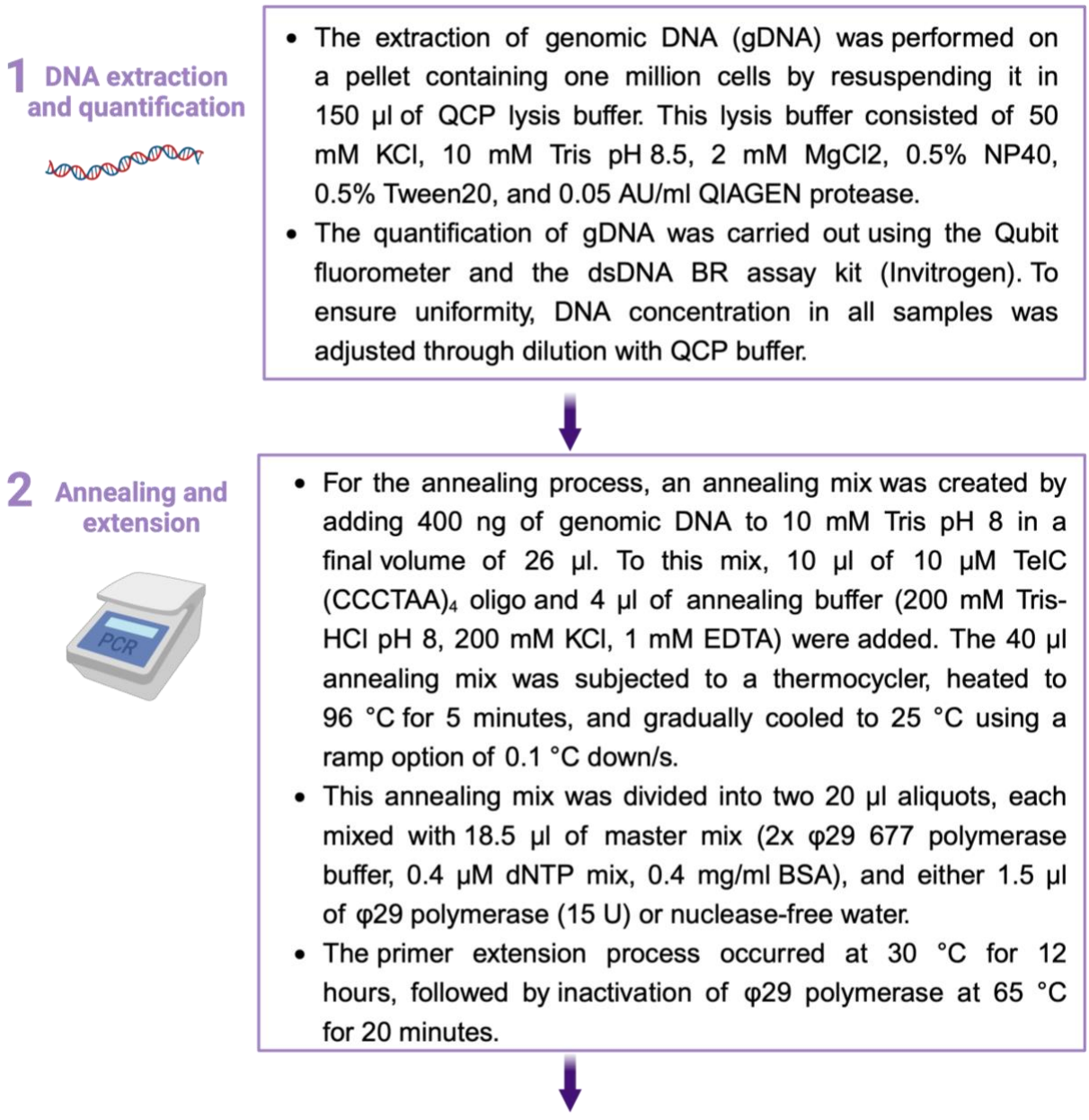

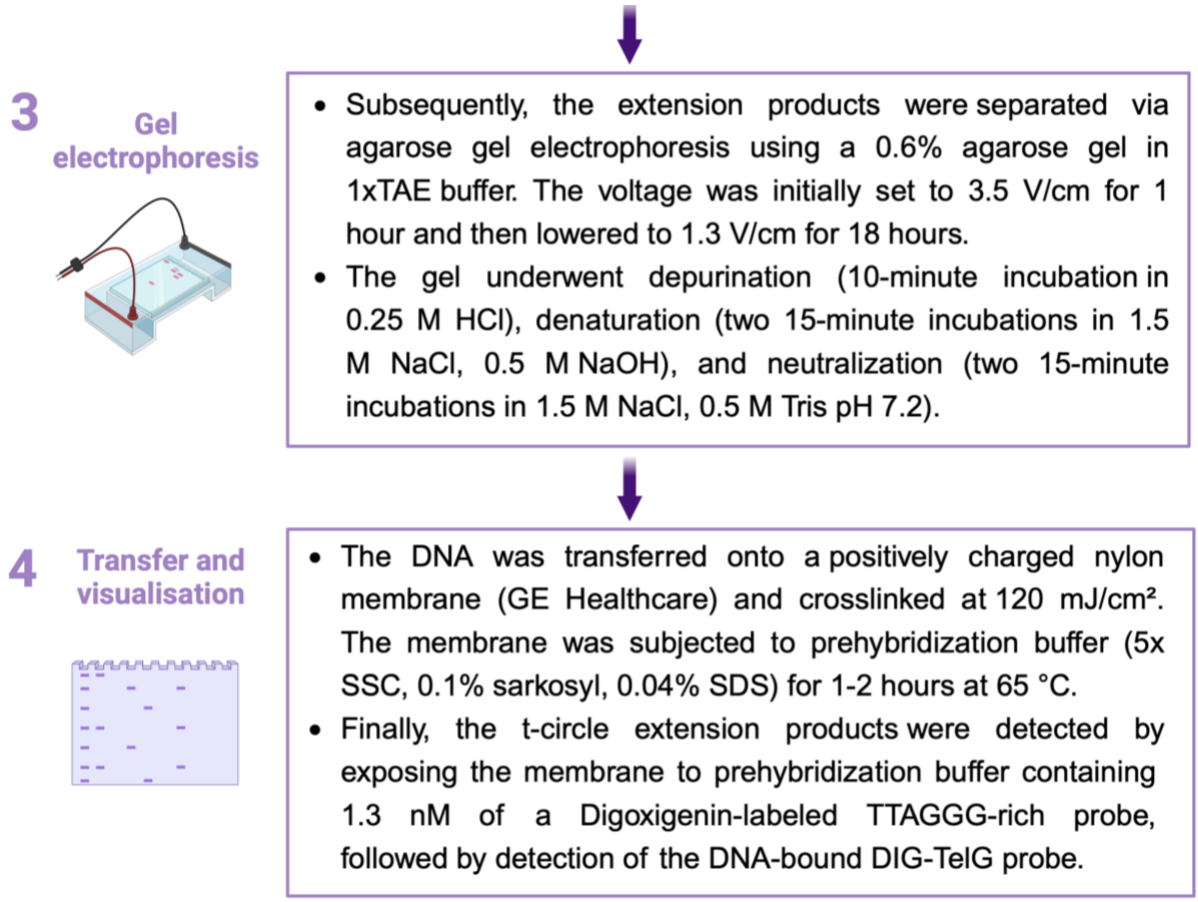

Figure 23: T-circle assay.

Detection of the DNA-bound DIG-TelG probe was done as elaborated by Kimura et al [246].

7.2 c-circle assay

1 DNA extraction and quantification

- Genomic DNA (gDNA) was isolated from cell pellets containing one million cells and assessed using the method outlined previously for the t-circle assay.
- To ensure uniformity, DNA concentration was adjusted across all samples by dilution with QCP buffer.

2 Amplification

- Rolling circle amplification reactions involving φ29 polymerase were conducted using input DNA quantities of 10 and 50 ng, along with a negative control devoid of φ29 utilizing 50 ng of input DNA.
- PCR conditions were as follows: After polymerase was added the samples were incubated at 30 °C for 4 h, following with 70 °C for 20 min and then kept at 4 °C.

3 Transfer and crosslink

- Subsequently, the reaction products were transferred onto a positively charged nylon membrane via a dot-blot manifold. The DNA was crosslinked to the membrane employing the method described earlier for the t-circle assay.

4 Hybridisation and visualisation

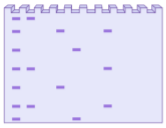

- Following this, the membrane was prehybridized with CHURCH buffer (comprising 500 ml of 0.5M NaPi pH 7.2, 2 ml of 0.5 M EDTA pH 8, 70 g of SDS, 10 g of BSA, and fill with miliQ water to 1 l, followed by filtration) for a duration of 1 hour at 65 °C.
- Subsequent hybridization was carried out using CHURCH buffer containing a 32P-klenow labeled TelC probe at 65 °C overnight. The protocol for creating the TelC probe was sourced from Titia de Lange's lab website.
- The membrane then underwent 2-3 brief washes with 2xSSC to eliminate excessive radioactivity, followed by 2 washes each with (2xSSC, 0.1% SDS) and (2xSSC), all for a 5-minute duration at 65 °C.
- Finally, the membrane was exposed to a Storage Phosphor Screen from GE Healthcare and scanned using a Thyphoon9400 Phosphorimager from Amersham, GE Healthcare. Subsequent quantitation of the dot blot signals was executed via ImageQuant TL software. The analysis involved subtracting the average intensity of the -φ29 sample from the respective φ29-containing sample, and the values were normalized in relation to the designated control sample.

Figure 24: C-circle assay.

7.3 Plasmids and transductions

The following figure describes the retroviral vector transfection and transduction of cell lines.

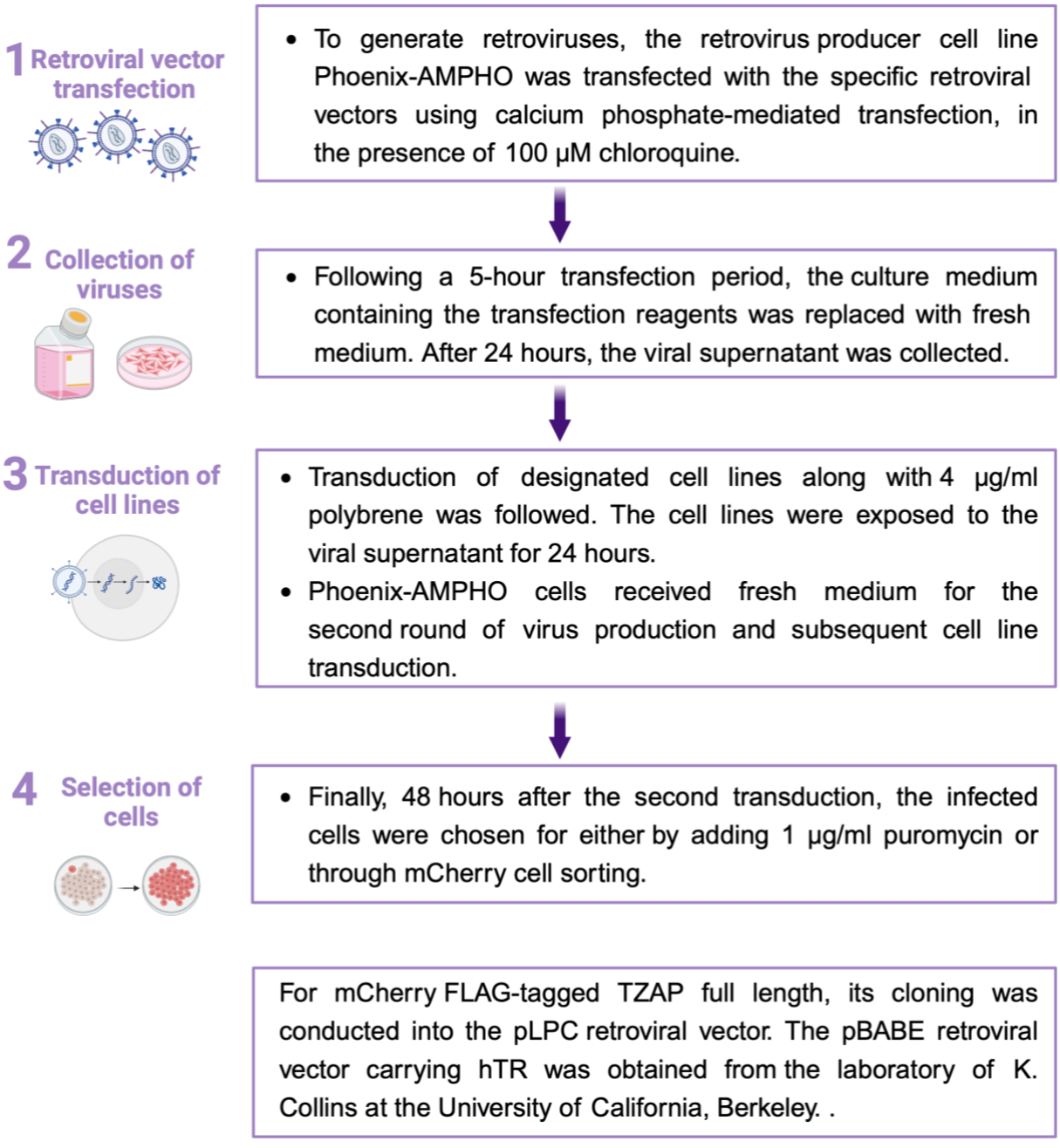

Figure 25: Retroviral vector transfection and transduction of cell lines.

7.4 Cell culture

Following cell lines and media were used in the study:

	Product name	Company
Cell lines 	• U2-OS	ATCC
	• GM847	Coriell Institute
	• HT-1080	ATCC
	• HeLa1.2.11	Generated in Titia de Langes' Lab
	• HeLa-LT	Generated in the Karlseder Lab
Media 	• Glutamax-Dulbecco's Modified Eagle's Medium	Gibco
	• Fetal Bovine Serum (FBS)	Avantor
	• Nonessential Amino Acids	Corning
	• Penicillin-streptomycin solution	Corning

Figure 26: Cell lines and Media used in the study.

Assessment of cells regarding whether they are free of mycoplasma was done in all cells.

7.5 siRNAs and transfections

Following siRNAs were used in the study:

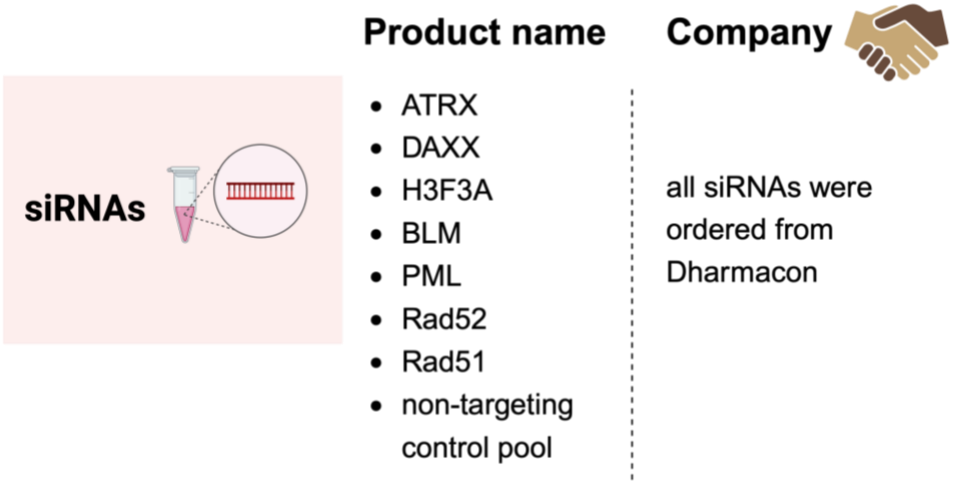

Figure 27: siRNAs used in the study.

siRNA transfection:

The following scheme shows how siRNA transfection was done: see next page:

1 Seeding cells

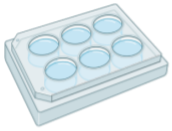

- First day: Cells were seeded in a 6-well plate (10^5 cells per well)
- On the second day, cells were incubated with antibiotic free media.

2 Transfection with siRNA

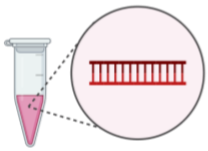

- Preparation of transfection solution was as follows: mixing 250 µl of OptiMEM containing the specified siRNAs at a final concentration of either 30 nM (for a single siRNA) or 25 nM (for two siRNAs), along with 250 µl of OptiMEM containing Lipofectamine RNAiMAX at a final concentration of 2.5 µg/ml. Transfection solution was incubated for 15 minutes at RT after thoroughly mixing it.
- Transfection solution was added dropwise to the cells

3 Selection

- Eight hours later, the media was replaced with antibiotic-containing media, and the cells were either transfected again or harvested 72 hours later.

Transfection variation in experiments

- For Western Blotting, immunofluorescence (IF), IF-FISH, c-circle, and t-circle assays, we performed two consecutive siRNA transfections. However, for ATSA and TRF assays, three consecutive siRNA transfections were carried out.

Figure 28: siRNA transfection procedure.

7.6 Antibody sources

The following table lists antibodies used in this study.

Antibody name	Company
α-GAPDH	Abnova
α-γH2A.x Ser 139	Millipore
α-Myc-tag	Cell Signaling
α-p-Chk1 Ser 345	Cell Signaling
α-PML	Santa Cruz
α-p-Chk2 Thr 68	Cell Signaling
α-p-ATR Thr 1989	Abcam
α-p-ATM Ser 1981	Cell Signaling
α-ATRX	Santa Cruz
α-DAXX	Santa Cruz
α-H3.3	Abcam
α-RMI1	Novus
α-FLAG-tag	Sigma
α-RPA32	Abcam
α-RPA70	Santa Cruz
α-BLM	generated in-house
α-TRF1	generated in-house
α-TRF2	generated in-house
Secondary antibodies for WB	
anti-mouse IgG	Amersham
anti-rabbit IgG	Amersham
Secondary antibodies for IF	
AlexaFluor 488 anti-IgG mouse	Invitrogen
AlexaFluor 594 anti-IgG rabbit	Invitrogen
AlexaFluor 568 anti-IgG mouse	Invitrogen

Figure 29: List of antibodies that were used in this study.

7.7 Western Blotting

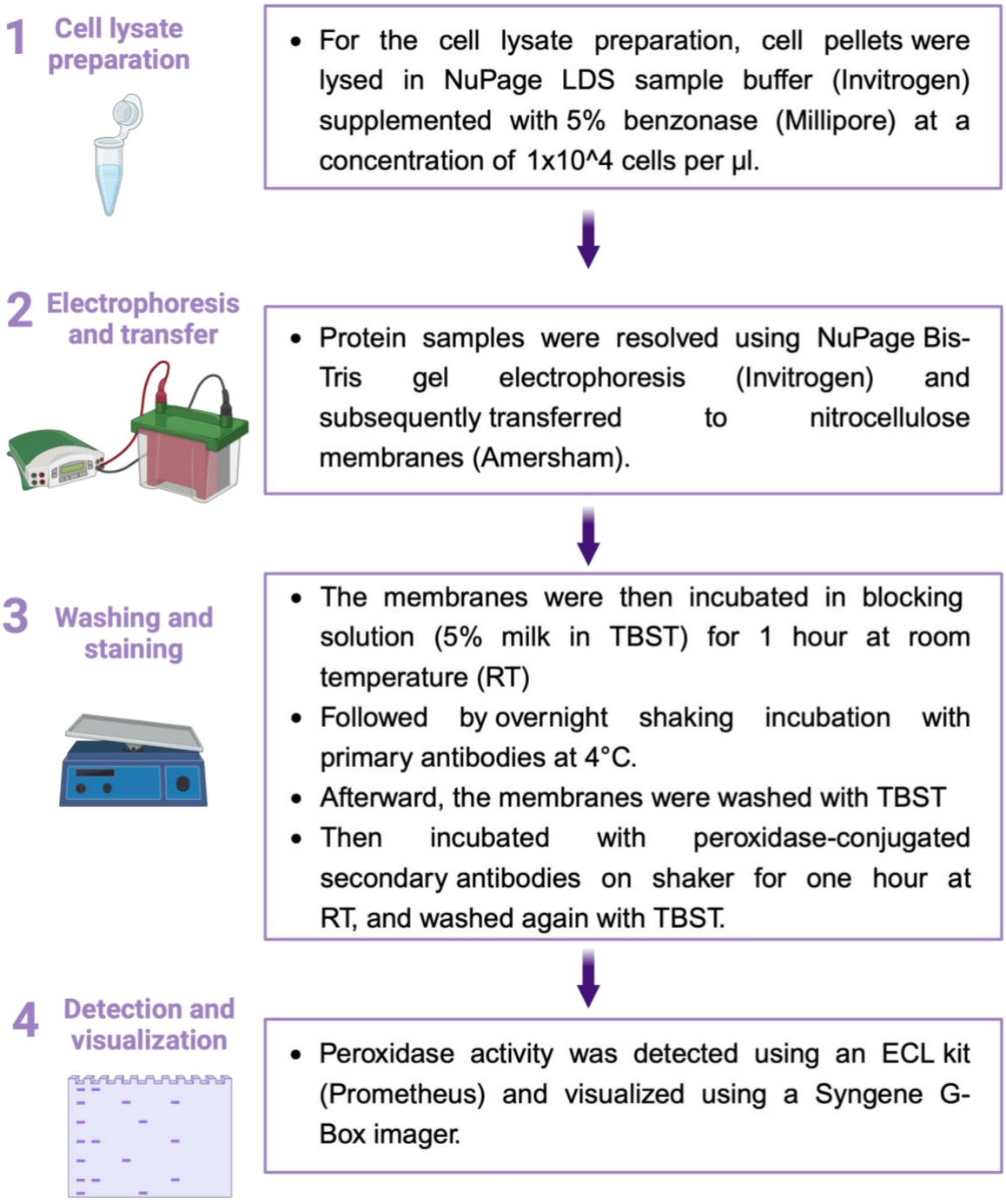

Figure 30: Western blotting procedure.

All primary antibodies were diluted in 5% milk in TBST.

7.8 Immuno-Fluorescence (IF)

1 Fix cells

- Cells were placed onto glass coverslips a day before the experiment. Subsequently, they were fixed using 4% paraformaldehyde in PBS for a duration of 10 minutes, followed by PBS washing.

2 Cell permeabilisation

- The cells were exposed to a permeabilization solution (0.2% Triton X-100, 30 nM glycine in PBS) for 15 minutes, gently shaken at room temperature (RT).

3 Blocking and first antibody incubation

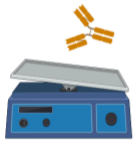

- Following this, the cells underwent blocking in a solution containing 5% BSA in PBS for 1 hour at RT
- Subsequently, the primary antibodies were applied and incubated with the cells either for 2 hours at RT or overnight at 4 °C within a humidity chamber.

4 Secondary antibody incubation and mounting

- After PBS washing, the cells were subjected to secondary antibodies for 1 hour at RT. Lastly, PBS washing was performed, and the cells were mounted in ProLong Diamond with DAPI (Invitrogen).

3 Microscopy

- The confocal microscopy sessions were conducted using a Zeiss LSM 880 microscope. For the experiments depicted in Figures 34C-D, 34E-F, 35E-F, Z-stack image acquisition was performed, while single-plane image acquisition was carried out for the experiments illustrated in Figures 36B, 37A-B. Imaris software was utilized for Z-stack analysis, and ImageJ was employed for the analysis of single-plane images. Prior to assembling representative images, raw images were processed using Zeiss ZEN (blue edition).
- In the experiment presented in Figure 35B, cells on coverslips underwent pre-extraction prior to fixation by being subjected to pre-extraction buffer (25 mM HEPES pH 7.4, 50 mM NaCl, 1 mM EDTA, 3 mM MgCl2, 300 mM Sucrose, 0.5% Triton X-100) for 5 minutes at 4 °C. Subsequently, the coverslips were fixed, stained, and mounted according to above explained protocol.

Figure 31: Immunofluorescence procedure.

7.9 ATSA assay (ALT telomere DNA synthesis in APBs)

The protocol for this assay was adapted from [247].

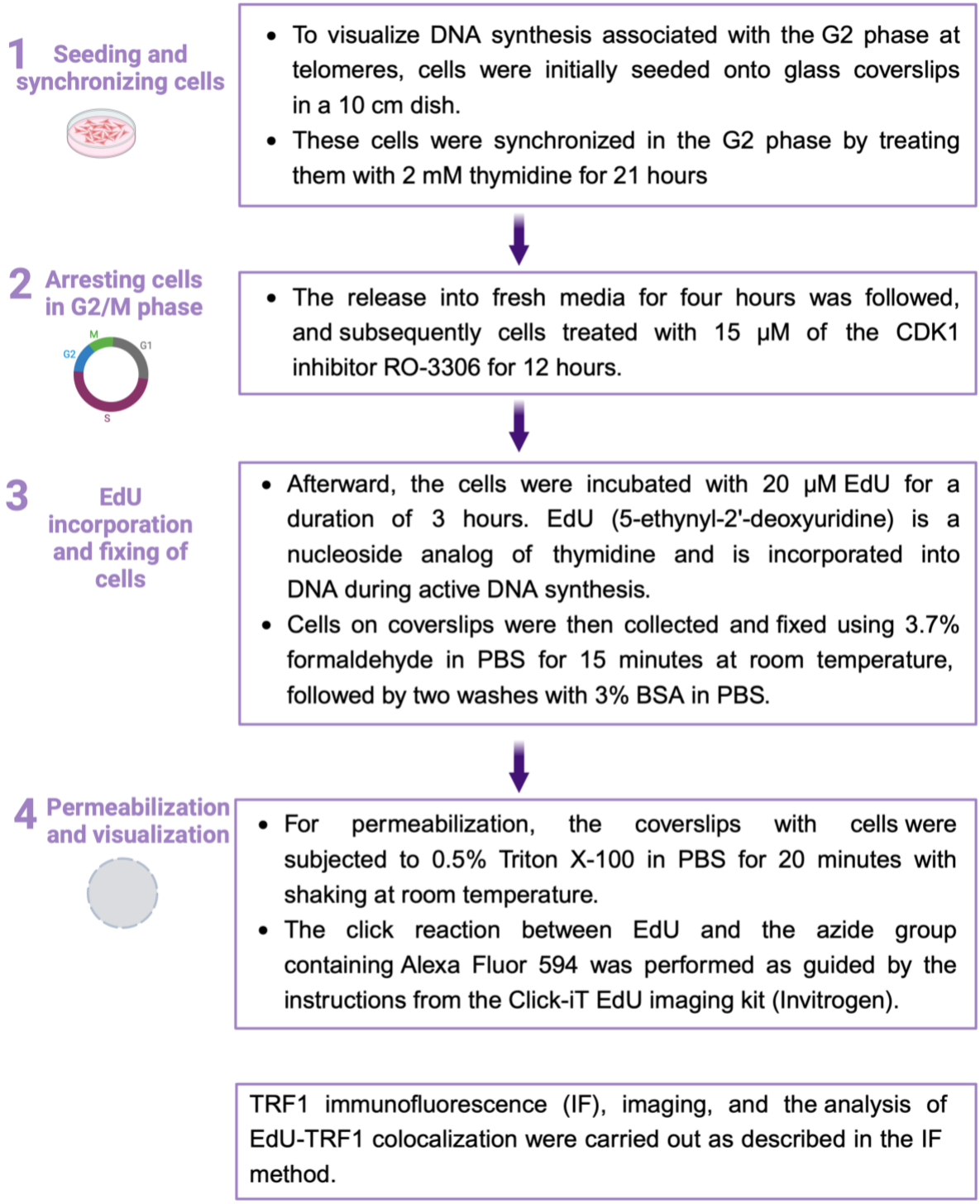

Figure 32: ATSA assay (ALT telomere DNA synthesis in APBs).

8 Results

8.1 Overexpression of TZAP in ALT positive cells leads to aggravation of ALT phenotypes

Elevated expression of TZAP within ALT+ cells goes along with elevation of ECTRs and APBs, both of which are established indicators of the ALT pathway [3]. Notably, these markers are also detectable at at lower counts of cells where shortening of telomeres occurs [248, 249]. To further explore this phenomenon, we aimed to ascertain whether the augmentation of these traits would also manifest in cancer cells that are telomerase positive (characterized by long telomeres) and overexpress TZAP. To this end, we conducted a c-circle assay encompassing two cell lines that are ALT positive, namely U-2 OS and GM847, as well as cell lines that are telomerase positive, HeLa1.2.11 and HT-1080 hTR. Each cell line was subjected to the assay in both the presence and absence of TZAP overexpression, as illustrated in Figure 33A. Although the introduction of TZAP exhibited an evident elevation in ECTR levels in ALT, but telomerase positivity was not affected by this change (Figure 33A). Meaning that the generation of ECTRs following TZAP upregulation is exclusive to ALT positive cells, hinting at their initiation through an ALT-like pathway. Subsequently, an in-depth exploration of other ALT markers was conducted in U-2 OS cells to unravel the impact of TZAP overexpression. This inquiry unveiled that the DNA damage response (ATM, ATR) is tightly linked with ALT, and was stimulated in response to TZAP overexpression (Figure 33B) [250, 251]. Moreover, delving into the correlation between the RPA and the TRF1, it was observed that TZAP led to an amplified recruitment in RPA32 (Figure 33C-D) which is recognized as an indicator of replication stress [252], suggesting that TZAP prompts a state of telomeric replication stress, a hallmark characteristic of ALT [253]. Lastly, the assessment of DNA synthesis at telomeres in G2 phase, yet another ALT marker, was performed through the implementation of the ATSA assay [254]. This analysis unveiled a substantial escalation in this trait following TZAP overexpression in U-2 OS cells (Figure 33E-F). Collectively, these observations signify that the higher levels of TZAP in U-2 OS cells prompts the initiation of replication stress at telomeres, effectively activating a pathway akin to ALT.

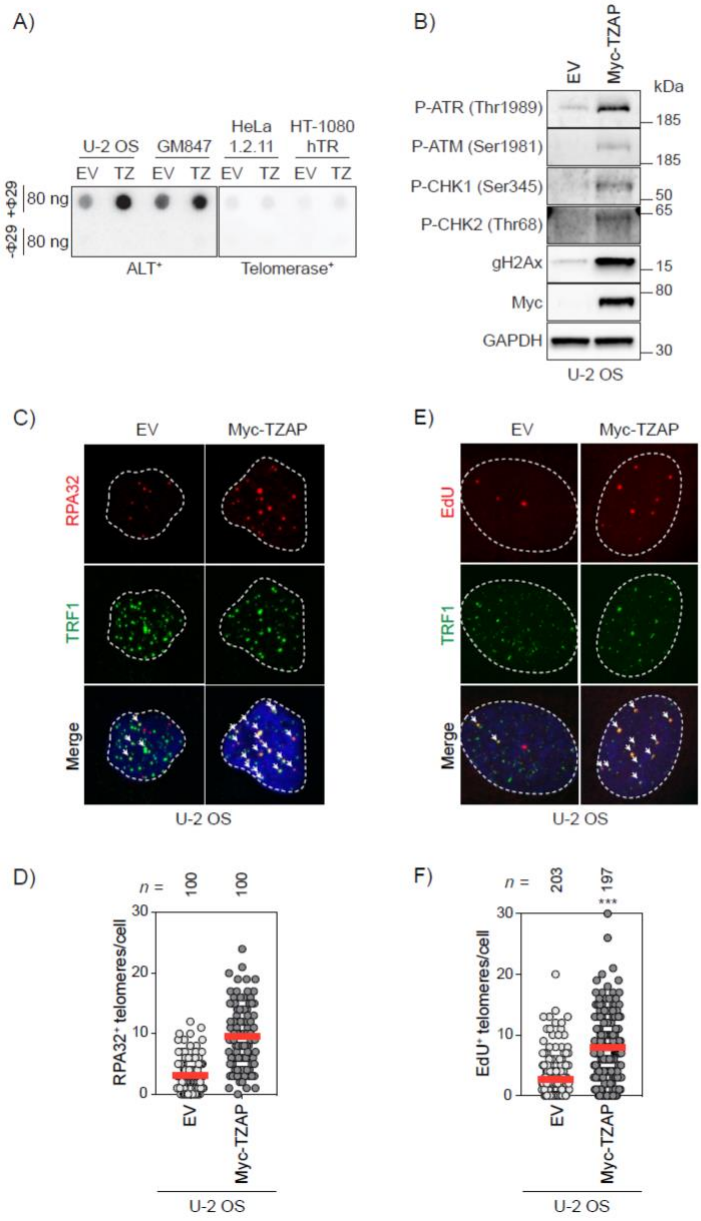

Figure 33: ALT phenotypes in ALT⁺ cells is enhanced by TZAP overexpression.
A) C-circle blots of ALT positive and telomerase positive cells with Myc-TZAP (TZ) or empty vector (EV). **B)** Western blot in U-2 OS cells either Myc-TZAP or EV. **C)** Representative immunofluorescence images in U-2 OS cells either Myc-TZAP or EV with the nuclear localization of TRF1 and RPA32. Arrows are indicating RPA32-TRF1 colocalizations. **D)** Quantification of previous experiment (C) shown as a scatter blot. For every sample there were 100 nuclei analyzed. Line in the centre indicates the mean. n is the analyzed number of cells. **E)** Representative immunofluorescence images of U-2 OS cells synchronized in G2, Myc-TZAP or EV with nuclear localization of TRF1 and EdU incorporated into DNA that is newly synthesized. Arrows show EdU-TRF1 colocalizations **F)** Quantification of previous experiment (E) as a scatter blot. 197 nuclei were analyzed for each sample in total. Centre line indicates the mean. n is the analyzed amount of cells. *** $P < 0.001$, ns: non-significant, the t-test was used for the calculation of the p-value Adapted from Moreno et al., 2023 [214] with permission of the publisher Elsevier.

8.2 ATRX/DAXX is responsible for the repression of telomere trimming induced by TZAP in telomerase positive cells with long telomeres which is not dependent on H3.3

A notable distinction between telomerase-positive and ALT-positive cancer cells resides in the frequent deficiency of the chromatin remodeling entity ATRX/DAXX [255]. Evaluation of ATRX/DAXX status across the spectrum of cell lines employed in our study through Western Blot analysis demonstrated that cells with telomerase expressed also exhibited certain expression in ATRX plus DAXX, but that ALT-positive cells only retained detectable DAXX but showed a complete loss of ATRX (Figure 37A). Consequently, our hypothesis emerged that TZAP-induced telomere trimming could be repressed by ATRX/DAXX in telomerase^{+} cells. To scrutinize this proposition, we orchestrated the upregulation of TZAP in HeLa1.2.11 cells concurrently subjected to siRNA-mediated knockdown of ATRX, DAXX, and the histone variant H3.3 (Figure 34A). Intriguingly, the elevation of TZAP led to augmented levels of extrachromosomal telomeric repeats (ECTRs) in the configuration of circular c-circles (Figure 34B-C) and t-circles (Figure 34D) within ATRX and DAXX deficient cells, while control and H3.3 silenced cells did not display such trends. Furthermore, the upregulation of TZAP in HeLa1.2.11 cells prompted the emergence of DNA synthesis at telomeres during the G2 phase, notably when ATRX or DAXX was not present, whereas control or H3.3 depleted cells did not exhibit similar outcomes (Figure 34E-F). Lastly, Telomere Restriction Fragments (TRF) assay conducted on HeLa1.2.11 cells with heightened TZAP expression unveiled a distribution of lower telomeric lengths within ATRX or DAXX depleted cells compared to control counterparts, indicative of telomere trimming (Figure 34G). Consequently, this observation underscores the association of ECTRs and G2-associated DNA synthesis at telomeres detected in ATRX or DAXX deficient HeLa1.2.11 cells with the process of telomere trimming.

These findings collectively affirm that the initiation of telomere trimming by TZAP within telomerase+ cells is counteracted by a functional influence exerted by the ATRX/DAXX complex, an effect that operates independently of deposition of H3.3. Of note, considering ATRX's recognized role as an ALT repressor [256], our experimental

outcomes substantiate the notion that TZAP-driven telomere trimming is facilitated through a pathway reminiscent of ALT mechanisms.

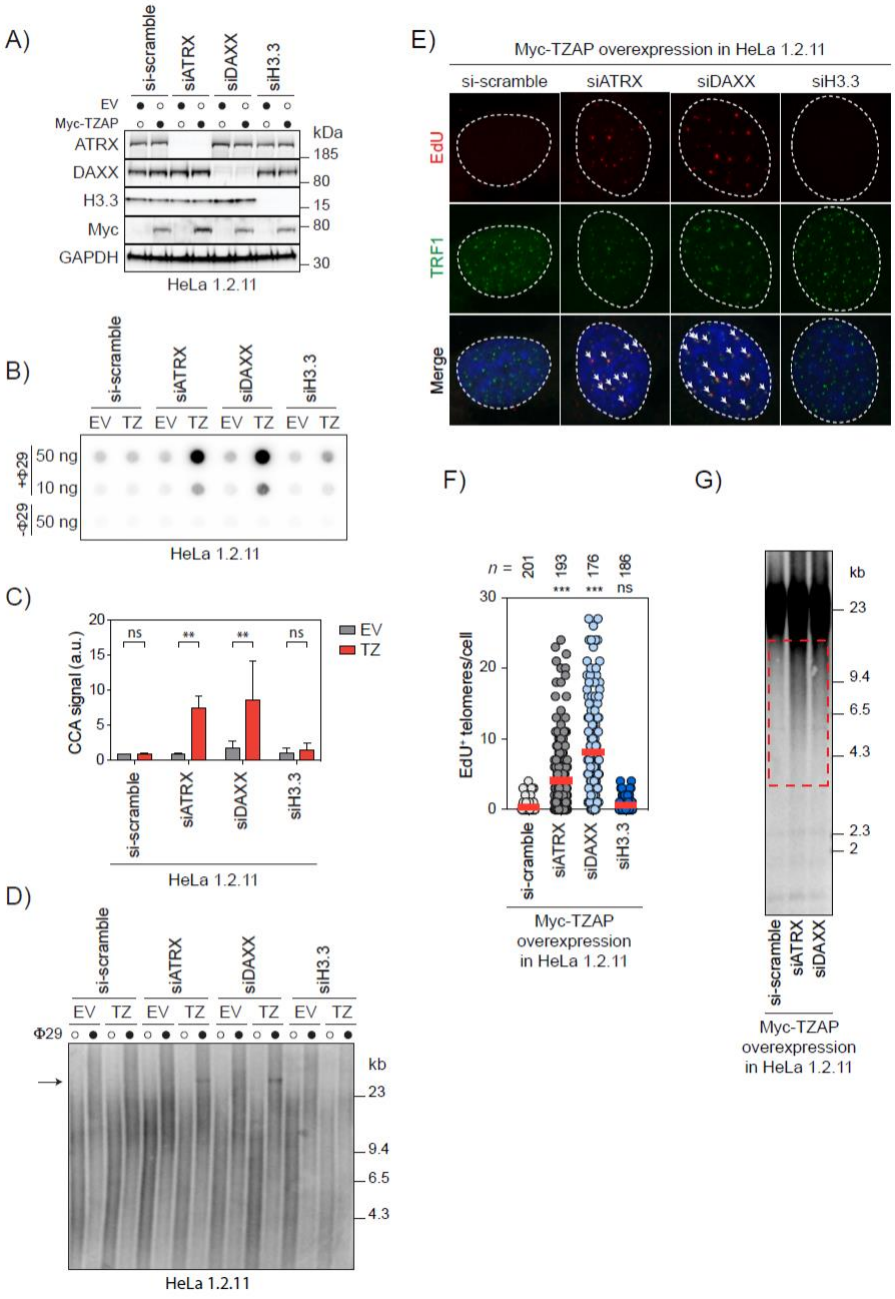

Figure 34: ATRX/DAXX represses the induction of ALT-like phenotypes in HeLa1.2.11 cells overexpressing TZAP
A) HeLa1.2.11 cells with Myc-TZAP or EV were transfected with siRNAs. Lysate was analyzed using western blotting **B)** C-circle blots of cells described in A). **C)** Quantification of C-circle blot results in B) was done relative to si-scramble treated HeLa1.2.11 with EV. The bars indicate the mean ± SD. ** $P < 0.01$, ns: non-significant. **D)** Here T-circle of cells described in A) is shown. An arrow indicates where the results of rolling circle amplification of TTAGGG-rich circular extrachromosomal DNA should be. **E)** Immunofluorescence images of G2-synchronized HeLa1.2.11 (synchronized in G2) cells with Myc-TZAP and siRNAs treated. TRF1 nuclear localization and EdU incorporated into DNA that is newly synthesized. Arrows indicate the EdU-TRF1 colocalizations. **F)** Quantification of Experiment E) as a scatter blot. 176 nuclei for every sample were analyzed. The data are representative of 2

experiments performed independently. Centre line indicates the mean. n is the analyzed number of cells. *** $P <$ 0.001, ns: non-significant. **G)** Telomere restriction fragment analysis of HeLa1.2.11 cells that overexpress Myc-TZAP and that are treated with siRNAs. The box (red dash-line) contains the short telomere restriction fragments that are generated due to telomere trimming upon siATRX and siDAXX treatments. Adapted from Moreno et al., 2023 [214] with kind permission of the publisher Elsevier.

8.3 The BTR complex is the main regulator of TZAP-induced telomere trimming

These findings underscore that the process of telomere trimming instigated by TZAP is orchestrated through a pathway bearing resemblance to Alternative Lengthening of Telomeres (ALT). Given the proposed pivotal role of the BTR (BLM-TOP3A-RMI1) complex in governing ALT [257,258], this investigation delved into the necessity of this complex for the induction of TZAP-driven telomere trimming. Leveraging the CRISPR/Cas9 methodology, U-2 OS Knock-Out (KO) clones were generated, targeting the genes encoding the BLM and RMI1 constituents of the BTR complex (259). Following this, TZAP overexpression was realized within the parental U-2 OS cells as well as these BLM and RMI1 KO clones (Figure 35A). Notably, while APB (Alt-associated PML Body) foci exhibited a substantial upsurge in both number and dimensions after upregulation of TZAP in the parental U-2 OS, as previously reported [260], these foci virtually disappeared in the BLM and RMI1 KO cells (Figure 35B), despite observable TZAP presence at telomeres (Figure 37B). Intriguingly, the heightened production of ECTRs witnessed in c-circle (Figure 35C-D) and t-circle (Figure 35E) assays in the parental U-2 OS cells upon TZAP overexpression was conspicuously inhibited in the BLM and RMI1 KO clones. Crucially, this impairment in c-circle and t-circle generation wasn't attributed to extensive telomere shortening due to a dysfunctional BTR complex, as the overall telomere length in BLM and RMI1 KO cells remained unaffected (Figure 37C). The inquiry then turned to if the BLM helicase held a requisite role in the TZAP-induced telomere trimming phenomena seen for telomerase positive cells that do not have ATRX/DAXX. For ensuing experiments, the HeLa-LT clone, a sub-clone of HeLa1.2.11 featuring an average TL of approximately 23 kb, was employed. Notably, the recruitment of the BLM at telomeres in HeLa-LT cells with upregulated TZAP, subsequent to the knock-down of ATRX and DAXX, exhibited a observable increase compared to the control and when H3.3 is knocked-

down (Figure 36A-B). Additionally, the depletion of BLM within DAXX-deficient HeLa-LT cells overexpressing TZAP (Figure 36C) significantly curtailed both c-circles (Figure 36D-E) and t-circles (Figure 36F). Furthermore, the smear of shorter telomeres observed in TRF assay upon upregulated TZAP in DAXX deficient HeLa-LT cells was obviated upon simultaneous BLM depletion (Figure 36G). Finally, the examination extended to assess the importance of other constituents of the ALT pathway - Rad52 and PML [261] - for the process of TZAP-induced telomere trimming. Additionally, scrutiny was directed towards Rad51, suggested to govern ALT by initiating homology searches between telomeres in ALT cells and mitigating replication stress at ALT telomeres [262,263]. Importantly, whereas PML played an indispensable role for TZAP-driven c-circles in DAXX-deficient HeLa-LT cells, Rad51 and Rad52 exhibited only partial necessity (Figure 37D-E).

These observations emphasize the indispensability of BTR within the pathway of TZAP-triggered telomere trimming. Furthermore, the participation of Rad51, Rad52, and PML proteins in the efficient production of c-circles within DAXX-deficient HeLa-LT cells with upregulated TZAP underscores their significance within the ALT process. The collective involvement of these factors, all vital to the correct execution of ALT, further substantiates the notion that TZAP-mediated telomere trimming finds its origins in a pathway akin to ALT.

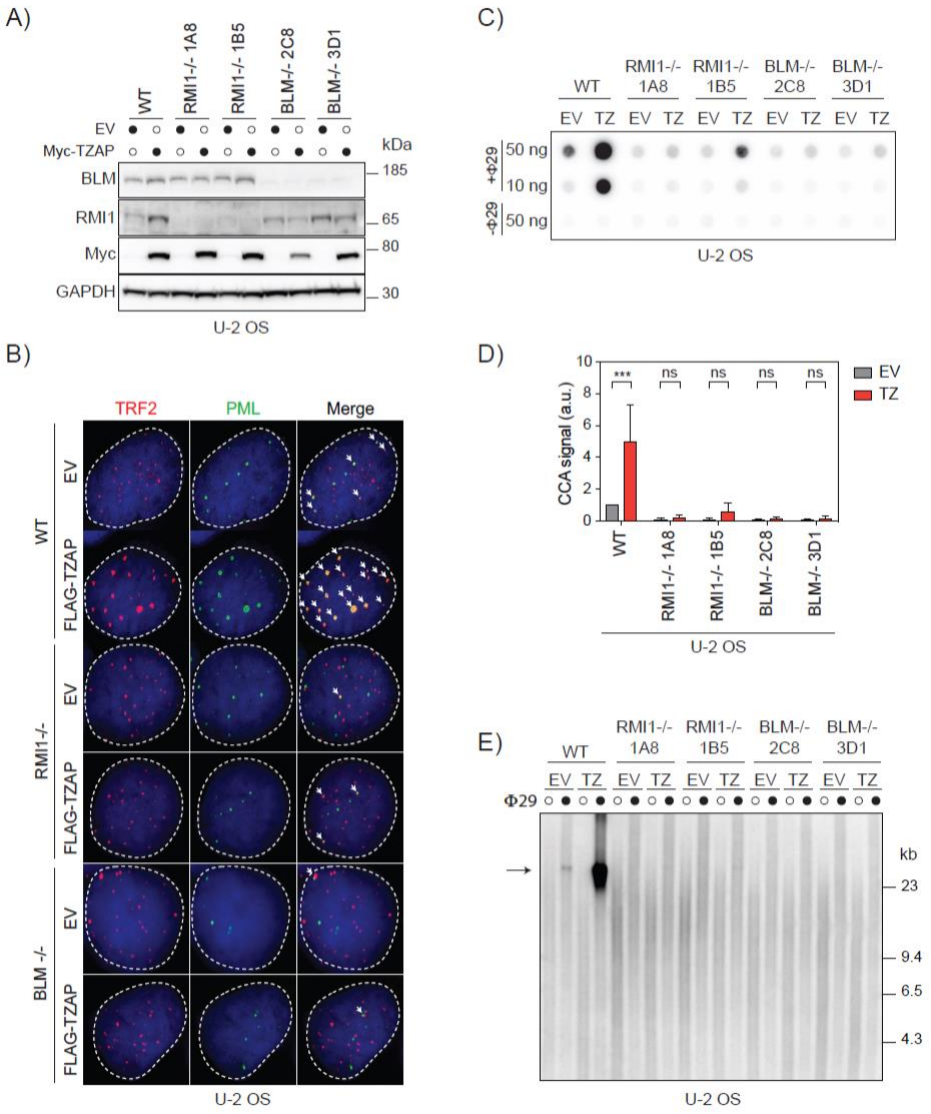

Figure 35: The BTR complex is essential for ALT phenotypes generated when TZAP is upregulated in U-2 OS. **A)** Western blot analysis (WT- parental), RMI1-/- (1A8, 1B5) and BLM-/- (2C8, 3D1) knock-out (KO) clones that overexpress Myc-TZAP or EV. **B)** Representative immunofluorescence images of parental U-2 OS and the indicated RM1-/- and BLM-/- KO clones overexpressing EV or FLAG-TZAP, showing the nuclear localization of TRF2 and PML. Arrows indicate PML-TRF2 colocalizations. **C)** C-circle assays of cells described in A). **D)** Quantification of C-circle assay signals in C), performed relative to parental U-2 OS overexpressing EV. Bars represent the mean ± SD. *** $P < 0.001$, ns: non-significant, two-way ANOVA test was used to calculate the p-values. **E)** T-circle assay of the cells described in A). Arrow is indicating where the products of rolling circle amplification of TTAGGG-rich circular extrachromosomal DNA should be. The experiment was repeated three times. Adapted from Moreno et al., 2023 [214] with kind permission of publisher “Elsevier”.

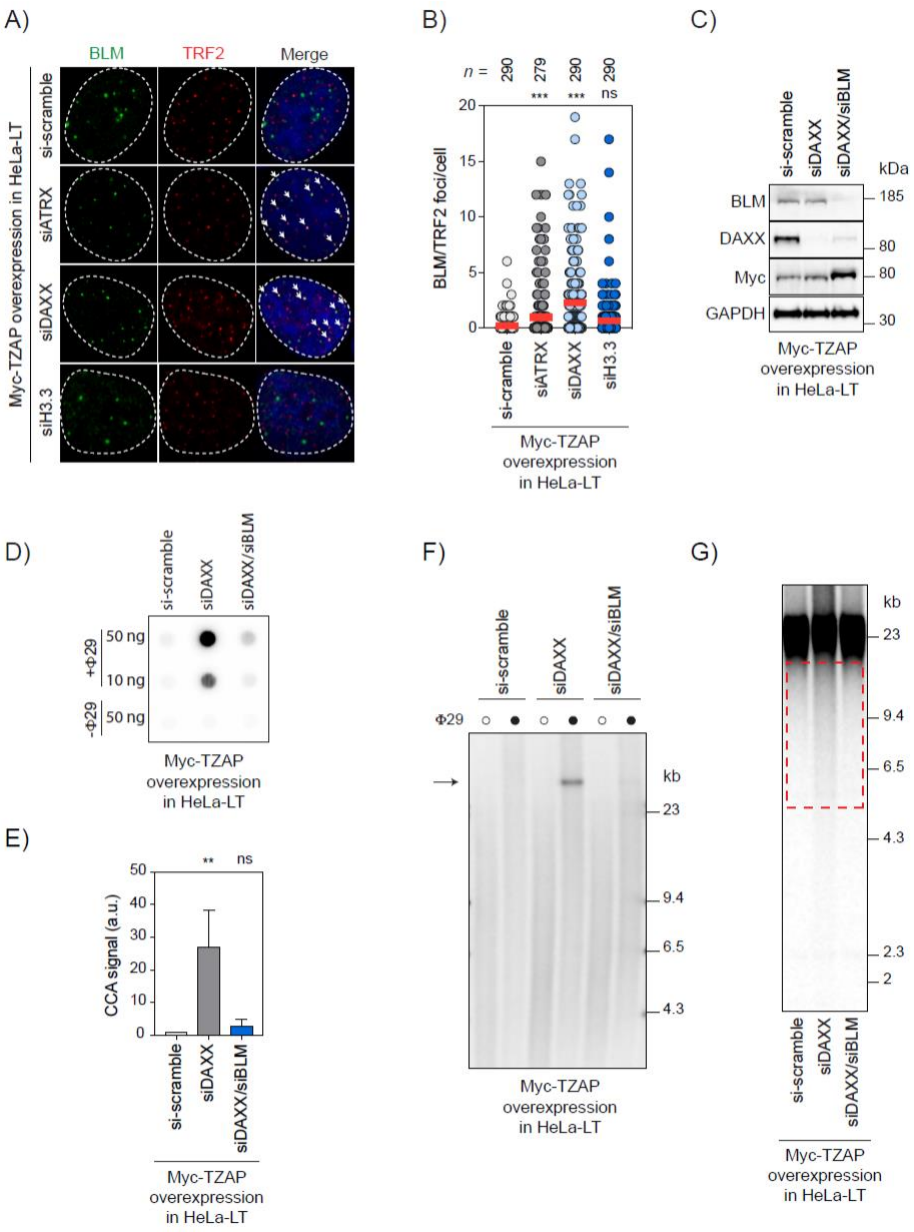

Figure 36: BLM is required for the induction of ALT-like phenotypes and telomere trimming generated upon TZAP overexpression in DAXX deficient HeLa-LT cells. **A)** Representative immunofluorescence images of HeLa-LT cells overexpressing Myc-TZAP and that are treated with siRNAs, showing localization of TRF2 and BLM in the nucleus. Arrows indicate BLM-TRF2 colocalizations. **B)** Quantification of experiment A) shown in a Scatter plot. 279 nuclei were analyzed for every sample. Data are representative of 2 independent experiments. Centre line indicates the mean. n is the analyzed number of cells. *** $P < 0.001$, ns: non-significant, one-way ANOVA test was used for the calculation of the p-value. **C)** Western blot analysis of the indicated proteins in HeLa-LT cells that overexpress Myc-TZAP and that are treated with siRNAs. **D)** C-circle assays of cells described in C). **E)** Quantification of C-circle assays signals in D) was done relative to si-scramble treated HeLa-LT cells that overexpress TZAP. Bars show the mean ± SD of three experiments done independently. ** $P < 0.01$, ns: non-significant, one-way ANOVA test was used to calculate the p-values. **F)** T-circle assay of cells described in C). Arrow indicates where the result of rolling circle amplification of TTAGGG-rich circular extrachromosomal DNA should be. The experiment was done three times independently. **G)** TRF assay of HeLa-LT cells that overexpress Myc-TZAP and that are treated with si-RNAs. The box (red dash-line) contains the short telomere restriction fragments that are generated due to telomere trimming upon siDAXX treatment alone. The experiment was done two times. Adapted from Moreno et al., 2023 [214] with permission of the publisher Elsevier.

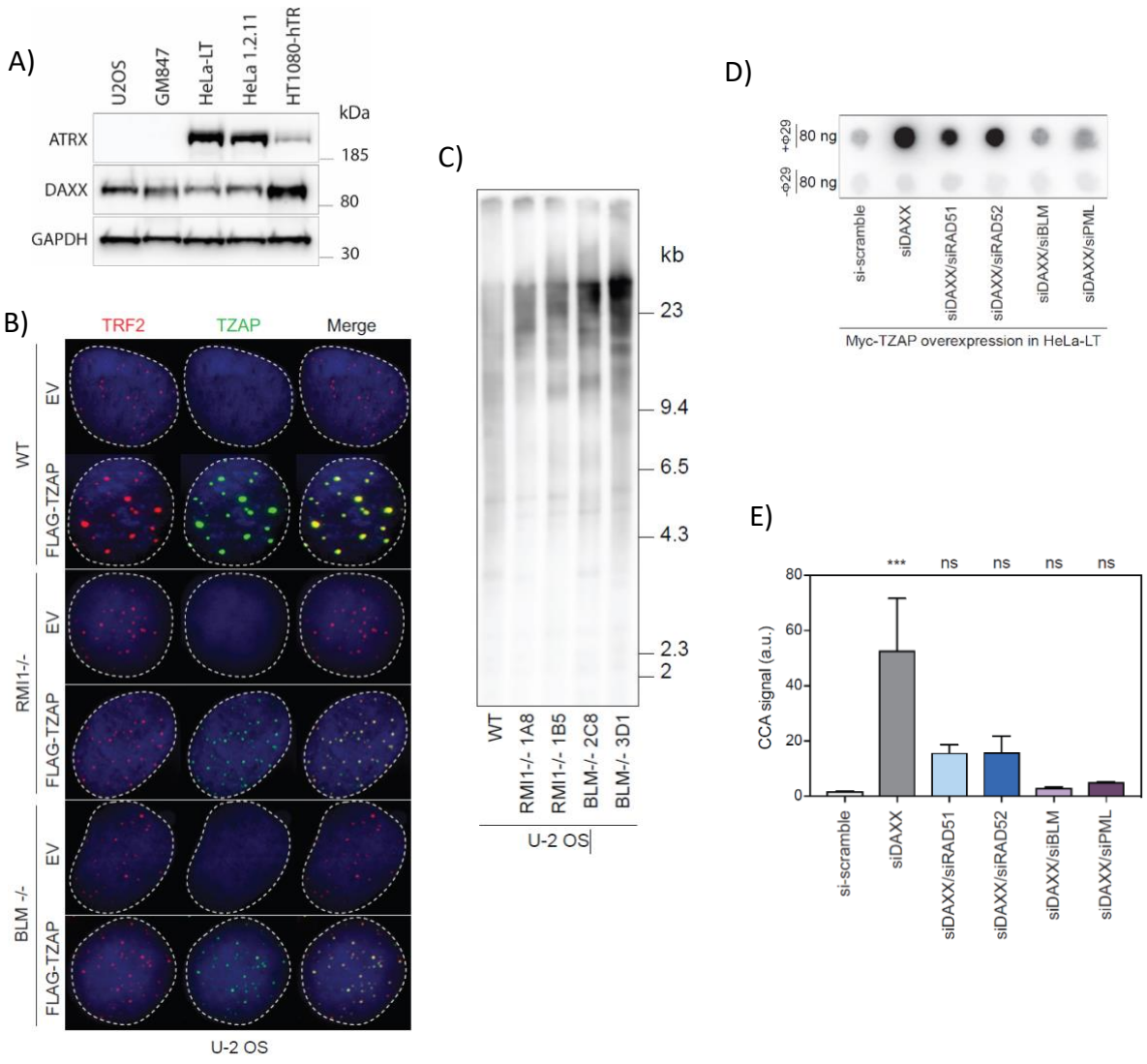

Figure 37: A) Western blot analysis of ATRX, DAXX and GAPDH in ALT positive (U2OS, GM847) and telomerase positive (HeLa-LT, HeLa 1.2.11 and HT1080-hTR) cell lines. B) Representative immunofluorescence images of parental U2OS (WT) and the indicated RM1-/- an BLM -/- KO clones that overexpress FLAG-TZAP or empty vector (EV), showing the nuclear localization of TRF2 and FLAG-TZAP. C) TRF analysis of parental U2OS cells, as well as RMI1 -/- (1A8, 1B5) and BLM -/- (2C8, 3D1) KO clones. D) CCA of HeLa-LT cells with upregulated TZAP and treated with indicated siRNAs. E) Quantification of CCA signals in D), performed relative to si-scramble treated HeLa-LT cells that overexpress TZAP. Bars represent the mean SD of three experiments performed independently ($p<0.001$) Adapted from Moreno et al., 2023 [214] with kind permission of the publisher Elsevier.

9 Discussion

Telomere trimming, originally thought to depend solely on HR-dependent excision of the t-loop, lacks conclusive experimental evidence supporting this as the sole mechanism governing regulated telomere trimming. Conversely, it is well-documented that long telomeres are susceptible to replication stress. Cells exposed to replication-stress-inducing drugs or lacking key DNA replication proteins exhibit elevated levels of ECTRs, telomere loss, and dysfunction, all indicative of intensified telomere trimming [264, 265, 266]. Intriguingly, cells undergoing telomere trimming often display hallmarks of ALT^+ cells, including ECTRs and APBs [267]. Like ALT, telomere trimming relies on HR factors [268]. However, the common regulatory pathways governing telomere trimming and ALT have been relatively unexplored, primarily because trimming leads to telomere shortening, while ALT typically results in telomere elongation. The findings at hand show that overexpression of TZAP can induce stress at telomeres during replication. This is evident from the upregulation of ATR (Figure 33B), upregulation of RPA (Figure 33C-D), and the exacerbation of ECTRs (Figure 35C-E). Moreover, a heightened telomeric DNA synthesis during the G2 phase was observed (Figure 33E-F). Notably, all these phenotypes align with established ALT characteristics. However, ALT^+ cells with elevated TZAP experience cell death and telomere attrition [3]. Of note, FANCM-deficient ALT^+ cells exhibit analogous traits (58). In the absence of FANCM, the stress of replication intensifies, and mechanisms of repair that go along ALT fail to sustain telomeric stability, culminating in cell death. Consequently, it has been brought forward that FANCM alleviates stress of replication at ALT telomeres by facilitating the reinitiation of replication forks [269] Therefore, it is possible that the introduction of TZAP onto telomeres triggers trimming by inducing stalled replication forks, depleting enzymes engaged in replication fork remodeling and reinitiation. This sequence of events culminates in inefficient activation of ALT, ensuing the loss of telomers, and cell death [3]. The BTR complex, consisting of three main proteins - BLM, TOP3A, and RMI1 - is crucial in not just repair, but also in recombination and replication [270]. This complex has also been identified as a central component of ALT [271]. The findings at hand reveal that the upregulation of TZAP leads to upregulated APB formation in ALT cells, contingent on the intact BTR complex (Figure 35B). This outcome indicates that

TZAP-induced recruitment of telomeres to APBs mirrors the BTR-dependent mechanism previously observed in ALT [272]. Furthermore, it was observed that the emergence of ECTRs induced by upregulated TZAP relies on the BTR complex in ALT (Figure 35C-E) which aligns with earlier research where in FANCM-deficient ALT$^+$ cells, the generation of ECTRs showed to be relying on BTR [273]. Additionally, the findings indicate that ECTRs resulting from upregulated TZAP in telomerase positive but DAXX-negative cells are relying on BLM (Figure 36D-F). It is likely that BTR has a role in resolving telomeric replication stress in telomere trimming that is triggered by TZAP. To conclude, the data suggest a trimming of telomeres induced through TZAP in cells that lack ATRX/DAXX, in which endogenous TZAP would sense and load on very long telomeres, leading to telomere trimming through the engagement of a pathway similar to ALT and which relies on BTR (Figure 38).

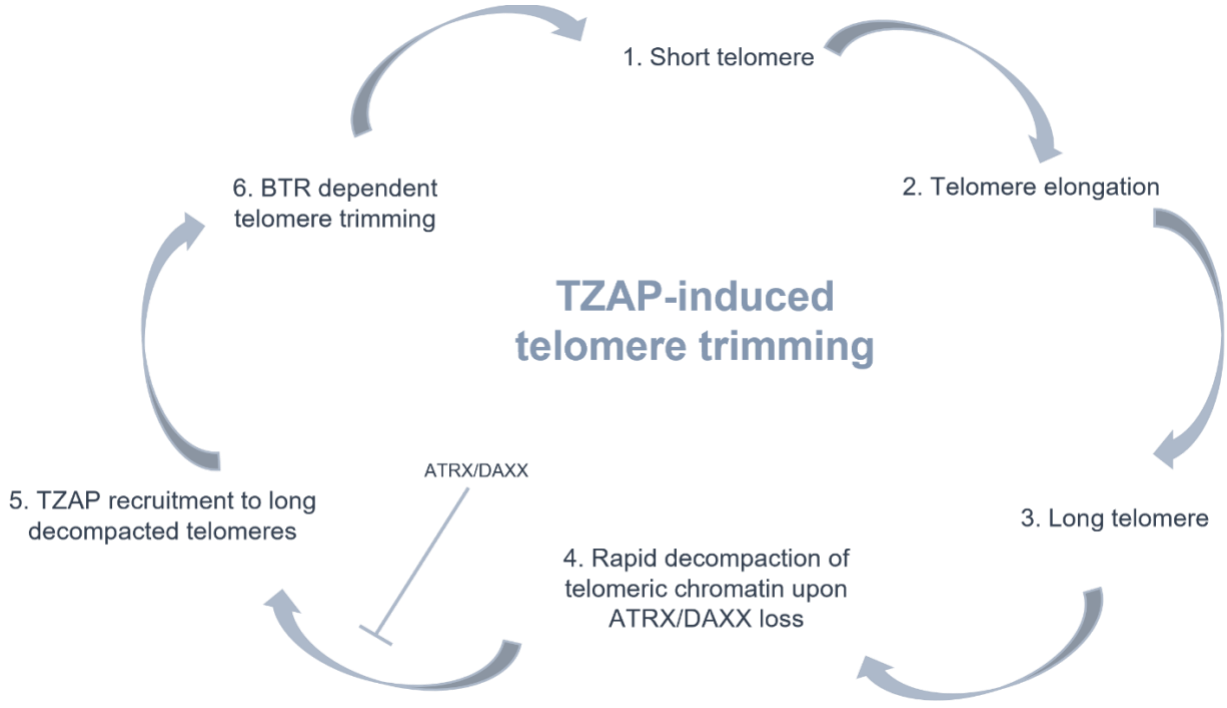

Figure 38: Hypothetical model of TZAP induced telomere trimming. Telomere elongation leads to over-elongated telomeres. Telomeres become rapidly de-compacted in the absence of ATRX/DAXX. TZAP is recruited to long and de-compacted telomeres. This results in the induction of replication stress at telomeres and the engagement of a BTR-dependent ALT-like pathway that promotes telomere trimming. Image created with Microsoft PowerPoint.

10 Bibliography

1 Rossiello F, Jurk D, Passos JF, d'Adda di Fagagna F. Telomere dysfunction in ageing and age-related diseases. Nat Cell Biol. 2022 Feb;24(2):135-147.

2 Kaiser M, Thurner EM, Mangge H, Herrmann M, Semeraro MD, Renner W, Langsenlehner T. Haptoglobin polymorphism and prostate cancer mortality. Sci Rep. 2020 Aug 4;10(1):13117.

3 Li JS, Miralles Fusté J, Simavorian T, Bartocci C, Tsai J, Karlseder J, Lazzerini Denchi E. TZAP: A telomere-associated protein involved in telomere length control. Science. 2017 Feb 10;355(6325):638-641.

4 Zaretsky, J.M.; Garcia-Diaz, A.; Shin, D.S.; Escuin-Ordinas, H.; Hugo,W.; Hu-Lieskovan, S.; Torrejon, D.Y.; Abril-Rodriguez, G.; Sandoval, S.; Barthly, L.; et al. Mutations Associated with Acquired Resistance to PD-1 Blockade in Melanoma. N. Engl. J. Med. 2016, 375, 819–829.

5 Topalian, S.L.; Hodi, F.S.; Brahmer, J.R.; Gettinger, S.N.; Smith, D.C.; McDermott, D.F.; Powderly, J.D.; Sosman, J.A.; Atkins, M.B.; Leming, P.D.; et al. Five-Year Survival and Correlates Among Patients with Advanced Melanoma, Renal Cell Carcinoma, or Non–Small Cell Lung Cancer Treated with Nivolumab. JAMA Oncol. 2019, 5, 1411–1420.

6 Champiat S., Dercle L., Ammari S., Massard C., Hollebecque A., Postel-Vinay S., Chaput N., Eggermont A.M., Marabelle A., Soria J.-C., et al. Hyperprogressive Disease Is a New Pattern of Progression in Cancer Patients Treated by Anti-PD-1/PD-L1. Clin. Cancer Res. 2017;23:1920–1928.

7 Postow MA, Sidlow R, Hellmann MD. Immune-Related Adverse Events Associated with Immune Checkpoint Blockade. N Engl J Med. 2018 Jan 11;378(2):158-168.

8 Ferlay, J.; Colombet, M.; Soerjomataram, I.; Mathers, C.; Parkin, D.M.; Piñeros, M.; Znaor, A.; Bray, F. Estimating the Global Cancer Incidence and Mortality in 2018: GLOBOCAN Sources and Methods. Int. J. Cancer 2019, 144, 1941–1953.

9 Havel JJ, Chowell D, Chan TA. The Evolving Landscape of Biomarkers for Checkpoint Inhibitor Immunotherapy. Nat Rev Cancer 2019, 19:133–50.

10 Lantuejoul S, Sound-Tsao M, Cooper WA, et al. PD-L1 testing for lung cancer in 2019: perspective from the IASLC pathology committee. J Thorac Oncol. 2020;15:499–519.

11 Sholl LM, Hirsch FR, Hwang D, et al. The promises and challenges of tumor mutation burden as an immunotherapy biomarker: a perspective from the International Association for the Study of Lung Cancer Pathology Committee. J Thorac Oncol. 2020;15:1409–1424.

12 Lee JS, Ruppin E. Multiomics prediction of response rates to therapies to inhibit programmed cell death 1 and programmed cell death 1 ligand 1. JAMA Oncol. 2019;5:1614–1618.

13 Lu S, Stein JE, Rimm DL, et al. Comparison of biomarker modalities for predicting response to PD-1/PD-L1 checkpoint blockade: a systematic review and metaanalysis. JAMA Oncol. 2019;5:1195–1204.

14 Ferrara R, Naigeon M, Auclin E, Duchemann B, Cassard L, Jouniaux JM, Boselli L, Grivel J, Desnoyer A, Mezquita L, Texier M, Caramella C, Hendriks L, Planchard D, Remon J, Sangaletti S, Proto C, Garassino MC, Soria JC, Marabelle A, Voisin AL, Farhane S, Besse B, Chaput N. Circulating T-cell Immunosenescence in Patients with Advanced Non-small Cell Lung Cancer Treated with Single-agent PD-1/PD-L1 Inhibitors or Platinum-based Chemotherapy. Clin Cancer Res. 2021 Jan 15;27(2):492-503.

15 Weischer M, Nordestgaard BG, Cawthon RM, Freiberg JJ, Tybjærg-Hansen A, Bojesen SE. Short telomere length, cancer survival, and cancer risk in 47102 individuals. J Natl Cancer Inst. 2013 Apr 3;105(7):459-68.

16 Dimri, G.P.; Lee, X.; Basile, G.; Acosta, M.; Scott, G.; Roskelley, C.; Medrano, E.E.; Linskens, M.; Rubelj, I.; Pereira-Smith, O.; et al. A biomarker that identifies senescent human cells in culture and in aging skin in vivo. Proc. Natl. Acad. Sci. USA 1995, 92, 9363–9367.

17 Faugeras E, Véronèse L, Jeannin G, Janicot H, Bailly S, Bay JO, Pereira B, Cayre A, Penault-Llorca F, Cachin F, Merle P, Tchirkov A. Telomere Status of Advanced Non-Small-Cell Lung Cancer Offers a Novel Promising Prognostic and Predictive Biomarker. Cancers (Basel). 2022 Dec 31;15(1):290.

18 Rolles B, Gorgulho J, Tometten M, Roderburg C, Vieri M, Abels A, Vucur M, Heymann F, Tacke F, Brümmendorf TH, Luedde T, Beier F, Loosen SH. Telomere Shortening in Peripheral Leukocytes Is Associated With Poor Survival in Cancer Patients Treated With Immune Checkpoint Inhibitor Therapy. Front Oncol. 2021 Aug 19;11:729207.

19 Lansdorp PM, Verwoerd NP, van de Rijke FM, Dragowska V, Little MT, Dirks RW, Raap AK, Tanke HJ. Heterogeneity in telomere length of human chromosomes. Hum Mol Genet. 1996 May;5(5):685-91.

20 Makarov VL, Hirose Y, Langmore JP. Long G tails at both ends of human chromosomes suggest a C strand degradation mechanism for telomere shortening. Cell. 1997;88(5):657-66.

21 McElligott R, Wellinger RJ. The terminal DNA structure of mammalian chromosomes. EMBO J. 1997;16(12):3705-14.

22 Kim SH, Kaminker P, Campisi J. TIN2, a new regulator of telomere length in human cells. Nat Genet. 1999 Dec;23(4):405-12.

23 Ye JZ, Donigian JR, van Overbeek M, Loayza D, Luo Y, Krutchinsky AN, Chait BT, de Lange T. TIN2 binds TRF1 and TRF2 simultaneously and stabilizes the TRF2 complex on telomeres. J Biol Chem. 2004 Nov 5;279(45):47264-71.

24 Frank AK, Tran DC, Qu RW, Stohr BA, Segal DJ, Xu L. The Shelterin TIN2 Subunit Mediates Recruitment of Telomerase to Telomeres. PLoS Genet. 2015 Jul 31;11(7):e1005410.

25 Xin H, Liu D, Wan M, Safari A, Kim H, Sun W, O'Connor MS, Songyang Z. TPP1 is a homologue of ciliate TEBP-beta and interacts with POT1 to recruit telomerase. Nature. 2007 Feb 1;445(7127):559-62.

26 Colgin LM, Baran K, Baumann P, Cech TR, Reddel RR. Human POT1 facilitates telomere elongation by telomerase. Curr Biol. 2003 May 27;13(11):942-6.

27 Hockemeyer D, Sfeir AJ, Shay JW, Wright WE, de Lange T. POT1 protects telomeres from a transient DNA damage response and determines how human chromosomes end. EMBO J. 2005 Jul 20;24(14):2667-78.

28 Rai R, Chen Y, Lei M, Chang S. TRF2-RAP1 is required to protect telomeres from engaging in homologous recombination-mediated deletions and fusions. Nat Commun. 2016 Mar 4;7:10881.

29 Griffith JD, Comeau L, Rosenfield S, Stansel RM, Bianchi A, Moss H, et al. Mammalian telomeres end in a large duplex loop. Cell. 1999;97(4):503-14.

30 Palm W, de Lange T. How shelterin protects mammalian telomeres. Annu Rev Genet. 2008;42:301-34.

31 Harley CB, Futcher AB, Greider CW. Telomeres shorten during ageing of human fibroblasts. Nature. 1990 May 31;345(6274):458-60.

32 Huffman KE, Levene SD, Tesmer VM, Shay JW, Wright WE. Telomere shortening is proportional to the size of the G-rich telomeric 3'-overhang. J Biol Chem. 2000 Jun 30;275(26):19719-22.

33 Zvereva MI, Shcherbakova DM, Dontsova OA. Telomerase: structure, functions, and activity regulation. Biochemistry (Mosc). 2010 Dec;75(13):1563-83.

34 Sharpless NE, DePinho RA. How stem cells age and why this makes us grow old. Nat Rev Mol Cell Biol. 2007 Sep;8(9):703-13.

35 Hastie ND, Dempster M, Dunlop MG, Thompson AM, Green DK, Allshire RC. Telomere reduction in human colorectal carcinoma and with ageing. Nature. 1990 Aug 30;346(6287):866-8.

36 Bodnar AG, Ouellette M, Frolkis M, Holt SE, Chiu CP, Morin GB, Harley CB, Shay JW, Lichtsteiner S, Wright WE. Extension of life-span by introduction of telomerase into normal human cells. Science. 1998 Jan 16;279(5349):349-52.

37 Rossiello F, Jurk D, Passos JF, d'Adda di Fagagna F. Telomere dysfunction in ageing and age-related diseases. Nat Cell Biol. 2022 Feb;24(2):135-147.

38 Maciejowski J, de Lange T. Telomeres in cancer: tumour suppression and genome instability. Nat Rev Mol Cell Biol. 2017 Mar;18(3):175-186.

39 Guterres AN, Villanueva J. Targeting telomerase for cancer therapy. Oncogene. 2020 Sep;39(36):5811-5824.

40 Ellingsen EB, Mangsbo SM, Hovig E, Gaudernack G. Telomerase as a Target for Therapeutic Cancer Vaccines and Considerations for Optimizing Their Clinical Potential. Front Immunol. 2021 Jul 5;12:682492.

41 MacKenzie D Jr, Watters AK, To JT, Young MW, Muratori J, Wilkoff MH, Abraham RG, Plummer MM, Zhang D. ALT Positivity in Human Cancers: Prevalence and Clinical Insights. Cancers (Basel). 2021 May 14;13(10):2384.

42 Kaiser M, Semeraro MD, Herrmann M, Absenger G, Gerger A, Renner W. Immune Aging and Immunotherapy in Cancer. Int J Mol Sci. 2021 Jun 29;22(13):7016.

43 Rafael Solana, Graham Pawelec, Raquel Tarazona. Aging and Innate Immunity, Immunity, Volume 24, Issue 5, 2006, Pages 491-494, ISSN 1074-7613.

44 David D. Chaplin. Overview of the Immune Response. J Allergy Clin Immunol. 2010 Feb; 125(2 Suppl 2): S3–23.

45 Childs BG, Durik M, Baker DJ, van Deursen JM. Cellular senescence in aging and age-related disease: from mechanisms to therapy. Nat Med. 2015;21(12):1424-1435.

46 Akbar AN, Fletcher JM. Memory T cell homeostasis and senescence during aging. Curr Opin Immunol. 2005 Oct;17(5):480-5.

47 Weng NP. Aging of the immune system: how much can the adaptive immune system adapt? Immunity. 2006 May;24(5):495-9.

48 Hayflick L, Moorehead P.S. The serial cultivation of human diploid cell strains. Exp Cell Res. 1961 Dec;25:585-621.

49 HAYFLICK L. THE LIMITED IN VITRO LIFETIME OF HUMAN DIPLOID CELL STRAINS. Exp Cell Res. 1965 Mar;37:614-36.

50 Harley CB, Futcher AB, Greider CW. Telomeres shorten during ageing of human fibroblasts. Nature. 1990 May 31; 345(6274):458-60.

51 de Lange T. Cell biology. Telomere capping--one strand fits all. Science. 2001 May 11;292(5519):1075-6.

52 Serrano M, Lin AW, McCurrach ME, Beach D, Lowe SW. Oncogenic ras provokes premature cell senescence associated with accumulation of p53 and p16INK4a. Cell. 1997 Mar 7;88(5):593-602.

53 te Poele RH, Okorokov AL, Jardine L, Cummings J, Joel SP. DNA damage is able to induce senescence in tumor cells in vitro and in vivo. Cancer Res. 2002 Mar 15;62(6):1876-83.

54 Charlotte Chandeck, Wolter J Mooi. Oncogene-induced cellular senescence. Adv Anat Pathol.2010 Jan;17(1):42-8.

55 Schwörer S, Becker F, Feller C, Baig AH, Köber U, Henze H, Kraus JM, Xin B, Lechel A, Lipka DB, Varghese CS, Schmidt M, Rohs R, Aebersold R, Medina KL, Kestler HA, Neri F, von Maltzahn J, Tümpel S, Rudolph KL. Epigenetic stress responses induce muscle stem-cell ageing by Hoxa9 developmental signals. Nature. 2016 Dec 15;540(7633):428-432.

56 Judith Campisi , Fabrizio d'Adda di Fagagna. Cellular senescence: when bad things happen to good cells. Nat Rev Mol Cell Biol. 2007 Sep;8(9):729-40.

57 Toussaint O, Medrano EE, von Zglinicki T. Cellular and molecular mechanisms of stress-induced premature senescence (SIPS) of human diploid fibroblasts and melanocytes. Exp Gerontol. (2000) 35:927–45.

58 Chen QM, Bartholomew JC, Campisi J, Acosta M, Reagan JD, Ames BN. Molecular analysis of H2O2-induced senescent-like growth arrest in normal human fibroblasts: p53 and Rb control G1 arrest but not cell replication. Biochem J. 1998 May 15;332 (Pt 1)(Pt 1):43-50.

59 J W Shay, O M Pereira-Smith, W E Wright. A role for both RB and p53 in the regulation of human cellular senescence. Exp Cell Res 1991 Sep;196(1):33-9.

60 Nassour, J., Aguiar, L.G., Correia, A. et al. Telomere-to-mitochondria signalling by ZBP1 mediates replicative crisis. Nature 614, 767–773 (2023).

61 Seoane, M., Costoya, J.A. & Arce, V.M. Uncoupling Oncogene-Induced Senescence (OIS) and DNA Damage Response (DDR) triggered by DNA hyper-replication: lessons from primary mouse embryo astrocytes (MEA). Sci Rep 7, 12991 (2017).

62 Criscione SW, Teo YV, Neretti N. The Chromatin Landscape of Cellular Senescence. Trends Genet. 2016;32(11):751-761.

63 Judith Campisi. Aging, cellular senescence, and cancer. Annu Rev Physiol. 2013;75:685-705.

64 Coppé JP, Desprez PY, Krtolica A, Campisi J. The senescence-associated secretory phenotype: the dark side of tumor suppression. Annu Rev Pathol. 2010;5:99-118.

65 Coppe, J. P. et al. Tumor suppressor and aging biomarker p16(INK4a) induces cellular senescence without the associated inflammatory secretory phenotype. J. Biol. Chem.286, 36396–36403 (2011).

66 Faget DV, Ren Q, Stewart SA. Unmasking senescence: context-dependent effects of SASP in cancer. Nat Rev Cancer. 2019 Aug;19(8):439-453.

67 Demaria M, Ohtani N, Youssef SA, Rodier F, Toussaint W, Mitchell JR, Laberge RM, Vijg J, Van Steeg H, Dollé ME, Hoeijmakers JH, de Bruin A, Hara E, Campisi J. An essential role for senescent cells in optimal wound healing through secretion of PDGF-AA. Dev Cell. 2014 Dec 22;31(6):722-33.

68 Coppe, J. P. et al. Senescence- associated secretory phenotypes reveal cell- nonautonomous functions of oncogenic RAS and the p53 tumor suppressor. PLOS Biol.6, 2853–2868 (2008).

69 Jean-Philippe Coppé, Pierre-Yves Desprez, Ana Krtolica, and Judith Campisi. The Senescence-Associated Secretory Phenotype: The Dark Side of Tumor Suppression. Annu Rev Pathol. 2010; 5: 99–118.

70 Jörg J Goronzy, Cornelia M Weyand. Mechanisms underlying T cell ageing. Nat Rev Immunol.2019;19(9):573-583.

71 Graham Pavelec. Immunosenescence and cancer. Biogerontology. 2017;18(4):717-721.

72 Rita B Effros. Roy Walford and the immunologic theory of aging. Immun Ageing. 2005; 2: 7.

73 Graham Pawelec. Hallmarks of human “immunosenescence”: adaptation or dysregulation? Immun Ageing. 2012; 9: 15.

74 Jörg J Goronzy & Cornelia M Weyand. Understanding immunosenescence to improve responses to vaccines. Nat Immunol 14, 428–436 (2013).

75 Rishi Vishal Luckheeram, Rui Zhou, Asha Devi Verma, and Bing Xia. CD4+T Cells: Differentiation and Functions. Clin Dev Immunol. 2012; 2012: 925135.

76 Brahma V. Kumar, Thomas Connors, and Donna L. Farber. Human T cell development, localization, and function throughout life. Immunity. 2018 Feb 20; 48(2): 202–213.

77 den Braber I, Mugwagwa T, Vrisekoop N, Westera L, Mögling R, de Boer AB, Willems N, Schrijver EH, Spierenburg G, Gaiser K, Mul E, Otto SA, Ruiter AF, Ackermans MT, Miedema F, Borghans JA, de Boer RJ, Tesselaar K. Maintenance of peripheral naive T cells is sustained by thymus output in mice but not humans. Immunity. 2012 Feb 24; 36(2):288-97.

78 Jörg J. Goronzy and Cornelia M. Weyand. Successful and Maladaptive T Cell Aging. Immunity. 2017 Mar 21; 46(3): 364–378.

79 Whiting CC, Siebert J, Newman AM, Du HW, Alizadeh AA, Goronzy J, Weyand CM, Krishnan E, Fathman CG, Maecker HT. Large-Scale and Comprehensive Immune Profiling and Functional Analysis of Normal Human Aging. PLoS One. 2015 Jul 21;10(7):e0133627.

80 Liset Westera, Julia Drylewicz, Ineke den Braber et. al. Closing the gap between T-cell life span estimates from stable isotope-labeling studies in mice and humans. Blood (2013) 122 (13): 2205–2212.

81 Ronald H. Schwartz. T Cell Anergy. Annual Review of Immunology 2003 21:1, 305-334.
82 Maier, C.C., Greene, M.I. Biochemical features of anergic T cells. Immunol Res 17, 133–140 (1998).
83 Andrew D. Wells. New Insights into the Molecular Basis of T Cell Anergy: Anergy Factors, Avoidance Sensors, and Epigenetic Imprinting. J Immunol June 15, 2009, 182 (12) 7331-7341.
84 Thomas RM, Chunder N, Chen C, Umetsu SE, Winandy S, Wells AD. Ikaros enforces the costimulatory requirement for IL2 gene expression and is required for anergy induction in CD4+ T lymphocytes. J Immunol. 2007 Dec 1;179(11):7305-15.
85 Gao B, Kong Q, Kemp K, Zhao YS, Fang D. Analysis of sirtuin 1 expression reveals a molecular explanation of IL-2-mediated reversal of T-cell tolerance. Proc Natl Acad Sci U S A. 2012 Jan 17;109(3):899-904.
86 Bandyopadhyay S, Duré M, Paroder M, Soto-Nieves N, Puga I, Macián F. Interleukin 2 gene transcription is regulated by Ikaros-induced changes in histone acetylation in anergic T cells. Blood. 2007 Apr 1;109(7):2878-86.
87 Zheng Y, Zha Y, Driessens G, Locke F, Gajewski TF. Transcriptional regulator early growth response gene 2 (Egr2) is required for T cell anergy in vitro and in vivo. J Exp Med. 2012 Nov 19;209(12):2157-63.
88 Jiang Y, Li Y, Zhu B. T-cell exhaustion in the tumor microenvironment. Cell Death Dis. 2015 Jun 18;6(6):e1792.
89 Barber DL, Wherry EJ, Masopust D, Zhu B, Allison JP, Sharpe AH, et al. Restoring function in exhausted CD8 T cells during chronic viral infection. Nature (2006) 439:682–7.
90 Zhou Q, Munger ME, Veenstra RG, Weigel BJ, Hirashima M, Munn DH, Murphy WJ, Azuma M, Anderson AC, Kuchroo VK, Blazar BR. Coexpression of Tim-3 and PD-1 identifies a CD8+ T-cell exhaustion phenotype in mice with disseminated acute myelogenous leukemia. Blood. 2011 Apr 28;117(17):4501-10.
91 Ferris RL, Lu B, Kane LP. Too much of a good thing? Tim-3 and TCR signaling in T cell exhaustion. J Immunol. (2014) 193:1525–30.
92 Richter K, Agnellini P, Oxenius A. On the role of the inhibitory receptor LAG-3 in acute and chronic LCMV infection. Int Immunol. (2010) 22:13–23.
93 Khaitan A, Unutmaz D. Revisiting immune exhaustion during HIV infection. Curr HIV/AIDS Rep. (2011) 8:4–11.
94 Chew GM, Fujita T, Webb GM, Burwitz BJ, Wu HL, Reed JS, et al. TIGIT marks exhausted T cells, correlates with disease progression, and serves as a target for immune restoration in HIV and SIV Infection. PLoS Pathog. (2016) 12:e1005349.
95 McLane, L. M., Abdel- Hakeem, M. S. & Wherry, E. J. CD8 T cell exhaustion during chronic viral infection and cancer. Annu. Rev. Immunol.37, 457–495 (2019)
96 Wherry, E. J. & Kurachi, M. Molecular and cellular insights into T cell exhaustion.Nat. Rev. Immunol.15, 486–499 (2015).
97 Pawelec G. Is There a Positive Side to T Cell Exhaustion?. Front Immunol. 2019;10:111. Published 2019 Jan 29. doi:10.3389/fimmu.2019.00111
98 Liu X, Mo W, Ye J, Li L, Zhang Y, Hsueh EC, Hoft DF, Peng G. Regulatory T cells trigger effector T cell DNA damage and senescence caused by metabolic competition. Nat Commun. 2018 Jan 16;9(1):249.
99 Ye J, Huang X, Hsueh EC, Zhang Q, Ma C, Zhang Y, Varvares MA, Hoft DF, Peng G. Human regulatory T cells induce T-lymphocyte senescence. Blood. 2012 Sep 6;120(10):2021-31.
100 Pawelec G. Is There a Positive Side to T Cell Exhaustion? Front Immunol. 2019 Jan 29;10:111.
101 Wherry EJ, Kurachi M. Molecular and cellular insights into T cell exhaustion. Nat Rev Immunol. 2015;15(8):486-499.
102 Dimri GP, Lee X, Basile G, et al. A biomarker that identifies senescent human cells in culture and in aging skin in vivo. Proc Natl Acad Sci U S A. 1995;92(20):9363-9367. doi:10.1073/pnas.92.20.9363

103 Brenchley JM, Karandikar NJ, Betts MR, Ambrozak DR, Hill BJ, Crotty LE, Casazza JP, Kuruppu J, Migueles SA, Connors M, Roederer M, Douek DC, Koup RA. Expression of CD57 defines replicative senescence and antigen-induced apoptotic death of CD8+ T cells. Blood. 2003 Apr 1;101(7):2711-20.

104 Di Mitri D, Azevedo RI, Henson SM, Libri V, Riddell NE, Macaulay R, Kipling D, Soares MV, Battistini L, Akbar AN. Reversible senescence in human CD4+CD45RA+CD27- memory T cells. J Immunol. 2011 Sep 1;187(5):2093-100.

105 Riddell NE, Griffiths SJ, Rivino L, King DC, Teo GH, Henson SM, Cantisan S, Solana R, Kemeny DM, MacAry PA, Larbi A, Akbar AN. Multifunctional cytomegalovirus (CMV)-specific CD8(+) T cells are not restricted by telomere-related senescence in young or old adults. Immunology. 2015 Apr;144(4):549-60.

106 Chou JP, Effros RB. T cell replicative senescence in human aging. Curr Pharm Des. 2013;19(9):1680-98.

107 Muñoz-Espín D, Serrano M. Cellular senescence: from physiology to pathology. Nat Rev Mol Cell Biol. 2014 Jul;15(7):482-96.

108 Ye J, Huang X, Hsueh EC, Zhang Q, Ma C, Zhang Y, Varvares MA, Hoft DF, Peng G. Human regulatory T cells induce T-lymphocyte senescence. Blood. 2012 Sep 6;120(10):2021-31.

109 Ye J, Ma C, Hsueh EC, Eickhoff CS, Zhang Y, Varvares MA, Hoft DF, Peng G. Tumor-derived γδ regulatory T cells suppress innate and adaptive immunity through the induction of immunosenescence. J Immunol. 2013 Mar 1;190(5):2403-14.

110 Yangjing Zhao, Qixiang Shao, and Guangyong Peng. Exhaustion and senescence: two crucial dysfunctional states of T cells in the tumor microenvironment. Cell Mol Immunol. 2020 Jan; 17(1): 27–35.

111 Callender LA, Carroll EC, Beal RWJ, et al. Human CD8+ EMRA T cells display a senescence-associated secretory phenotype regulated by p38 MAPK. Aging Cell. 2018;17(1):e12675. doi:10.1111/acel.12675

112 Ramos-Casals M, Brahmer JR, Callahan MK, Flores-Chávez A, Keegan N, Khamashta MA, Lambotte O, Mariette X, Prat A, Suárez-Almazor ME. Immune-related adverse events of checkpoint inhibitors. Nat Rev Dis Primers. 2020 May 7;6(1):38.

113 Okazaki T, Honjo T. PD-1 and PD-1 ligands: from discovery to clinical application. Int Immunol. 2007 Jul;19(7):813-24.

114 Pardoll DM. The blockade of immune checkpoints in cancer immunotherapy. Nat Rev Cancer. 2012 Mar 22;12(4):252-64.

115 Chambers CA, Kuhns MS, Egen JG, Allison JP. CTLA-4-mediated inhibition in regulation of T cell responses: mechanisms and manipulation in tumor immunotherapy. Annu Rev Immunol. 2001;19:565-94.

116 Wei SC, Duffy CR, Allison JP. Fundamental Mechanisms of Immune Checkpoint Blockade Therapy. Cancer Discov. 2018;8:1069-86.

117 Yan Y, Kumar AB, Finnes H, Markovic SN, Park S, Dronca RS, Dong H. Combining Immune Checkpoint Inhibitors With Conventional Cancer Therapy. Front Immunol. 2018;9:1739.

118 Shiravand Y, Khodadadi F, Kashani SMA, Hosseini-Fard SR, Hosseini S, Sadeghirad H, Ladwa R, O'Byrne K, Kulasinghe A. Immune Checkpoint Inhibitors in Cancer Therapy. Curr Oncol. 2022 Apr 24;29(5):3044-3060.

119 Chrétien S., Zerdes I., Bergh J., Matikas A., Foukakis T. Beyond PD-1/PD-L1 inhibition: What the future holds for breast cancer immunotherapy. Cancers. 2019;11:628.

120 Woo SR, Turnis ME, Goldberg MV, Bankoti J, Selby M, Nirschl CJ, Bettini ML, Gravano DM, Vogel P, Liu CL, Tangsombatvisit S, Grosso JF, Netto G, Smeltzer MP, Chaux A, Utz PJ, Workman CJ, Pardoll DM, Korman AJ, Drake CG, Vignali DA. Immune inhibitory molecules LAG-3 and PD-1 synergistically regulate T-cell function to promote tumoral immune escape. Cancer Res. 2012 Feb 15;72(4):917-27.

121 Okazaki T, Okazaki IM, Wang J, Sugiura D, Nakaki F, Yoshida T, Kato Y, Fagarasan S, Muramatsu M, Eto T, Hioki K, Honjo T. PD-1 and LAG-3 inhibitory co-receptors act synergistically to prevent autoimmunity in mice. J Exp Med. 2011 Feb 14;208(2):395-407.

122 Ruffo E, Wu RC, Bruno TC, Workman CJ, Vignali DAA. Lymphocyte-activation gene 3 (LAG3): The next immune checkpoint receptor. Semin Immunol. 2019;42:101305. doi:10.1016/j.smim.2019.101305

123 Koyama S, Akbay EA, Li YY, et al. Adaptive resistance to therapeutic PD-1 blockade is associated with upregulation of alternative immune checkpoints. Nat Commun. 2016;7:10501.

124 Cyriac G, Gandhi L. Emerging biomarkers for immune checkpoint inhibition in lung cancer. Semin Cancer Biol. 2018;52:269-77.

125 Doroshow, D.B., Bhalla, S., Beasley, M.B. et al. PD-L1 as a biomarker of response to immune-checkpoint inhibitors. Nat Rev Clin Oncol (2021).

126 Davis, A.A., Patel, V.G. The role of PD-L1 expression as a predictive biomarker: an analysis of all US Food and Drug Administration (FDA) approvals of immune checkpoint inhibitors. j. immunotherapy cancer 7, 278 (2019).

127 O'Malley DM, Oaknin A, Monk BJ, Leary A, Selle F, Alexandre J, et al. LBA34 Single-agent anti-PD-1 balstilimab or in combination with anti-CTLA-4 zalifrelimab for recurrent/metastatic (R/M) cervical cancer (CC): Preliminary results of two independent phase II trials. Ann Oncol. 2020;31:S1164–S1165.

128 Grossman, J.E., Vasudevan, D., Joyce, C.E. et al. Is PD-L1 a consistent biomarker for anti-PD-1 therapy? The model of balstilimab in a virally-driven tumor. Oncogene 40, 1393–1395 (2021).

129 Zhao, Y., Shao, Q. & Peng, G. Exhaustion and senescence: two crucial dysfunctional states of T cells in the tumor microenvironment. Cell Mol Immunol 17, 27–35 (2020).

130 Tsukishiro T, Donnenberg AD, Whiteside TL. Rapid turnover of the CD8(+)CD28(-) T-cell subset of effector cells in the circulation of patients with head and neck cancer. Cancer Immunol Immunother. 2003 Oct;52(10):599-607.

131 Meloni F, Morosini M, Solari N, Passadore I, Nascimbene C, Novo M, Ferrari M, Cosentino M, Marino F, Pozzi E, Fietta AM. Foxp3 expressing CD4+ CD25+ and CD8+CD28- T regulatory cells in the peripheral blood of patients with lung cancer and pleural mesothelioma. Hum Immunol. 2006 Jan-Feb;67(1-2):1-12.

132 Gruber IV, El Yousfi S, Dürr-Störzer S, Wallwiener D, Solomayer EF, Fehm T. Down-regulation of CD28, TCR-zeta (zeta) and up-regulation of FAS in peripheral cytotoxic T-cells of primary breast cancer patients. Anticancer Res. 2008 Mar-Apr;28(2A):779-84.

133 Urbaniak-Kujda D, Kapelko-Słowik K, Wołowiec D, Dybko J, Hałoń A, Jaźwiec B, Maj J, Jankowska-Konsur A, Kuliczkowski K. Increased percentage of CD8+CD28- suppressor lymphocytes in peripheral blood and skin infiltrates correlates with advanced disease in patients with cutaneous T-cell lymphomas. Postepy Hig Med Dosw (Online). 2009 Jul 21;63:355-9.

134 Ye J, Peng G. Controlling T cell senescence in the tumor microenvironment for tumor immunotherapy. Oncoimmunology. 2015;4(3):e994398. Published 2015 Jan 22.

135 Zhao, Y., Shao, Q. & Peng, G. Exhaustion and senescence: two crucial dysfunctional states of T cells in the tumor microenvironment. Cell Mol Immunol 17, 27–35 (2020).

136 Patrick MS, Cheng NL, Kim J, et al. Human T Cell Differentiation Negatively Regulates Telomerase Expression Resulting in Reduced Activation-Induced Proliferation and Survival. Front Immunol. 2019;10:1993

137 Qian Y, Yang L, Cao S. Telomeres and telomerase in T cells of tumor immunity. Cell Immunol. 2014 May-Jun;289(1-2):63-9.

138 Shen X, Zhou J, Hathcock KS, Robbins P, Powell DJ Jr, Rosenberg SA, Hodes RJ. Persistence of tumor infiltrating lymphocytes in adoptive immunotherapy correlates with telomere length. J Immunother. 2007 Jan;30(1):123-9.

139 Ayers M, Lunceford J, Nebozhyn M, Murphy E, Loboda A, Kaufman DR, Albright A, Cheng JD, Kang SP, Shankaran V, Piha-Paul SA, Yearley J, Seiwert TY, Ribas A, McClanahan TK. IFN-γ-related mRNA profile predicts clinical response to PD-1 blockade. J Clin Invest. 2017 Aug 1;127(8):2930-2940.

140 Litchfield K, Reading JL, Puttick C, Thakkar K, Abbosh C, Bentham R, Watkins TBK, Rosenthal R, Biswas D, Rowan A, Lim E, Al Bakir M, Turati V, Guerra-Assunção JA, Conde L, Furness AJS, Saini SK, Hadrup SR, Herrero J, Lee SH, Van Loo P, Enver T, Larkin J, Hellmann MD, Turajlic S, Quezada SA, McGranahan N, Swanton C. Meta-analysis of tumor- and T cell-intrinsic mechanisms of sensitization to checkpoint inhibition. Cell. 2021 Feb 4;184(3):596-614.e14.

141 Olson DJ, Luke JJ. The T-cell-inflamed tumor microenvironment as a paradigm for immunotherapy drug development. Immunotherapy. 2019;11(3):155-159. doi:10.2217/imt-2018-0171

142 Cristescu R, Mogg R, Ayers M, et al. Pan-tumor genomic biomarkers for PD-1 checkpoint blockade-based immunotherapy [published correction appears in Science. 2019 Mar 1;363(6430):]. Science. 2018;362(6411):eaar3593.

143 O'Donnell JS, Smyth MJ, Teng MWL. PD1 functions by inhibiting CD28-mediated co-stimulation. Clin Transl Immunology. 2017 May 5;6(5):e138.

144 Hui E, Cheung J, Zhu J, Su X, Taylor MJ, Wallweber HA, Sasmal DK, Huang J, Kim JM, Mellman I, Vale RD. T cell costimulatory receptor CD28 is a primary target for PD-1-mediated inhibition. Science. 2017 Mar 31;355(6332):1428-1433.

145 Kamphorst AO, Wieland A, Nasti T, Yang S, Zhang R, Barber DL et al. Rescue of exhausted CD8 T cells by PD-1-targeted therapies is CD28-dependent. Science 2017; 355: 1423–1427.

146 Hui E, Cheung J, Zhu J, et al. T cell costimulatory receptor CD28 is a primary target for PD-1-mediated inhibition. Science. 2017;355(6332):1428-1433. doi:10.1126/science.aaf1292

147 Moreira A, Gross S, Kirchberger MC, Erdmann M, Schuler G, Heinzerling L. Senescence markers: Predictive for response to checkpoint inhibitors. Int J Cancer. 2019 Mar 1;144(5):1147-1150.

148 Ferrara R, Naigeon M, Auclin E, Duchemann B, Cassard L, Jouniaux JM, Boselli L, Grivel J, Desnoyer A, Mezquita L, Texier M, Caramella C, Hendriks L, Planchard D, Remon J, Sangaletti S, Proto C, Garassino MC, Soria JC, Marabelle A, Voisin AL, Farhane S, Besse B, Chaput N. Circulating T-cell Immunosenescence in Patients with Advanced Non-small Cell Lung Cancer Treated with Single-agent PD-1/PD-L1 Inhibitors or Platinum-based Chemotherapy. Clin Cancer Res. 2021 Jan 15;27(2):492-503.

149 Iwahori, K., Shintani, Y., Funaki, S. et al. Peripheral T cell cytotoxicity predicts T cell function in the tumor microenvironment. Sci Rep 9, 2636 (2019).

150 Yost KE, Satpathy AT, Wells DK, Qi Y, Wang C, Kageyama R, McNamara KL, Granja JM, Sarin KY, Brown RA, Gupta RK, Curtis C, Bucktrout SL, Davis MM, Chang ALS, Chang HY. Clonal replacement of tumor-specific T cells following PD-1 blockade. Nat Med. 2019 Aug;25(8):1251-1259.

151 Zhang J, Ji Z, Caushi JX, El Asmar M, Anagnostou V, Cottrell TR, Chan HY, Suri P, Guo H, Merghoub T, Chaft JE, Reuss JE, Tam AJ, Blosser RL, Abu-Akeel M, Sidhom JW, Zhao N, Ha JS, Jones DR, Marrone KA, Naidoo J, Gabrielson E, Taube JM, Velculescu VE, Brahmer JR, Housseau F, Hellmann MD, Forde PM, Pardoll DM, Ji H, Smith KN. Compartmental Analysis of T-cell Clonal Dynamics as a Function of Pathologic Response to Neoadjuvant PD-1 Blockade in Resectable Non-Small Cell Lung Cancer. Clin Cancer Res. 2020 Mar 15;26(6):1327-1337.

152 Galon J, Costes A, Sanchez-Cabo F, Kirilovsky A, Mlecnik B, Lagorce-Pagès C, Tosolini M, Camus M, Berger A, Wind P, Zinzindohoué F, Bruneval P, Cugnenc PH, Trajanoski Z, Fridman WH, Pagès F. Type, density, and location of immune cells within human colorectal tumors predict clinical outcome. Science. 2006 Sep 29;313(5795):1960-4.

153 Mahmoud SM, Paish EC, Powe DG, Macmillan RD, Grainge MJ, Lee AH, Ellis IO, Green AR. Tumor-infiltrating CD8+ lymphocytes predict clinical outcome in breast cancer. J Clin Oncol. 2011 May 20;29(15):1949-55.

154 Sharma P, Shen Y, Wen S, Yamada S, Jungbluth AA, Gnjatic S, Bajorin DF, Reuter VE, Herr H, Old LJ, Sato E. CD8 tumor-infiltrating lymphocytes are predictive of survival in muscle-invasive urothelial carcinoma. Proc Natl Acad Sci U S A. 2007 Mar 6;104(10):3967-72.

155 Sade-Feldman M, Yizhak K, Bjorgaard SL, et al. Defining T Cell States Associated with Response to Checkpoint Immunotherapy in Melanoma [published correction appears in Cell. 2019 Jan 10;176(1-2):404].

156 Sanmamed MF, Nie X, Desai SS, Villaroel-Espindola F, Badri T, Zhao D, Kim AW, Ji L, Zhang T, Quinlan E, Cheng X, Han X, Vesely MD, Nassar AF, Sun J, Zhang Y, Kim TK, Wang J, Melero I, Herbst RS, Schalper KA, Chen L. A burned-out CD8+ T-cell subset expands in the tumor microenvironment and curbs cancer immunotherapy. Cancer Discov. 2021 Mar 3:candisc.0962.2020.

157 Goswami S, Chen Y, Anandhan S, Szabo PM, Basu S, Blando JM, Liu W, Zhang J, Natarajan SM, Xiong L, Guan B, Yadav SS, Saci A, Allison JP, Galsky MD, Sharma P. ARID1A mutation plus CXCL13 expression act as combinatorial biomarkers to predict responses to immune checkpoint therapy in mUCC. Sci Transl Med. 2020 Jun 17;12(548):eabc4220.

158 Thommen DS, Koelzer VH, Herzig P, et al. A transcriptionally and functionally distinct PD-1+ CD8+ T cell pool with predictive potential in non-small-cell lung cancer treated with PD-1 blockade. Nat Med. 2018;24(7):994-1004.

159 Litchfield K, Reading JL, Puttick C, Thakkar K, Abbosh C, Bentham R, Watkins TBK, Rosenthal R, Biswas D, Rowan A, Lim E, Al Bakir M, Turati V, Guerra-Assunção JA, Conde L, Furness AJS, Saini SK, Hadrup SR, Herrero J, Lee SH, Van Loo P, Enver T, Larkin J, Hellmann MD, Turajlic S, Quezada SA, McGranahan N, Swanton C. Meta-analysis of tumor- and T cell-intrinsic mechanisms of sensitization to checkpoint inhibition. Cell. 2021 Feb 4;184(3):596-614.e14.

160 Beauséjour CM, Krtolica A, Galimi F, et al. Reversal of human cellular senescence: roles of the p53 and p16 pathways. EMBO J. 2003;22(16):4212-4222.

161 Lanna A, Henson SM, Escors D, Akbar AN. The kinase p38 activated by the metabolic regulator AMPK and scaffold TAB1 drives the senescence of human T cells. Nat Immunol. 2014;15:965–972.

162 Henson SM, Macaulay R, Riddell NE, Nunn CJ, Akbar AN. Blockade of PD-1 or p38 MAP kinase signaling enhances senescent human CD8(+) T-cell proliferation by distinct pathways. Eur J Immunol. 2015 May;45(5):1441-51.

163 Matthews N, Watkins JF. Tumour-necrosis factor from the rabbit. I. Mode of action, specificity and physicochemical properties. Br J Cancer. 1978 Aug;38(2):302-9.

164 Green S, Dobrjansky A, Chiasson MA. Murine tumor necrosis-inducing factor: purification and effects on myelomonocytic leukemia cells. J Natl Cancer Inst. 1982 Jun;68(6):997-1003.

165 Freund A, Patil CK, Campisi J. p38MAPK is a novel DNA damage response-independent regulator of the senescence-associated secretory phenotype. EMBO J. 2011 Apr 20;30(8):1536-48.

166 Akbar AN, Henson SM. Are senescence and exhaustion intertwined or unrelated processes that compromise immunity? Nat Rev Immunol. 2011 Apr;11(4):289-95.

167 Lanna A, Gomes DC, Muller-Durovic B, McDonnell T, Escors D, Gilroy DW, Lee JH, Karin M, Akbar AN. A sestrin-dependent Erk-Jnk-p38 MAPK activation complex inhibits immunity during aging. Nat Immunol. 2017 Mar;18(3):354-363.

168 Hu-Lieskovan S, Mok S, Homet Moreno B, et al. Improved antitumor activity of immunotherapy with BRAF and MEK inhibitors in BRAF V600E melanoma. Sci Transl Med. 2015;7:279ra41.

169 Liu L, Mayes PA, Eastman S, et al. The BRAF and MEK inhibitors dabrafenib and trametinib: effects on immune function and in combination with immunomodulatory antibodies targeting PD-1, PD-L1, and CTLA-4. Clin Cancer Res. 2015;21:1639-1651.

170 Ribas A, Butler M, Lutzky J, et al. Phase I study combining anti-PD-L1 (MEDI4736) with BRAF (dabrafenib) and/or MEK (trametinib) inhibitors in advanced melanoma. J Clin Oncol. 2015;33(15_suppl):3003.

171 Ebert PJR, Cheung J, Yang Y, et al. MAP kinase inhibition promotes T cell and anti-tumor activity in combination with PD-L1 checkpoint blockade. Immunity. 2016;44:609-621.

172 Fares CM, Van Allen EM, Drake CG, Allison JP, Hu-Lieskovan S. Mechanisms of Resistance to Immune Checkpoint Blockade: Why Does Checkpoint Inhibitor Immunotherapy Not Work for All Patients? Am Soc Clin Oncol Educ Book. 2019 Jan;39:147-164.

173 Gurusamy D, Henning AN, Yamamoto TN, Yu Z, Zacharakis N, Krishna S, Kishton RJ, Vodnala SK, Eidizadeh A, Jia L, Kariya CM, Black MA, Eil R, Palmer DC, Pan JH, Sukumar M, Patel SJ, Restifo NP. Multi-phenotype CRISPR-Cas9 Screen Identifies p38 Kinase as a Target for Adoptive Immunotherapies. Cancer Cell. 2020 Jun 8;37(6):818-833.e9.

174 Chong EA, Melenhorst JJ, Lacey SF, Ambrose DE, Gonzalez V, Levine BL, June CH, Schuster SJ. PD-1 blockade modulates chimeric antigen receptor (CAR)-modified T cells: refueling the CAR. Blood. 2017 Feb 23;129(8):1039-1041.

175 Ye J, Huang X, Hsueh EC, et al. Human regulatory T cells induce T-lymphocyte senescence. Blood. 2012;120(10):2021-2031.

176 Li L, Liu X, Sanders KL, Edwards JL, Ye J, Si F, Gao A, Huang L, Hsueh EC, Ford DA, Hoft DF, Peng G. TLR8-Mediated Metabolic Control of Human Treg Function: A Mechanistic Target for Cancer Immunotherapy. Cell Metab. 2019 Jan 8;29(1):103-123.e5.

177 Liu X, Mo W, Ye J, Li L, Zhang Y, Hsueh EC, Hoft DF, Peng G. Regulatory T cells trigger effector T cell DNA damage and senescence caused by metabolic competition. Nat Commun. 2018 Jan 16;9(1):249.

178 Pauken KE, Sammons MA, Odorizzi PM, Manne S, Godec J, Khan O, Drake AM, Chen Z, Sen DR, Kurachi M, Barnitz RA, Bartman C, Bengsch B, Huang AC, Schenkel JM, Vahedi G, Haining WN, Berger SL, Wherry EJ. Epigenetic stability of exhausted T cells limits durability of reinvigoration by PD-1 blockade. Science. 2016 Dec 2;354(6316):1160-1165.

179 Scott AC, Dündar F, Zumbo P, Chandran SS, Klebanoff CA, Shakiba M, Trivedi P, Menocal L, Appleby H, Camara S, Zamarin D, Walther T, Snyder A, Femia MR, Comen EA, Wen HY, Hellmann MD, Anandasabapathy N, Liu Y, Altorki NK, Lauer P, Levy O, Glickman MS, Kaye J, Betel D, Philip M, Schietinger A. TOX is a critical regulator of tumour-specific T cell differentiation. Nature. 2019 Jul;571(7764):270-274.

180 Khan O, Giles JR, McDonald S, Manne S, Ngiow SF, Patel KP, Werner MT, Huang AC, Alexander KA, Wu JE, Attanasio J, Yan P, George SM, Bengsch B, Staupe RP, Donahue G, Xu W, Amaravadi RK, Xu X, Karakousis GC, Mitchell TC, Schuchter LM, Kaye J, Berger SL, Wherry EJ. TOX transcriptionally and epigenetically programs CD8+ T cell exhaustion. Nature. 2019 Jul;571(7764):211-218.

181 Alfei F, Kanev K, Hofmann M, Wu M, Ghoneim HE, Roelli P, Utzschneider DT, von Hoesslin M, Cullen JG, Fan Y, Eisenberg V, Wohlleber D, Steiger K, Merkler D, Delorenzi M, Knolle PA, Cohen CJ, Thimme R, Youngblood B, Zehn D. TOX reinforces the phenotype and longevity of exhausted T cells in chronic viral infection. Nature. 2019 Jul;571(7764):265-269.

182 Yao C, Sun HW, Lacey NE, Ji Y, Moseman EA, Shih HY, Heuston EF, Kirby M, Anderson S, Cheng J, Khan O, Handon R, Reilley J, Fioravanti J, Hu J, Gossa S, Wherry EJ, Gattinoni L, McGavern DB, O'Shea JJ, Schwartzberg PL, Wu T. Single-cell RNA-seq reveals TOX as a key regulator of CD8+ T cell persistence in chronic infection. Nat Immunol. 2019 Jul;20(7):890-901.

183 Seo H, Chen J, González-Avalos E, Samaniego-Castruita D, Das A, Wang YH, López-Moyado IF, Georges RO, Zhang W, Onodera A, Wu CJ, Lu LF, Hogan PG, Bhandoola A, Rao A. TOX and TOX2 transcription factors cooperate with NR4A transcription factors to impose CD8+ T cell exhaustion. Proc Natl Acad Sci U S A. 2019 Jun 18;116(25):12410-12415.

184 Goronzy JJ, Hu B, Kim C, Jadhav RR, Weyand CM. Epigenetics of T cell aging. J Leukoc Biol. 2018;104(4):691-699. R

185 Chauvin JM, Pagliano O, Fourcade J, Sun Z, Wang H, Sander C, Kirkwood JM, Chen TH, Maurer M, Korman AJ, Zarour HM. TIGIT and PD-1 impair tumor antigen-specific CD8$^+$ T cells in melanoma patients. J Clin Invest. 2015 May;125(5):2046-58.

186 Freepik Company S.L., "Download Free Icons and Stickers for your projects. Images made by and for designers in PNG, SVG, EPS, PSD and CSS formats.," [Online]. Available: https://www.flaticon.com/free-icon/cancer_1488119?related_id=1488119&origin=pack. [Accessed 29 February 2024].

187 Cawthon RM. Telomere measurement by quantitative PCR. Nucleic Acids Res. 2002 May 15;30(10):e47.

188 Lai TP, Zhang N, Noh J, Mender I, Tedone E, Huang E, Wright WE, Danuser G, Shay JW. A method for measuring the distribution of the shortest telomeres in cells and tissues. Nat Commun. 2017 Nov 7;8(1):1356.

189 Skvortsov D.A., Zvereva M.E., Shpanchenko O.V., Dontsova O.A. Assays for Detection of Telomerase Activity // Acta Naturae. - 2011. - Vol. 3. - N. 1. - P. 48-68.

190 Ludlow AT, Shelton D, Wright WE, Shay JW. ddTRAP: A Method for Sensitive and Precise Quantification of Telomerase Activity. Methods Mol Biol. 2018;1768:513-529.

191 Pooley KA, Bojesen SE, Weischer M, Nielsen SF, Thompson D, Amin Al Olama A, et al. A genome-wide association scan (GWAS) for mean telomere length within the COGS project: identified loci show little association with hormone-related cancer risk. Hum Mol Genet. 2013 Dec;22(24):5056–64.

192 Codd V, Nelson CP, Albrecht E, Mangino M, Deelen J, Buxton JL, et al. Identification of seven loci affecting mean telomere length and their association with disease. Nat Genet. 2013 Apr;45(4):422-427e4272.

193 Mangino M, Hwang S-J, Spector TD, Hunt SC, Kimura M, Fitzpatrick AL, et al. Genome-wide meta-analysis points to CTC1 and ZNF676 as genes regulating telomere homeostasis in humans. Hum Mol Genet. 2012/09/21. 2012 Dec 15;21(24):5385–94

194 Viktoria Topler (2020). Leukozyten-Telomerlänge als prognostischer Marker für das Prostatakarzinom. Unpublished bachelor thesis. FH Joaneum, Graz.

195 Zhang C, Doherty JA, Burgess S, Hung RJ, Lindström S, Kraft P, et al. Genetic determinants of telomere length and risk of common cancers: a Mendelian randomization study. Hum Mol Genet. 2015 Sep;24(18):5356–66.

196 Pooley KA, Bojesen SE, Weischer M, Nielsen SF, Thompson D, Amin Al Olama A, et al. A genome-wide association scan (GWAS) for mean telomere length within the COGS project: identified loci show little association with hormone-related cancer risk. Hum Mol Genet. 2013 Dec;22(24):5056–64.

197 Codd V, Nelson CP, Albrecht E, Mangino M, Deelen J, Buxton JL, et al. Identification of seven loci affecting mean telomere length and their association with disease. Nat Genet. 2013 Apr;45(4):422-427e4272.

198 Mangino M, Hwang S-J, Spector TD, Hunt SC, Kimura M, Fitzpatrick AL, et al. Genome-wide meta-analysis points to CTC1 and ZNF676 as genes regulating telomere homeostasis in humans. Hum Mol Genet. 2012/09/21. 2012 Dec 15;21(24):5385–94.

199 Bai R, Lv Z, Xu D, Cui J. Predictive Biomarkers for Cancer Immunotherapy With Immune Checkpoint Inhibitors. Biomark Res (2020) 8:1–17.

200 Zhang J, He T, Xue L, Guo H. Senescent T cells: a potential biomarker and target for cancer therapy. EBioMedicine. 2021 Jun;68:103409.

201 Levy T, Agoulnik I, Atkinson EN, Tong XW, Gause HM, Hasenburg A, Runnebaum IB, Stickeler E, Möbus VJ, Kaplan AL, Kieback DG. Telomere length in human white blood cells remains constant with age and is shorter in breast cancer patients. Anticancer Res. 1998 May-Jun;18(3A):1345-9.

202 Gallicchio L, Gadalla SM, Murphy JD, Simonds NI. The Effect of Cancer Treatments on Telomere Length: A Systematic Review of the Literature. J Natl Cancer Inst. 2018 Oct 1;110(10):1048-1058.

203 Beauséjour, C.M.; Krtolica, A.; Galimi, F.; Narita, M.; Lowe, S.W.; Yaswen, P.; Campisi, J. Reversal of human cellular senescence: Roles of the p53 and p16 pathways. EMBO J. 2003, 22, 4212–4222.

204 Lanna, A.; Henson, S.M.; Escors, D.; Akbar, A.N. The kinase p38 activated by the metabolic regulator AMPK and scaffold TAB1 drives the senescence of human T cells. Nat. Immunol. 2014, 15, 965–972.

205 Henson, S.M.; Macaulay, R.; Riddell, N.; Nunn, C.J.; Akbar, A.N. Blockade of PD-1 or p38 MAP kinase signaling enhances senescent human CD8+T-cell proliferation by distinct pathways. Eur. J. Immunol. 2015, 45, 1441–1451.

206 Huang EE, Tedone E, O'Hara R, Cornelius C, Lai TP, Ludlow A, Wright WE, Shay JW. The Maintenance of Telomere Length in CD28+ T Cells During T Lymphocyte Stimulation. Sci Rep. 2017 Jul 28;7(1):6785.

207 Waldman AD, Fritz JM, Lenardo MJ. A guide to cancer immunotherapy: from T cell basic science to clinical practice. Nat Rev Immunol. 2020 Nov;20(11):651-668.

208 Ugolini A, Zizzari IG, Ceccarelli F, Botticelli A, Colasanti T, Strigari L, Rughetti A, Rahimi H, Conti F, Valesini G, Marchetti P, Nuti M. IgM-Rheumatoid factor confers primary resistance to anti-PD-1 immunotherapies in NSCLC patients by reducing CD137+T-cells. EBioMedicine. 2020 Dec;62:103098.

209 Coleman, N., Yap, T.A., Heymach, J.V. et al. Antibody-drug conjugates in lung cancer: dawn of a new era?. npj Precis. Onc. 7, 5 (2023).

210 Müller, P. et al. Trastuzumab emtansine (T-DM1) renders HER2+ breast cancer highly susceptible to CTLA-4/PD-1 blockade. Sci. Transl. Med. 7, 315 (2015).

211 Dumbrava, E. I. et al. Abstract OT-03-02: Phase 1/2 study of a novel HER2 targeting TLR7/8 immune stimulating antibody conjugate (ISAC), BDC-1001, as a single agent and in combination with an immune checkpoint inhibitor in patients with advanced HER2-expressing solid tumors. Cancer Res. 81, OT-03-02–OT-03-02 (2021).

212 Kuhn CK, Meister J, Kreft S, Stiller M, Puppel SH, Zaremba A, Scheffler B, Ullrich V, Schöneberg T, Schadendorf D, Horn S. TERT expression is associated with metastasis from thin primaries, exhausted CD4+ T cells in melanoma and with DNA repair across cancer entities. PLoS One. 2023 Jul 7;18(7):e0281487.

213 Lee JY, Kannan B, Lim BY, Li Z, Lim AH, Loh JW, Ko TK, Ng CC, Chan JY. The Multi-Dimensional Biomarker Landscape in Cancer Immunotherapy. Int J Mol Sci. 2022 Jul 16;23(14):7839.

214 Moreno SP, Fusté JM, Kaiser M, Li JSZ, Nassour J, Haggblom C, Denchi EL, Karlseder J. TZAP overexpression induces telomere dysfunction and ALT-like activity in ATRX/DAXX-deficient cells. iScience. 2023 Mar 14;26(4):106405.

215 Zhang J.M., Zou L. Alternative lengthening of telomeres: from molecular mechanisms to therapeutic outlooks. Cell Biosci. 2020;10:30. doi: 10.1186/s13578-020-00391-6.

216 Bryan T.M., Englezou A., Gupta J., Bacchetti S., Reddel R.R. Telomere elongation in immortal human cells without detectable telomerase activity. EMBO J. 1995;14:4240–4248.

217 MacKenzie D Jr, Watters AK, To JT, Young MW, Muratori J, Wilkoff MH, Abraham RG, Plummer MM, Zhang D. ALT Positivity in Human Cancers: Prevalence and Clinical Insights. Cancers (Basel). 2021 May 14;13(10):2384.

218 Bryan TM, Englezou A, Gupta J, Bacchetti S, Reddel RR. Telomere elongation in immortal human cells without detectable telomerase activity. EMBO J. 1995;14(17):4240-8.

219 Roumelioti FM, Sotiriou SK, Katsini V, Chiourea M, Halazonetis TD, Gagos S. Alternative lengthening of human telomeres is a conservative DNA replication process with features of break-induced replication. EMBO Rep. 2016;17(12):1731-7.

220 Dilley RL, Verma P, Cho NW, Winters HD, Wondisford AR, Greenberg RA. Break-induced telomere synthesis underlies alternative telomere maintenance. Nature. 2016;539(7627):54-8.

221 Yeager TR, Neumann AA, Englezou A, Huschtscha LI, Noble JR, Reddel RR. Telomerase-negative immortalized human cells contain a novel type of promyelocytic leukemia (PML) body. Cancer Res. 1999;59(17):4175-9.

222 Xue Y, Gibbons R, Yan Z, Yang D, McDowell TL, Sechi S, Qin J, Zhou S, Higgs D, Wang W. The ATRX syndrome protein forms a chromatin-remodeling complex with Daxx and localizes in promyelocytic leukemia nuclear bodies. Proc Natl Acad Sci U S A. 2003 Sep 16;100(19):10635-40.

223 Heaphy CM, de Wilde RF, Jiao Y, Klein AP, Edil BH, Shi C, et al. Altered telomeres in tumors with ATRX and DAXX mutations. Science. 2011;333(6041):425.

224 Picketts DJ, Higgs DR, Bachoo S, Blake DJ, Quarrell OW, Gibbons RJ. ATRX encodes a novel member of the SNF2 family of proteins: mutations point to a common mechanism underlying the ATR-X syndrome. Hum Mol Genet. 1996;5(12):1899-907.

225 Lewis PW, Elsaesser SJ, Noh KM, Stadler SC, Allis CD. Daxx is an H3.3-specific histone chaperone and cooperates with ATRX in replication-independent chromatin assembly at telomeres. Proc Natl Acad Sci U S A. 2010;107(32):14075-80.

226 Lovejoy CA, Li W, Reisenweber S, Thongthip S, Bruno J, de Lange T, et al. Loss of ATRX, genome instability, and an altered DNA damage response are hallmarks of the alternative lengthening of telomeres pathway. PLoS Genet. 2012;8(7):e1002772.

227 Heaphy CM, de Wilde RF, Jiao Y, Klein AP, Edil BH, Shi C, Bettegowda C, Rodriguez FJ, Eberhart CG, Hebbar S, Offerhaus GJ, McLendon R, Rasheed BA, He Y, Yan H, Bigner DD, Oba-Shinjo SM, Marie SK, Riggins GJ, Kinzler KW, Vogelstein B, Hruban RH, Maitra A, Papadopoulos N, Meeker AK. Altered telomeres in tumors with ATRX and DAXX mutations. Science. 2011 Jul 22;333(6041):425.

228 Pan X, Chen Y, Biju B, Ahmed N, Kong J, Goldenberg M, et al. FANCM suppresses DNA replication stress at ALT telomeres by disrupting TERRA R-loops. Sci Rep. 2019;9(1):19110.

229 Heaphy CM, de Wilde RF, Jiao Y, Klein AP, Edil BH, Shi C, Bettegowda C, Rodriguez FJ, Eberhart CG, Hebbar S, Offerhaus GJ, McLendon R, Rasheed BA, He Y, Yan H, Bigner DD, Oba-Shinjo SM, Marie SK, Riggins GJ, Kinzler KW, Vogelstein B, Hruban RH, Maitra A, Papadopoulos N, Meeker AK. Altered telomeres in tumors with ATRX and DAXX mutations. Science. 2011 Jul 22;333(6041):425.

230 Clynes D, Jelinska C, Xella B, Ayyub H, Scott C, Mitson M, et al. Suppression of the alternative lengthening of telomere pathway by the chromatin remodelling factor ATRX. Nat Commun. 2015;6:7538.

231 Napier CE, Huschtscha LI, Harvey A, Bower K, Noble JR, Hendrickson EA, et al. ATRX represses alternative lengthening of telomeres. Oncotarget. 2015;6(18):16543-58.

232 Cong YS, Wright WE, Shay JW. Human telomerase and its regulation. Microbiol Mol Biol Rev. 2002 Sep;66(3):407-25.

233 Hiyama K, Hirai Y, Kyoizumi S, Akiyama M, Hiyama E, Piatyszek MA, Shay JW (1995) Activation of telomerase in human lymphocytes and hematopoietic progenitor cells. J Immunol 155: 3711–3715.

234 Morrison SJ, Prowse KR, Ho P, Weissman IL (1996) Telomerase activity in hematopoietic cells is associated with self-renewal potential. Immunity 5: 207–216.

235 Yuan X, Larsson C, Xu D. Mechanisms underlying the activation of TERT transcription and telomerase activity in human cancer: old actors and new players. Oncogene. 2019 Aug;38(34):6172-6183.

236 Blasco MA. Telomeres and human disease: ageing, cancer and beyond. Nat Rev Genet. 2005 Aug;6(8):611-22.

237 Dratwa M, Wysoczańska B, Łacina P, Kubik T, Bogunia-Kubik K. TERT-Regulation and Roles in Cancer Formation. Front Immunol. 2020 Nov 19;11:589929.

238 Lipinska N, Romaniuk A, Paszel-Jaworska A, Toton E, Kopczynski P, Rubis B. Telomerase and drug resistance in cancer. Cell Mol Life Sci. 2017 Nov;74(22):4121-4132.

239 Artandi SE, DePinho RA. Telomeres and telomerase in cancer. Carcinogenesis. 2010 Jan;31(1):9-18.

240 Fernández-Marcelo T, Sánchez-Pernaute A, Pascua I, De Juan C, Head J, Torres-García AJ, Iniesta P. Clinical Relevance of Telomere Status and Telomerase Activity in Colorectal Cancer. PLoS One. 2016 Feb 25;11(2):e0149626.

241 Guterres AN, Villanueva J. Targeting telomerase for cancer therapy. Oncogene. 2020 Sep;39(36):5811-5824.

242 Fragkiadaki P, Renieri E, Kalliantasi K, Kouvidi E, Apalaki E, Vakonaki E, Mamoulakis C, Spandidos DA, Tsatsakis A. Telomerase inhibitors and activators in aging and cancer: A systematic review. Mol Med Rep. 2022 May;25(5):158.

243 Aamdal E, Inderberg EM, Ellingsen EB, Rasch W, Brunsvig PF, Aamdal S, Heintz KM, Vodák D, Nakken S, Hovig E, Nyakas M, Guren TK, Gaudernack G. Combining a Universal Telomerase Based Cancer Vaccine With Ipilimumab in Patients With Metastatic Melanoma - Five-Year Follow Up of a Phase I/IIa Trial. Front Immunol. 2021 May 11;12:663865.

244 Zanetti M. A second chance for telomerase reverse transcriptase in anticancer immunotherapy. Nat Rev Clin Oncol. 2017 Feb;14(2):115-128.

245 Thompson CAH, Wong JMY. Non-canonical Functions of Telomerase Reverse Transcriptase: Emerging Roles and Biological Relevance. Curr Top Med Chem. 2020;20(6):498-507.

246 Kimura M, Stone RC, Hunt SC, Skurnick J, Lu X, Cao X, et al. Measurement of telomere length by the Southern blot analysis of terminal restriction fragment lengths. Nat Protoc. 2010;5(9):1596-607.

247 Zhang JM, Yadav T, Ouyang J, Lan L, Zou L. Alternative Lengthening of Telomeres through Two Distinct Break-Induced Replication Pathways. Cell Rep. 2019;26(4):955-68 e3.

248 Pickett HA, Cesare AJ, Johnston RL, Neumann AA, Reddel RR. Control of telomere length by a trimming mechanism that involves generation of t-circles. EMBO J. 2009;28(7):799-809.

249 Rivera T, Haggblom C, Cosconati S, Karlseder J. A balance between elongation and trimming regulates telomere stability in stem cells. Nat Struct Mol Biol. 2017;24(1):30-9.

250 Koneru B, Farooqi A, Nguyen TH, Chen WH, Hindle A, Eslinger C, et al. ALT neuroblastoma chemoresistance due to telomere dysfunction-induced ATM activation is reversible with ATM inhibitor AZD0156. Sci Transl Med. 2021;13(607).

251 Zhang JM, Genois MM, Ouyang J, Lan L, Zou L. Alternative lengthening of telomeres is a self-perpetuating process in ALT-associated PML bodies. Mol Cell. 2021;81(5):1027-42 e4.

252 Gaillard H, Garcia-Muse T, Aguilera A. Replication stress and cancer. Nat Rev Cancer. 2015;15(5):276-89.

253 Cesare AJ, Kaul Z, Cohen SB, Napier CE, Pickett HA, Neumann AA, Reddel RR. 2009. Spontaneous occurrence of telomeric DNA damage response in the absence of chromosome fusions. Nat. Struct. Mol. Biol. 16, 1244-1251.

254 Min J, Wright WE, Shay JW. Alternative Lengthening of Telomeres Mediated by Mitotic DNA Synthesis Engages Break-Induced Replication Processes. Mol Cell Biol. 2017 Sep 26;37(20):e00226-17.

255 Heaphy CM, de Wilde RF, Jiao Y, Klein AP, Edil BH, Shi C, et al. Altered telomeres in tumors with ATRX and DAXX mutations. Science. 2011;333(6041):425.

256 Clynes D, Jelinska C, Xella B, Ayyub H, Scott C, Mitson M, et al. Suppression of the alternative lengthening of telomere pathway by the chromatin remodelling factor ATRX. Nat Commun. 2015;6:7538.

257 Zhang JM, Genois MM, Ouyang J, Lan L, Zou L. Alternative lengthening of telomeres is a self-perpetuating process in ALT-associated PML bodies. Mol Cell. 2021;81(5):1027-42 e4

258 Sobinoff AP, Allen JA, Neumann AA, Yang SF, Walsh ME, Henson JD, et al. BLM and SLX4 play opposing roles in recombination-dependent replication at human telomeres. EMBO J. 2017;36(19):2907-19.

259 Loe TK, Li JSZ, Zhang Y, Azeroglu B, Boddy MN, Denchi EL. Telomere length heterogeneity in ALT cells is maintained by PML-dependent localization of the BTR complex to telomeres. Genes Dev. 2020;34(9-10):650-62.

260 Li JS, Miralles Fuste J, Simavorian T, Bartocci C, Tsai J, Karlseder J, et al. TZAP: A telomere-associated protein involved in telomere length control. Science. 2017;355(6325):638-41.

261 Zhang JM, Yadav T, Ouyang J, Lan L, Zou L. Alternative Lengthening of Telomeres through Two Distinct Break-Induced Replication Pathways. Cell Rep. 2019;26(4):955-68 e3.

262 Cho NW, Dilley RL, Lampson MA, Greenberg RA. Interchromosomal homology searches drive directional ALT telomere movement and synapsis. Cell. 2014;159(1):108-21.

263 Pan X, Drosopoulos WC, Sethi L, Madireddy A, Schildkraut CL, Zhang D. FANCM, BRCA1, and BLM cooperatively resolve the replication stress at the ALT telomeres. Proc Natl Acad Sci U S A. 2017;114(29):E5940-E9.

264 Zhang T, Zhang Z, Li F, Hu Q, Liu H, Tang M, et al. Looping-out mechanism for resolution of replicative stress at telomeres. EMBO Rep. 2017;18(8):1412-28.

265 Deng Z, Dheekollu J, Broccoli D, Dutta A, Lieberman PM. The origin recognition complex localizes to telomere repeats and prevents telomere-circle formation. Curr Biol. 2007;17(22):1989-95.

266 Cox KE, Marechal A, Flynn RL. SMARCAL1 Resolves Replication Stress at ALT Telomeres. Cell Rep. 2016;14(5):1032-40.

267 Pickett HA, Reddel RR. The role of telomere trimming in normal telomere length dynamics. Cell Cycle. 2012;11(7):1309-15.

268 Pickett HA, Henson JD, Au AY, Neumann AA, Reddel RR. Normal mammalian cells negatively regulate telomere length by telomere trimming. Hum Mol Genet. 2011;20(23):4684-92.

269 Lu R, O'Rourke JJ, Sobinoff AP, Allen JAM, Nelson CB, Tomlinson CG, et al. The FANCM-BLM-TOP3A-RMI complex suppresses alternative lengthening of telomeres (ALT). Nat Commun. 2019;10(1):2252.

270 Manthei KA, Keck JL. The BLM dissolvasome in DNA replication and repair. Cell Mol Life Sci. 2013 Nov;70(21):4067-84.

271 Loe TK, Li JSZ, Zhang Y, Azeroglu B, Boddy MN, Denchi EL. Telomere length heterogeneity in ALT cells is maintained by PML-dependent localization of the BTR complex to telomeres. Genes Dev. 2020 May 1;34(9-10):650-662.

272 Zhang JM, Yadav T, Ouyang J, Lan L, Zou L. Alternative Lengthening of Telomeres through Two Distinct Break-Induced Replication Pathways. Cell Rep. 2019;26(4):955-68 e3.

273 Lu R, O'Rourke JJ, Sobinoff AP, Allen JAM, Nelson CB, Tomlinson CG, et al. The FANCM-BLM-TOP3A-RMI complex suppresses alternative lengthening of telomeres (ALT). Nat Commun. 2019;10(1):2252.